The Dissertation Committee for Mary Gazell Mapili Call Certifies that this is the approved version of the following dissertation:

Microfabrication of Spatially-Patterned, Polymer Scaffolds for Applications in Stem Cell and Tissue Engineering

Committee:

Krishnendu Roy, Supervisor

Shaochen Chen

Wolfgang Frey

Anshu Mathur

Christine Schmidt

Microfabrication of Spatially-Patterned, Polymer Scaffolds for Applications in Stem Cell and Tissue Engineering

by

Mary Gazell Mapili Call, B.S.; M.S.

Dissertation

Presented to the Faculty of the Graduate School of

The University of Texas at Austin

in Partial Fulfillment

of the Requirements

for the Degree of

Doctor of Philosophy

The University of Texas at Austin

August 2007

Dedication

I would like to dedicate this dissertation and Ph.D. studies to my husband, Seth, my family, and close friends for their unconditional love, support, and constant encouragement while growing up and throughout the years at the University of Texas.

Acknowledgements

I would like to thank Dr. Krishnendu Roy, my Ph.D. adviser, for giving me the invaluable opportunity to research in his lab over the past five years. My experience at the University of Texas will always be a memorable one. You taught me how to correctly approach science and served as an excellent mentor for balancing life in general with the challenges of research and courses. Thank you for your guidance and constant encouragement throughout the process of my doctoral studies.

My sincere thanks go to Dr. Shaochen Chen for giving me the opportunity to work in collaboration in using their stereolithography systems for creating the scaffolds. I would also like to thank Yi Lu for his help in using these systems and for our numerous research discussions. Thanks to Curt Deister for his help with tissue histology. I would like to also thank Dr. Andrea Gore and Sarah Dickerson from the College of Pharmacy for their help with real time PCR. Thanks to the rest of my committee members, Drs. Wolfgang Frey, Anshu Mathur, and Christine Schmidt, for their advice and invaluable input on the direction of my Ph.D. project.

I would also like to thank Julie Rytlewski, Myung Hee Kim, and Sindura Bandi, my undergraduate research assistants, who all helped me with my research from start to finish. Especially to Julie, I would like to thank her for her commitment, sincere interest, and eagerness to learn all aspects of my project. Thanks to Sabia Taqvi, Sonia Kumar, and Hunter Lauten for always being such wonderful friends throughout these past five years. Everyone else in the lab, I appreciate all of our discussions and for making the lab environment an enjoyable place to work. I would also like to thank everyone at the

ICMB Core Facility for their help with instruments: specifically Dr. Angela Bardo and John Mendenhall for their help with confocal and SEM microscopy; Shawn Tucker and Cecil Harkey for their help in using the Biomek robots and real time PCR instruments.

My special thanks also go to my parents, Rey and Dia, and immediate family, whose never-ending prayers and encouragement have always reminded me that loved ones are the most important in life. Most of all, I would like to thank my husband and best friend, Seth, for his unconditional love, support, and patience through even the most difficult times of being a graduate student.

Microfabrication of Spatially-Patterned, Polymer Scaffolds for Applications in Stem Cell and Tissue Engineering

Publication No._____

Mary Gazell Mapili Call, Ph.D.

The University of Texas at Austin, 2007

Supervisor: Krishnendu Roy

Tissue engineering is a recently developed field that combines material science, cell biology, and engineering to create or improve functional tissues/organs. The field of tissue engineering has progressed from a fledgling science to an emerging technology, in large part due to parallel advances in the application of biomaterials and understanding stem cell behavior. Current studies have evaluated certain types of natural and synthetic biomaterials for feasibility of replicating the physio-chemical microenvironments of stem cells. Furthermore, technologies derived from micro-machining and solid free-form fabrication industries have utilized these biomaterials to create scaffolds that resemble tissue-like structures.

Recent scaffold fabrication methods have attempted to overcome certain challenges in engineering tissues and organs. One of the fundamental limitations in current tissue engineering efforts has been the inability to develop multiple tissue types (i.e. bone, cartilage, muscles, ligaments) within a single scaffold structure in a pre-designed manner. The differentiation of multiple cells within a three-dimensional (3D)

scaffold using a single stem cell population has yet to be developed due to challenges in integrating various biochemical factors in a spatially-patterned method.

This dissertation discusses scaffold micro-fabrication techniques that use layer-by-layer, ultraviolet-based (UV) stereolithography systems. These approaches in micro-fabricating scaffolds provide an optimal, biomimetic environment for the pre-patterned differentiation of mesenchymal stem cells into skeletal-type tissues. We demonstrated both laser-based and digital micromirror device-based stereolithography systems for creating intricate scaffold architectures with multiple bio-factors encapsulated in pre-determined regions. We showed that micro-stereolithography has the powerful capability of building 3D complex scaffolds with specific pore sizes and shapes in a layer-by-layer fashion using photo-crosslinkable monomers. These polymer-based scaffolds were functionalized with specific signaling proteins to create a biomimetic niche in which stem cells can respond, attach, and differentiate. The ultimate goal of this project is to integrate novel concepts of micro-manufacturing along with polymer-controlled release kinetics and stem cell biology to attain pre-designed architectures of tissue structures.

Table of Contents

List of Tables

List of Figures

CHAPTER ONE

Introduction: Specific Aims and Overview

1.1 INTRODUCTION

Over the past few decades, significant advances in the field of tissue engineering have established a substantial groundwork for future, novel therapies in repairing and reconstructing tissues of the body. Therapies and regenerative medicine in tissue engineering have vastly improved due to the tremendous need for organs and tissues. Increased interest in such studies is due to the lack of tissue and organ supplies needed for transplantations. From January 2005 to December 2005, approximately 90,000 people were on an organ transplant waiting list while only 27,527 people received them [1]. A current strategy to remedy this statistic has involved the development of tissue engineering constructs, or scaffolds, to serve as a synthetic niche for the organization of cells into a three-dimensional (3D) architecture and to provide the stimuli in directing cell proliferation and differentiation. A unique approach to this technique is undertaken in this dissertation, with the hopes that it could eventually be refined to allow for arbitrarily complex control over the differentiation of stem cells.

An approach for creating scaffolds capable of engineering functional tissues and organs must first overcome a few basic challenges. One such fundamental limitations in current scaffold-derived efforts has been the inability to develop multiple tissue types (i.e. bone, cartilage, muscles, ligaments) in a pre-designed manner, within a single scaffold structure [2, 3]. Adult progenitor and embryonic stem cells have been shown to differentiate into a variety of cell types; however, the simultaneous development of

hybrid tissue structures inside a single 3D environment which mimics the complex architecture of organs has yet to be reported.

Growth of multiple cells within a 3D tissue engineering scaffold using a single stem cell population have yet to be produced due to the difficulty in integrating multiple bio-factors in a spatially-patterned method. Current methods in fabricating scaffolds only allow the incorporation of bio-factors in a bulk manner, (i.e., the factors are randomly dispersed all through-out the matrix), creating a microenvironment suitable only for the differentiation of a single tissue lineage. Recent attempts in scaffolding techniques, such as solid free-form fabrication (SFF) [4] and constructing scaffolds with various bio-factors [6], still do not have a prescribed manner of being compartmentalized.. Two crucial aspects that must be incorporated into a scaffold design in order to achieve patterned microenvironments for the hybrid stem cell differentiation include: (a) creating localized concentrations of multiple growth factors (GFs) by controlled spatial-incorporation while preventing their diffusion to surrounding areas and (b) creating a temporal profile of GFs for their precise administration, similarly to the molecular signaling present in the physiological environment. The development of a model scaffolding system that incorporates these key features is the emphasis of this dissertation. One measure of success for this system will be the simultaneous differentiation of marrow-derived progenitor cells into bone and cartilage inside a single 3D scaffold environment.

Another challenge limiting the fabrication of such intricate tissue structures is our lack of understanding on how stem cells behave and differentiate under spatially distributed biochemical and physical microenvironments, similar to those encountered during organ development. This dissertation is only minimally focused on this issue;

however, the proposed scaffolding system offers a method by which this information could be applied, once discovered.

Therapies for orthopedic tissue engineering have dramatically increased within recent years and include the harvesting and transplanting of tissue-generating progenitor cells, systemic and local administration of growth factors or hormones, and biomimetic scaffolds that incorporate various physical and chemical properties [7]. One ultimate application of this project is to enable osteochondral replacements and the fabrication of specific craniofacial structures, (involving fibrous cartilage, alveolar bone, cementum, skeletal muscles, ligaments, etc.) within a single microfabricated scaffold. However, such a proposed method for engineering scaffolds could be applied to a variety of tissue regeneration applications. This research project will significantly advance current efforts in the development of complex tissues and organs. Additionally, our novel methods of fabricating intricate scaffold designs would create a new platform for developmental biology since cells are driven by specific bioactive chemicals and physical factors.

Research presented here will attempt to overcome the challenges already iterated with two distinct areas of investigation. One will be an analysis into the feasibility of ultraviolet-based (UV), layer-by-layer stereolithography (SL) processes that have the capability of creating precise, spatial distribution of bio-factors within 3D scaffolds. Once this technique is well understood, the other focus will be to investigate how physical structure and material of the scaffolds directly affect the differentiation of mesenchymal stem cells (MSCs) into multiple cell lineages. We hypothesize that micro-fabricated scaffolds through our UV-based SL techniques will ultimately provide an optimal, biomimetic environment for the pre-patterned differentiation of MSCs into the skeletal tissues. The long-term goal of this project is to integrate novel concepts of

micro-manufacturing along with polymer-controlled release and stem cell biology to attain pre-designed architectures of tissue structures.

1.2 SPECIFIC AIMS

In order to fulfill these objectives, the three specific aims for this project are as follows:

1.2.1 Aim 1: To employ a layer-by-layer SL photo-polymerization technique that would microfabricate 3D polymer scaffolds with (a) variable porosities and pre-determined architectures as well as with (b) the precise, spatial distribution of various bio-chemical cues and controlled-release microparticles.

We hypothesized that a layer-by-layer photo-polymerization process would enable versatile designs of scaffolds at the micron-level to fabricate complex features found in the physiological environment. The spatial distributions of biochemical and physical properties could be pre-designed within the architecture of the 3D scaffold due to the nature in which they are created. Two methods were developed to create these temporal spatially-patterned scaffolds: UV laser-based and digital micro-mirror device-based layer-by-layer SL systems. With these methods, three controllable biomimetic factors present themselves: macro-porosities within the scaffold material, polymeric microparticles encapsulated in the scaffold material, and functionalizing with extracellular matrix components.

1.2.2 Aim 2: To study whether the covalent functionalization of micro-fabricated scaffolds with specific extracellular matrix (ECM) components can (a) provide efficient stem cell seeding and (b) mesenchymal stem cell (MSC) differentiation into

either osteogenesis and chondrogenic pathway, and (c) create immobilized regions of growth factors in order to mimic the physiological environment.

We hypothesized that the functional modification of these scaffolds with conjugated fibronectin and the fibronectin-derived peptide, RGD, would allow for optimal cell seeding. Scaffolds were created with poly(ethylene glycol) diacrylate (PEGDA), a non-ionic and hydrophilic monomer characterized to limit cell and protein adsorption. Surfaces were therefore modified with either fibronectin or RGD to mediate cellular attachment. Additionally, the immobilization of heparin/heparan sulfate was completed by conjugating it to PEG-esters, thus preventing the diffusion of soluble growth factors and creating optimal local concentrations similar to *in vivo* cellular environments. Specifically basic fibroblast growth factor (FGF-2) was effectively sequestered and protected by heparin-modified materials.

1.2.3 Aim 3: To study the osteogenic growth and differentiation of MSCs within microfabricated polymer scaffolds that integrate varying physical and biochemical properties.

This aim was combined with the first two aims to ultimately create a micro-patterned, polymer-based scaffold with complex architectures and functionalized ECM. By creating physical and biochemical microenvironments within the 3D scaffold, MSC differentiation would be optimally directed to the formation of osteoblasts. Using PEGDA as the biomaterial, patterned scaffolds were created with various architectures, and changes in osteoblast gene expression levels were measured. Fibronectin was conjugated to the PEGDA scaffolds upon fabrication to allow MSCs to attach, proliferate, and then undergo osteoblast differentiation. Furthermore, we demonstrated that PEGDA crosslinking density alters osteoblast gene expression levels of differentiated MSCs.

1.3 OVERVIEW

The following *Chapter Two* discusses background and significance of this research study and highlights the most recent advances in the fabrication of tissue engineering scaffolds and how these cellular microenvironments effect stem cell growth and behavior. *Chapter Three* discusses a UV laser stereolithography system that can precisely pattern ligands, extracellular-matrix components, growth factors, and controlled release particles within a single scaffold. *Chapter Four* discusses another layer-by-layer SL system consisting of a UV light source, a digital micro-mirror masking device, and a conventional computer projector. This system allows fabrication of complex internal features coupled with precise spatial distribution of biological factors inside a scaffold. This chapter also demonstrates microfabricated scaffolds that allow for the osteogenic differentiation using marrow-derived progenitor cells. Both this system and the one introduced in *Chapter Three* can produce pre-designed, complex internal architectures and porosities in the micro- and macro-scale. *Chapter Five* discusses osteogenic differentiation of mesenchymal stem cells onto microfabricated polymer scaffolds. Analyses of extracellular matrix through histology and gene expression show successful differentiation of this progenitor cell population into osteoblasts. *Chapter Six* discusses preliminary studies with the simultaneous differentiation of MSCs into bone- and cartilage-like cells using multi-layered scaffolds. Finally *Chapter Seven* discusses the overall conclusions from this study and recommendations for future work.

1.4 REFERENCES

1. *Scientific Registry of Transplant Recipients. http://www.ustransplant.org.*
2. Griffith, L.G., *Emerging design principles in biomaterials and scaffolds for tissue engineering.* Ann N Y Acad Sci, 2002. **961**: p. 83-95.
3. Orban, J.M., K.G. Marra, and J.O. Hollinger, *Composition options for tissue-engineered bone.* Tissue Eng, 2002. **8**(4): p. 529-39.
4. Park, A., B. Wu, and L.G. Griffith, *Integration of surface modification and 3D fabrication techniques to prepare patterned poly(L-lactide) substrates allowing regionally selective cell adhesion.* J Biomater Sci Polym Ed, 1998. **9**(2): p. 89-110.
5. Park, H., et al., *Delivery of TGF-beta1 and chondrocytes via injectable, biodegradable hydrogels for cartilage tissue engineering applications.* Biomaterials, 2005. **26**(34): p. 7095-103.
6. Richardson, T.P., et al., *Polymeric system for dual growth factor delivery.* Nat Biotechnol, 2001. **19**(11): p. 1029-34.
7. Bolland, B.J., et al., *Adult mesenchymal stem cells and impaction grafting: a new clinical paradigm shift.* Expert Rev Med Devices, 2007. **4**(3): p. 393-404.

CHAPTER TWO

Background and Significance

2.1 CURRENT TRENDS IN TISSUE ENGINEERING

Although organ transplantations have steadily advanced over the past several decades, there still exists an immense shortage of organ donors. State of the art techniques in the field of tissue engineering have progressed from a fledgling science to an emerging technology, in large part due to parallel advances in modifying biomaterials and understanding stem cell behavior in the nano- and micro-scales. Therapies in modern medicine have included the prevention, control, or eradication of diseases and disorders, and more recently, the restoration and replacement of non-functional organs through tissue engineering methods are becoming a possibility [1]. Complete tissue and organ replacement using stem cells is still a milestone in which current studies are laying the necessary groundwork.

Current research studies have evaluated how certain types of materials have been used as substrates to mimic the physiochemical microenvironments of cells and tissues [2, 3]. Multiple, pre-differentiated stem cell populations combined with biomaterials have also been utilized to form hybrid constructs that closely mimic native tissue [4, 5]. Presently, there exist many studies in clinically and experimentally designing biodegradable and bioresorbable materials to regenerate skin, bone, and cartilage for orthopedic, dental, and craniofacial applications. Three general approaches have been used to devise systems for the regeneration of these tissues: (a) the use of scaffolding materials to draw specific cells into the defect site and provide a protective, regenerative environment, (b) the release of tissue inductive factors either directly integrated or

released from the matrix, and (c) the use of cell transplantation in which precursor cells are seeded into an appropriate environment and then moved to the defect site to form structurally and functionally integrated tissue.

2.2 STEM CELLS IN TISSUE ENGINEERING

Recent developments in tissue engineering have been driven by novel discoveries in stem cell expansion, differentiation, and methods of culture. Stem cells are simply defined as a progeny of cells that have the potential to differentiate into lineages of any phenotype. In literature, embryonic and adult stem cells are the two classifications and are distinguished by their differentiation potential. It is well-established that the fertilized egg is classified as the ultimate stem cell, with the defining characteristic of giving rise to a plethora of undifferentiated cell lineages. The term totipotent has been commonly used to classify stem cells that have the capability of differentiating into all tissues of the body. Embryonic stem cells are daughter cells that form from early divisions of a fertilized egg and retain their complete totipotent capability.

Tissue renewal in adults, however, involves adult stem cells that are less totipotent and are more committed than embryonic stem cells. Adult stem cells are referred to as progenitor, multipotent, or pluripotent cells since they have a more limited differentiation capacity and are found in several adult tissues, such as the bone marrow. Bone-marrow derived progenitor cells or mesenchymal stem cells (MSCs) have been regarded as an attractive cell population for the field of tissue engineering because of (a) their multipotent differentiation into end-state mesenchymal cell types and (b) their ease in harvest, isolation and expansion *in vitro*. Before surveying the vast range of methods and materials currently used to understand MSCs behavior, their isolation, characterization, and differentiation lineages should first be examined.

2.3 SOURCES, CHARACTERIZATION, AND DIFFERENTIATION LINEAGES OF MESENCHYMAL STEM CELLS

The primary source for isolating MSCs is in the bone marrow, but their existence in smaller populations have also been found in other tissues, such as in adipose tissue, muscle and peripheral blood [6-9]. Cells derived from the bone marrow are a heterogeneous population that includes both committed and progenitor cells [10]. Bone-marrow derived MSCs have a fibroblast-like morphology in culture and are adherent to tissue-culture treated surfaces. Since these progenitor cells coexist in the marrow with non-adherent hematopoietic cells, MSCs can be easily separated from this population by aspirating the floating cells 3-4 days after plating the marrow-derived cells in a treated plate. Another purification method involves fractionating aspirated bone marrow based on a density gradient solution, such as Percoll.

Because the marrow consists of a variety of subpopulations, an array of MSC-specific surface markers have been determined to further purify these progenitor cells. As examples, the STRO-1 antibody reacts with non-hematopoietic bone marrow stromal cells [11-13], and the SB-10 antibody reacts with an antigen (CD166) specific to undifferentiated MSC populations [14, 15]. Additionally, SH-2 binds to endoglin of transforming growth factor-β (TGF-β) [16], and SH-3/SH-4 antibodies recognize the CD73 antigen on undifferentiated cells [17]. These antibodies do not react with osteogenic, differentiated MSCs, and with hematopoietic cells. Hematopoietic cells can also be removed from MSC cultures by their negative selection using anti-CD1, anti-CD14, anti-CD31 markers [18].

MSCs differentiate into a variety of end-state cell types, such as adipose tissue, bone, cartilage, fibroblasts, muscle, ligament, and tendon , as depicted in **Figure 2.1** [19-24]. The adipocyte phenotypic pathway for MSCs and their presence in the marrow are

still not yet well-established. One theory suggests adipogenic MSCs act as space-regulatory cells to expand or contract based on the need for hematopoiesis. For instance, population of adipogenic cells within the marrow increases when hematopoiesis declines and vice versa. MSCs undergoing adipogenesis *in vitro* have a rounded morphology and increased lipid content.

Previous studies suggest that cell morphology and the amount of tension presented by the cytoskeleton can regulate MSC differentiation into either the adipogenic or osteogenic pathway based on RhoA activity, a small G-protein part of the Rho signaling family. In response to extracellular signals, RhoA controls cell morphology and structure through actin cytoskeleton reorganization. Various factors downstream of the RhoA signaling cascade act on cytoskeletal morphology to affect overall stress fiber formation. Because RhoA activity within osteogenic precursor cells increases, osteoblasts adopt a more flattened morphology than adipocytes [25]. In addition to the Rho intracellular signaling pathway, osteogenesis of human MSCs can be chemically induced both *in vitro* and *in vivo*, using the mitogen, basic fibroblast growth factor (FGF-2) [26]. Matrix mineralization and gene expression of bone-specific molecules, such as osteopontin, osteocalcin, and alkaline phosphatase, are generally used to classify *in vitro* osteogenesis for MSCs.

Chondrogenic pathway of MSCs is initiated *in vitro* only in the absence of serum in culture media and in a three-dimensional (3D) organization or pellet-form. Chemical induction into this cell lineage can be achieved using a member of the transforming growth factor-β (TGF-β) family [27]. TGF-β1, TGF-β2 and TGF-β3 expressions are continuously found during the chondrogenic differentiation of MSCs and may act simultaneously with other TGF-β members; however TGF-β3 and TGF-β4 may also aid in the process of de-differentiation, indicating capability of MSCs to also retain their

plasticity [28]. Biosynthesis of glycosaminoglycans and expression of cartilage-specific extracellular matrix (ECM) genes, such as aggrecan, collagen type-II, collagen type-X, and Sox9 have been used to mark MSCs differentiation into the chondrogenic pathway [29].

More recently, undifferentiated MSCs also been found to express markers for other cell types unrelated to connective tissues, such as neural cells, endothelial cells, and cardiomyocytes. In one study, human and mouse bone-marrow derived progenitor cells were induced to differentiate into neural cells in the presence of epidermal growth factor and brain-derived neurotrophic factor [30]. Bone-marrow derived progenitor cells have also been induced into the neural lineage *in vitro* through other chemical exposures such as, serum withdrawal following β-mercaptoethanol treatment [31] and the addition of isobutylmethylxanthine and dibutyryl cyclic AMP [32]. Additionally murine MSCs have been shown to transform into cardiomyocytes, endothelial cells, and smooth muscle cells by their direct injection into the heart [33, 34]. MSC transplantations have further shown improved cardiac function in a rat model through the initiation of angiogenesis and myogenesis [35]. Since MSCs are the most, well-characterized type of adult stem cells both in 2D and 3D cultures, biomaterials have been exclusively modified for this population to further establish complex intracellular signaling and differentiation pathways. Various methods of creating 3D environments have been utilized when studying MSCs behavior and should be discussed in further detail.

2.4 MICROFABRICATION OF TISSUE ENGINEERING SCAFFOLDS

Efforts in scaffold design must incorporate porous constructs that provide appropriate diffusion of biochemical cues and cellular waste as well as mechanical properties that mimic the target tissue that is being generated. Soft tissues have a

Young's moduli of 0.4-350 MPa, whereas hard tissues are in the range of 10-1,500 MPa [36]. These structures not only have to integrate the critical properties of permeability and strength, but also should be easily produced in complex 3D anatomical-like constructs. A vast array of scaffold manufacturing techniques over the past decade has enabled significant leaps in creating constructs in the micro- and nano-scales. These fabrications technologies are well-summarized in a review by Tsang and Bhatia, as shown in **Table 2.1 [37]**. Current, popular methods in scaffold fabrication have been adopted from the microelectronics manufacturing industry as well as phase separation chemistry.

Advances in coupling computational topography design and solid free-form fabrication (SFF) have recently made it possible to generate scaffolds with controlled architectures. **Figure 2.2** illustrates SFF techniques that generally use 2D planar slices of the target tissue/organ structure based on computer-aided design (CAD) and re-build a synthetic 3D construct on a platform through a layer-by-layer technique, without the use of sacrificial materials or molds. Each 2D planar slice or layer represents a cross-section of the model that is being regenerated. Commercially available systems are commonly grouped into three major categories: (1) laser-based machines that photo-polymerize liquid macromer solutions or sintered powder compounds, (2) printer-based machines that can print a binder to chemically combine powdered materials or direct construct materials, cells, and proteins and (3) nozzle-based systems that extrude materials, processing them either through chemical or thermal means [36].

Scaffold fabrication based on laser technology is considered to be the pioneer of rapid prototyping techniques and generally involves a laser beam directed over the top of a photocurable polymeric material. The light initiates a chain reaction in polymer crosslinking, causing material solidification only in the exposed areas by the laser beam.

The liquid polymer solution is contained in a vat, and a pre-designed 3D construct can be developed on a stage through a layer-by-layer, raster scanning style process. Laser technology can also provide heat energy to sinter particles together where the laser interaction increases the temperature to the transition temperature of the material. The exposed regions of particles, thereby, fuse together.

Another prevalent, scaffold fabrication method is based on inkjet printing technology and uses droplet formation to melt materials together. The deposited droplet is a thermoplastic material that hardens when it cools. The multiple jet heads, as found in a color printer, could contain various materials to create a construct with higher chemical complexity. The ModelMakerII™ uses a wax-like material in a jet head as the support substrate and the polymeric material to build the scaffold in another jet head. Additionally single cells or cell aggregates can be printed onto support substrates, as demonstrated by Boland et. al. [38]. Approaches in laser printing technology for cellular guidance have also been investigated by Ringeisen et. al. [39].

A nozzle-based system to extrude molten ceramics and polymeric substrates in a layer-by-layer fashion is another method of creating complex tissue engineering scaffolds, as demonstrated by Hutmacher et.al.[40]. This computer-guided and filament deposition modeling method was used to create bioresorbable poly(ε-caprolactone) with feature sizes ranging from 160-700μm. Limitation to this system is that the height of a scaffold layer is limited to the diameter of the nozzle and that the operating temperature to extrude these materials is too high to use proteins during the fabrication process.

Aside from SFF technology, other conventional means of creating scaffolds with micro-scale features include solvent casting and particulate leaching, gas foaming, and negative molding techniques [41]. Phase separation chemistries have also used to create bioactive polymeric constructs. Synthetic materials are dissolved in molten phenol or

naphthalene, liquid-liquid phase separation occurs due to a decrease in temperature, and a two-phased solid is produced. The solvent is removed through sublimation as shown by Lo et. al. to create a porous construct with integrating bioactive molecules [42]. Methods discussed in this section can use both natural and synthetic, as discussed in the following section.

2.5 SCAFFOLD BIOMATERIALS USED FOR STUDYING MSCS

Natural materials used for developing scaffolds can consist of components found in tissue, such as collagen, fibrinogen, and hyaluronan, and therefore have the advantage of being bioactive and biocompatible, as well as having the same mechanical properties of native tissue. Additionally some natural materials can be made into components that can be more easily processed through chemical modifications. For example, hyaluronan is present in tissue as a gel-like substance but can be chemically adjusted so that it can be processed as fibers, membranes, or microspheres, and is commercially known as Hyaff® [43]. Silk fibroin is also classified as a natural material and can be isolated from silkworm cocoons. Silk has been developed into porous scaffolds using gas foaming or salt leaching methods [44, 45] and widely used as suture materials for surgical methods.

Other natural materials used for studies in MSC differentiation include chitosan and coralline. Chitosan is hydrophilic in nature, biodegradable, biocompatible, and has similar properties to glycosaminoglycans, deeming it as an attractive material for tissue engineering studies. One particular study combined this chitosan with coralline, exoskeletons of marine species or coral, as a composite scaffold to study MSCs osteogenesis since coral is composed of calcium carbonate, a component found in bone [46]. Another material that has been used as a chitosan-composite for bone tissue engineering is hydroxyapatite, a natural, inorganic component of bone mineral [47].

Calcium phosphates, bioactive glasses, and other bioceramics are desirable materials for studies in MSCs osteogenesis since these materials have high mechanical properties and can integrate with bone to a higher degree than soft biomaterials, thereby enhancing mineralization and matrix formation. Disadvantages of using natural materials over synthetic materials include uncontrolled degradation rates, biocompatibility of degradation by-products, difficulty in sterilization and pathogen/viral issues when isolated from different sources.

Polyglycolides (PGA), polylactides, (PLA), polylactide-co-glycolide (PLGA) and their amorphous forms have been extensively used as synthetic polymers for evaluating cell behavior in 3D scaffolding environments [48, 49]. These materials are hydrolytically degradable through bulk erosion due to the presence of ester bonds, and the glycolic/lactic acid by-products can be physiologically removed via metabolic pathways. PLA/PGA molecular weight, copolymerization ratio, and their polydispersity can be adjusted to control the degradation rate, making them attractive synthetic materials for tissue engineering. Furthermore standard methods (e.g., salt leaching, sintering, porogen melting, nanofiber electrospinning) have been widely established for these materials to incorporate interconnective porosity within 3D scaffolds [49-51].

Non-woven fabrics developed from polyethylene terepthalate (PET) have also been used to study MSCs seeding, proliferation, and aggregation for tissue regeneration [52, 53]. Adipogenesis, chondrogenesis, and osteogenesis have all been successfully studied differentiation pathways on biodegradable, nanofibrous 3D scaffolds fabricated from poly(ε-caprolactone) (PCL) [54, 55]. Acrylated polymers that form hydrogels, such as poly(ethylene glycol) diacrylates (PEGDA) and poly(6-aminohexyl phosphate acryloyl) (PPE-HA-acryl), are widely studied for MSC cell and bio-chemical molecule encapsulation capabilities during photo-crosslinking [29, 54, 56, 57]. Though synthetic

materials provide the versatility of creating structures with tunable features (i.e., mechanical properties, degradation rates, and porosities), disadvantages for choosing such materials include poor compatibility and acidic by-products.

2.6 MODIFICATIONS TO SCAFFOLD BIOMATERIALS TO MIMIC CELLULAR NICHE

Chemical modifications to biomaterials can directly govern the intracellular signaling pathway in which MSCs can undergo due to the transformation of mechanical integrity, signals presented by the microenvironment, degradation rate, and overall porosity. Because biomaterials can be designed to fine-tune their degradation kinetics and/or the release of biological molecules in response to their microenvironment, they have also been termed as intelligent or bioresponsive materials. Furthermore, the intrinsic mechanical integrity of a material is a significant feature since the manner of forces exert by cells are dependent on their type. For instance, chondrocytes exert contractile forces when integrated onto substrates and can change the overall microstructure of the scaffold during tissue development depending on the mechanical properties of the material [58, 59]. Therefore it is essential to distinguish the types of soft and hard materials that have been used for studying the differentiation lineages of MSCs.

Overall mechanical integrity of scaffolding materials is a key element that needs to be addressed when evaluating material properties that effect differentiation pathways of stem cells. Bone marrow-derived stromal cells are highly sensitive and responsive to mechanical stimulation *in vitro* [60, 61]. It can be speculated that mechanical stimuli activate cell surface receptors and focal adhesion sites, which in turn triggers intracellular signaling cascades that involve switching on genes that activate for ECM secretion. Differentiation of MSCs by the physical microenvironment is administered either by mechanical cyclical stresses applied directly to the cells [60-62] or by the compositional

properties inherent to the material itself (i.e. material integrity, crystallinity, crosslinking density, overall structural micro- and macro-porosity).

Soft substrates or gel-like materials, such as hydrogels and collagen, closely resemble the consistency of soft, native tissues, making them attractive materials for use as scaffolds. Additionally collagen is the most abundant protein found in the ECM of bone formation, and can therefore be regarded as the "gold standard" of scaffolding materials for tissue regeneration; however these materials are not suitable for studying cell lineages and tissues that undergo high cyclical stress *in vivo*. When differentiating MSCs into the connective tissue lineages (i.e. bone, cartilage, ligaments, tendons) materials with high mechanical strength must be chosen to closely mimic the types of stresses these native tissues must physiologically undergo.

Collagen and other gel-like materials, however, can be modified to have an increased modulus of elasticity, making them more suitable for applications in connective tissue engineering. Collagen can be adjusted to have a higher modulus by adding hydroxyapatite, a brittle, yet stronger material than collagen, thereby mimicking the structure of bone which is mostly composed of collagen fibers and phosphate minerals. Adding hydroxyapatite to collagen at a 1:1 ratio alone increases the modulus from 0.392 MPa to 0.422 MPa, which is more similar to trabecular bone (E = 0.443 MPa) [63]. These porous collagen-hydroxyapatite composites, prepared through phase-separation techniques, have been used to study rat MSCs seeding and proliferation [63].

Other composite scaffolds can be formulated using both natural and synthetic materials, and at the same time reinforce the mechanical integrity of the entire structure. Studies have also fabricated composites with collagen to contain poly-lactic-acid and chitin fibers, further reinforcing the mechanical integrity. Chitin fibers were crosslinked within PLA materials through dicyclohexylcarbodimide chemistries to strengthen

scaffolds even further, which resulted in higher human MSC attachment due to the neutralization of acidic by-products (due to PLA) with alkaline chitin [64].

Silk-based materials have also been commonly used for MSC scaffolding materials [65-67] since they provide increased modulus of elasticity over other natural materials, such as collagen. However decontamination and purification methods of silk, prior to their use *in vivo*, are extremely critical in order to avoid inflammatory and immunogenic reactions that are associated with this material in its natural form. Silk-based scaffolds seeded with hMSCs were positively evaluated for advanced bone formation in critical-sized, cranial defect models (larger than 4mm) using nude mice, indicated by the presence of bone sialoprotein, osteopontin, and osteocalcin [65]. In addition, positive results in gene expression and immunohistochemical staining for cartilage formation were seen when differentiating MSCs into the chondrogenic pathway [45].

In addition to natural materials, synthetic materials can also be chemically modified to increase mechanical strength. Increasing acrylate concentration in photo-crosslinkable polymers has been shown to increase the modulus of elasticity, such as within PPE-HA-acryl (poly(6-aminohexyl phosphate acryloyl)) hydrogels [57]. By increasing the amount of acrylated-PEG that was reacted with PPE-HA by four times, the shear modulus was increased almost 10-fold (3 to 26 kPa). Additionally this particular biodegradable phosphate-based synthetic material is highly favorable for bone tissue engineering due to a phosphate degradation product, which could aid in the overall scaffold mineralization when encapsulating MSCs and placed in osteogenic medium [57].

MSC differentiation induced by mechanical stimulation has also been extensively investigated using bioreactors [68-70], or *in vitro* systems that provide dynamic culturing conditions. Cells *in vivo* consistently undergo fluid shear stress and mechanical strain,

thereby influencing cellular interactions and responses. A copious amount of interest in mimicking these forces *in vitro*, specifically for connective tissue differentiation of MSCs, has resulted from our increased understanding of how cells behave physiologically.

In a study performed by Datta and colleagues [71], titanium fiber meshes seeded with rat MSCs were cultured in a perfusion bioreactor to study effects on osteoblast differentiation. Levels of mineralization formed by osteoblasts within the scaffolds were compared between plain titanium meshes and pre-generated, bone ECM-deposited titanium meshes. Results concluded that synergistic effects of both mechanical stimulation through shear stress and the presence of ECM deposition onto scaffolding substrates profoundly enhanced the osteoblast differentiation as indicated by increased calcium content.

Stem cell differentiation can be indirectly mediated by transforming the intrinsic mechanical properties of materials or directly mediated by chemically altering the bio-chemicals present in their microenvironment. Many studies have determined certain hormones and cytokines that can enhance proliferation and the differentiation potential of MSCs. Several families of growth factors are marked as critical bioactive molecules that guide MSCs differentiation into specific cell lineages. FGF-2 is shown to increase the self-renewal and the maintenance of MSCs multi-lineage differentiation potential [26, 72-74]. Additionally bone morphogenetic proteins (BMPs) are part of the TGF-β superfamily that have significant roles in the regeneration and growth of skeletal tissues [75, 76]. At least 20 human BMPs have been identified and are known to be involved in skeletal formation.

Scaffolds have directly integrated these growth factors, hormones, and chemicals in a variety of ways, other than exogenous delivery within culture media. Soluble growth

factors can be directly encapsulated or incorporated during the scaffold fabrication process [77, 78], but would also require a method to sequester these bio-factors in a localized microenvironment to prevent their diffusion into other regions of the scaffolds and within the media. Heparan sulfates, a type of glycosaminoglycans, have been known to bind and protect growth factors, especially FGF-2, from pH and heat denaturation within the body. In our studies, we have successfully demonstrated the effective binding of FGF-2 within photo-polymerizable PEGDA scaffolds by covalently conjugating acrylated-PEG moieties to heparan sulfate [79]. Using immuno-histochemistry we effectively demonstrated that FGF-2 was only localized or sequestered in a region of a multi-layered scaffold that had heparin-PEG-acrylate.

Physical adsorption of biomolecules onto substrate surfaces is shown to be an effective technique of delivery. In situ osteogenesis was demonstrated by Carstens et al, using absorbable collagen sponges as delivery vehicles for recombinant human BMP-2 (rhBMP-2) within a craniofacial mandibular defect to induce MSCs into the osteogenic pathway [80]. Instead of using natural materials found in bone tissues, such as hydroxyapatite, which would require longer times for bone reformation alone, an absorbable collagen sponge with rhBMP-2 adsorbed onto the surfaces was implanted into a mandibular defect of an adolescent Yorkshire pig. Because of the chemotactic effects presented by the rhBMP-2, MSCs were found to be in the vicinity of the implanted collagen sponges and were characterized to be spindle-shaped and in osteoblast precursor form. BMPs are osteogenic-specific proteins and are characterized to initiate bone formation by homing and binding to MSCs. Another adsorption study uses titanium fiber mesh scaffold coated with a short, amino acid sequence, RGD (arginin-glycine-aspartic acid) [81], which is found in numerous cell adhesive proteins, such as fibronectin and laminin and takes part in cell integrin binding. MSCs attached more strongly to RGD-

coated titanium scaffolds, but did not however change ECM secretion of the differentiating cells into the osteoblast lineage.

Although protein adsorption to scaffold surfaces can be an effective route for biochemical presentation [82, 83], covalently conjugating proteins to surfaces could provide a more dependable method since conjugation density can be controlled. By incorporating methacrylic acid within PEGDA macromer solution prior to photo-polymerizing into 3D scaffolds, we have shown that carbodiimide bioconjugation chemistries successfully activate free carboxyl groups (from methacrylic acid), which in turn forms amide bonds with fibronectin, a glycoprotein dimer found in the ECM mediating for cell attachment [84]. Murine MSCs were then seeded onto the microfabricated scaffolds created by layer-by-layer stereolithography system, and cells effectively adhered and transformed into osteoblasts. These results are discussed in further detail in *Chapter Five*.

Furthermore RGD can be covalently conjugated to PEG-acrylates using N-hydroxysuccinimidyl-activated esters [85-88] and have also been used in PEGDA scaffolds for human MSCs differentiation into osteoblasts [89]. Cell integrin-matrix interactions were enhanced by incorporating RGD within the hydrogel scaffolds, leading to increased MSCs viability. Nuttelman and colleagues show increased viability of encapsulated human MSCs from 15% to 75% when incorporating RGD-PEG-acrylates to PEGDA hydrogels [89]. RGD acts as a signaling peptide that triggers conformational change to cell inetgrins, thus leading to an intracellular signaling pathway that prevents programmed cell death or apoptosis.

Additionally, Shin et al, shows that increasing concentrations of signaling peptide within oligo(PEG-fumarate) hydrogels increases alkaline phosphatase activity of osteoblasts when compared of hydrogels that do not contain the peptide [90]. This group

also compared effects between RGD and an osteopontin-derived peptide, and determined that hydrogels modified with osteopontin-derived peptide triggered greater osteoblast migration distance than RGD-modified hydrogels; however RGD was still found to be the dominating peptide for mediating cell-attachment [91].

Scaffolds also operate as effective delivery vehicles using degradable components for signaling biomolecules that direct MSC growth and organization, in addition to covalently conjugating and adsorbing proteins onto scaffold surfaces and throughout the matrix. The covalent conjugation and controlled-release of dexamethasone, a synthetic corticosteroid crucial for MSCs osteogenesis *in vitro*, within a scaffold polymer network is directly mediated by a hydrolytically-labile lactide component, a study performed by Nuttelman et al, [92]. Humans MSCs were encapsulated in a PEG-based hydrogel network with the controlled release of dexamethasone, which then lead to the osteogenic differentiation of entrapped progenitor cells. The polymer network used to fabricate the scaffold was composed of photo-polymerizable PEGDA and a biocompatible ultra-violet cleavable photoinitiator that initiated polymer crosslinking. The gene expression levels for two common osteogenic markers, alkaline phosphatase and core binding factor alpha 1 (cbfα−1), were increased for MSCs cultured in scaffolds containing the released dexamethasone. The concentration of the biomolecules to be delivered can be easily controlled by the amount loaded into the polymer network prior to photo-crosslinking. Furthermore the length of degradable lactide linkages attaching the biomolecules to be delivered can be chemically to control release kinetics.

Delivery of growth factors and chemicals can also be mediated using degradable particles, which could provide temporal release kinetics for signaling biomolecules over a prolonged period of time [93-96]. Osteogenic studies from rat MSCs using recombinant human TGF-β1 was encapsulated in polymer blends of PEG-PLGA particles (sized at an

average of 158 μm) by Peter et al, [97]. Here they show that a loading of 6.0ng TGF-β1/ 1mg of microparticle provided an optimal dose for growth factor delivery for enhancing MSC proliferation and transformation into osteoblasts, as demonstrated by increased alkaline phosphatase and osteocalcin secretion.

Scaffold mineralization due to MSCs osteogenesis can be mediated through other chemical modifications, such as adding a degradable unit to the monomer backbone, making it into bio-responsive vehicle. Adding a phosphoester to photo-polymerizable PEG-based hydrogels has not only been shown to act as the degradation component of the scaffold, but has also shown to promote the mineralization of encapsulated MCSs. The use of phosphoester-containing hydrogels marked increased levels of alkaline phosphatase and osteocalcin, as demonstrated by Wang and colleagues [98, 99]. Cell-matrix interactions and the viability of encapsulated MSCs increase in the presence of phosphate molecules within hydrogel scaffolds, as shown by Nuttelman [89]. Phosphate moieties contribute to the adsorption of osteopontin, a sialoprotein that binds to bone mineralization and mediates cell adhesion.

Components of bone mineralization have also been integrated within scaffolds for bone tissue engineering. A thin bone-like mineral layer, which consists of calcium phosphate components, influences osteogenic cell maturation when used within orthopedic and dental implantations. Osteoconductivity *in vivo* is greatly improved by utilizing substrates that contain calcium phosphate mineral, which have been used to bond orthopedic implants to native bone tissue and is mediated by fibroblasts in the marrow [100, 101]. This mineral substrate also enhances proliferation and gene expression of osteoblasts and osteogenic precursor cells [102, 103]. Murphy et al, exploited these concepts by using bone-like mineral films to analyze MSCs proliferation and differentiation *in vitro* [104]. Polymer sheets fabricated from PLGA were

mineralized by submersing in a solution that simulated body fluid, and soaked in fibronectin solution prior to human MSCs seeding. Though the mineralized PLGA sheets did promote MSCs proliferation, interestingly enough, osteogenic differentiation was inhibited. They speculate that osteogenic inhibition could be directly due to the material properties, such as low crystallinity, decreased crystal size, increased surface roughness, and rapid mineralization layer dissolution rate [105-108].

In addition to synthetic polymers, metals, and ceramics, natural materials can be chemically altered to improve specific properties for tissue engineering properties, such as their gelation state, degradation rate, and mechanical properties. Proteins, such as fibrinogen, can be linked with PEG polymers to enhance viability of entrapped MSCs by mimicking the hydrophilic nature of native tissues. Zhang and colleagues have created PEGylated fibrin patches to study the *in vitro* differentiation of MSCs into the endothelial cell lineage for a potential therapeutic tool in myocardial repair [109]. Chitosan is an example of a natural, biocompatible material that has been modified to be thermo-responsive [110, 111]. For instance, by conjugating hydroxybutyl groups onto the amino and hydroxyl reactive sites of chitosan, this polymer becomes water soluble and is capable of turning into a gel state when exposed to 37°C [112]. *In vitro* culture and encapsulation of human MSCs were used to study this modification of chitosan as an injectable material for the eventual use as a therapeutic agent in degenerative disk diseases. MSCs were effectively encapsulated within the chemically-modified chitosan gels of up to 5% wt polymer concentration, with minimal cell toxicity, and positive gene expression for the bone-specific markers, collagen I and aggrecan, was found [112]. Furthermore, oligo(PEG-fumarate) has been studied as a thermo-responsive hydrogel to encapsulate rat MSCs by the addition of a thermally reactive radical initiator that allows for the gelation of the monomer at 37°C [113]. These thermally-crosslinked hydrogels

show matrix calcification due transformation into osteoblasts and can be used as injectable cell delivery vehicles for bone regeneration studies.

2.7 MECHANISM OF *IN VIVO* AND *IN VITRO* BONE FORMATION

Bone is composed of four distinct cell types: osteoblasts, osteoclasts, bone lining cells, and osteocytes. Osteoprogenitor cells produce osteoblasts, osteocytes, and bone lining cells, whereas osteoclasts originate from various hemopoietic tissues. The morphology of osteoblasts, as described today, has not changed from when it was first characterized via microscopy in the late 19^{th}-century: flat, elongated, and polygonal. Sources of precursor osteoblasts are not only from undifferentiated mesenchymal progenitor cells, but also from differentiated chondrocytes. Osteoblasts are responsible for the production of bone matrix and classified to be fully differentiated cells. Osteocytes are mature osteoblasts found within the bone matrix and serve as "maintenance" cells. Bone lining cells are inactive cells found on the surfaces of bone that potentially serve as precursors for osteoblasts. Bone-resorbing cells are known as osteoclasts, which are characterized to be large, multi-nucleated, and are seen on bone surfaces when active.

The process of osteogenesis is an intricate, multi-step process and can be divided into three main categories: (1) progenitor or precursor cell proliferation and active osteoblasts differentiation, (2) bone matrix production, such as collagenous and non-collagenous bone proteins, and (3) bone matrix calcification, in which concentrations and deposition of calcium and phosphate are highly regulated at the site of calcification. Osteoblasts change into osteocytes as soon as the bone forming cell is surrounded by mineralized matrix. Intermediate stage is osteocytic osteoblast or osteoid-osteocyte.

Osteocytes appear to be more elongated and 30% less in size when compared to osteoblasts.

Bone matrix deposited by osteoblasts consists of multiple forms and can be divided into three main categories:

(1) compact bone: a dense, well-vascularized and mineralized tissue encompassing the cortex of the long bones, and connected to muscles to overcome the mechanical forces created during motility,

(2) trabecular bone: most commonly makes up the vertebral structure of humans and are characterized to be thin, flattened elements of well-mineralized bone. This forms during endochondral ossification along lines of stress, and continue to functions as such throughout adulthood, and

(3) chondroid bone: this tissue is characterized to have large cells, decreased cellular processes and function, a high collagen content, and increased amounts of proteoglycans than 'mature bone'.

Collagen I is the most abundant protein in bone matrix serving as 90% of the total ECM, whereas collagen V, the second class of collagen found in bone matrix, only makes up 3%. This protein also acts as a scaffolding material that binds and arranges other proteins that nucleate hydroxyapatite deposition. Collagen is present in the ECM associated with numerous, other proteins, serving as a scaffold upon which nucleators are oriented.

While collagen makes up most of the organic bone matrix, other non-collagenous glycoproteins also populate the bone ECM. Osteonectin is another prominent bone matrix protein known to bind to calcium, collagen, hydroxyapatite, as well nucleating hydroxyapatite deposition. Functionally this protein regulates cell progression through proliferation, shape, binding to growth factors and metal ions, and regulating enzymatic

activities. Fibronectin is also synthesized by bone, as well as other connective tissues, and initially seen during the first stages of osteogenesis. Sialoproteins found in bone matrix are composed of sialic acid, and the two best characterized are osteopontin and bone sialoprotein. Osteopontin is usually found during the later stages of osteoblast maturation, binds to calcium, and mediates cellular attachment *in vitro*. Bone sialoprotein is highly associated with mineralization, and is also a marker during the late stages of bone formation. Similarly to osteopontin, this molecule has a high affinity for calcium and can also mediate cell attachment. These are just some of the many constituents found in bone physiology, while other proteoglycans and glycoproteins are listed in **Table 2.2**.

Alkaline phosphatase activity during bone formation is abundant along the cell membrane and is characterized to hydrolyze many substrates with the release of a monophosphate from ATPase (adenosine triphosphate). Since alkaline phosphatases are concentrated within the cell surfaces, high binding affinities to positively charged calcium molecules occur, thus mediating calcium transport from blood vessels found in bone tissue. Younger osteoblasts tend to express increased alkaline phosphatase activity whereas mature osteocytes, found buried within the trabeculae, do not show evidence of cell membrane alkaline phosphatase.

It has been widely shown that introducing organic phosphate to *in vitro* culture medium stimulates matrix calcification. β-glycerophosphate, a non-physiological factor, is introduced solely for the *in vitro* mineralization of cell cultures. The rationale for using β-glycerophosphate is that this molecule acts as an organic phosphate around cells with a high alkaline phophatase activity, and therefore calcification of the matrix is triggered. Increased concentrations of β-glycerophosphate, however, have been shown to cause precipitation of calcium phosphate in the medium and to be inhibitory for cell growth.

Dexamethasone is another supplemented compound in osteogenic growth medium. In *in vitro* culture, this glucocorticoid increases vitamin D receptors and cell proliferation, and has been shown to inhibit bone resorption by indirectly inducing apoptosis of osteoclasts, the bone-resorbing cells. Lastly vitamin C, or ascorbic acid, is involved in collagen production, necessary to forming bone matrix, and is therefore another imperative supplement in osteogenic medium.

By combining knowledge gained from scaffold fabrication methods, material science, and stem cell biology surveyed from literature, this dissertation discusses attempts in creating a an ideal microenvironment for studying hybrid MSC differentiation. The ultimate goal of this research is to couple novel concepts of micro-manufacturing along with the ECM functionalization of polymers and stem cell biology to attain pre-designed architectures of tissue structures.

Table 2.1 Comparison of 3D Scaffolding Methods

	Resolution (μm)	Advantages	Disadvantages
Acellular 3-D Scaffolds			
		use of well-established fabrication methods, usually automated	must seed cells post-processing, less control in cell placement and distribution
Fabrication using Heat			
Micro Molding [6,7]	20–30	simple; reusable molds	limited to thin membranes, each layer must be contiguous structure, manual alignment required
Selective Laser Sintering [4,5,9]	400	high porosity, automated	high temperatures during process, powder may be trapped
Fused Deposition Modeling [3,4,10]	250–700	no trapped particles or solvents, automated	high temperatures during processing
3-D Plotting [11]	1000	use of hydrogel materials (agar, gelatin), automated	limited resolution
Fabrication using Light			
Stereolithography [5,12]	70–250	ease of use, easy to achieve small features, automated	limited choice of materials must be photosensitive and biocompatible; exposure of material to laser
Fabrication using Chemicals			
3-D Printing [14–16]	200–500	versatile; high porosity, automated	limited choice of materials (e.g. organic solvents as binders); difficult to reduce resolution below polymer particle size
Pressure Assisted Microsyringe [7]	10	high resolution, not subject to heat, automated	viscosity dependent, no inclusion of particles
Fabrication by Molding			
Matrix Molding [21]	200	use of biological matrix materials (collagen), mold fabrication can use automated methods (above)	features must be interconnected, weaker mechanical properties
Cell-Laden 3-D Scaffolds			
		precise placement of cells throughout construct, ability to place multiple cell types arbitrarily	limited fabrication conditions (sterility, temperature, pH), still in earlier phases of development
Cellular Assembly			
Organ Printing [24–26]	100	incorporation of cell aggregates or tissue explants, precise cell placement, automated	lack of structural support, dependence on self assembly
Laser-Guided Deposition [27]	< 1	precise single cell placement, automated	has yet to be extended to 3-D structures, lack of structural support
Cell/Biopolymer Hybrids			
Hydrogel Photopatterning [50]	100	incorporation of living cells within scaffold, leverages existing hydrogel chemistry (incorporation of peptides, degradation domains), versatile	not yet automated, exposure of cells to ultraviolet light, diffusion of large molecules limited by hydrogel pore size

****Table by Tsang and Bhatia [37]*

Table 2.2. Main Proteins found in Bone Matrix and their Functional Role [114]

Protein	Function
collagen Type I	Serves as scaffolding, binds to other proteins, orients other proteins to serve as nucleator
collagen Type X	Present in hypertrophic cartilage but does not regulate matrix mineralization
collagen Type III, V	Present in trace amounts, regulates collagen fibril diameter, may explain large diameter size of bone collagen fibrils
alkaline phosphatase	Potential Ca^{2++} carrier, hydrolyzes inhibitors of mineral deposition such as pyrophosphates
osteonectin	May mediate deposition of hydroxyapatite, binds to growth factors, may influence cell cycle
fibronectin	Cell attachment, binds to heparin, platelets, types I and V collagens, thrombin, fibrinogen, laminin, plasminogen, and plasminogen activator inhibitor, histidine rich glycoprotein
osteopontin	Binds to cells, may regulate mineralization, may regulate proliferation, inhibits nitric oxide synthase, may regulate resistance to viral infection
bone sialoprotein	Binds to cells, may initiate mineralization
osteocalcin	May regulate activity of osteoclasts and their precursors, may mark the turning point between bone formation and resorption
albumin	Inhibits hydroxyapatite crystal growth

Figure 2.1 Differentiation Capacity of Mesenchymal Stem Cells (MSCs). MSCs are characterized to proliferate and differentiate into multiple tissue types [115].

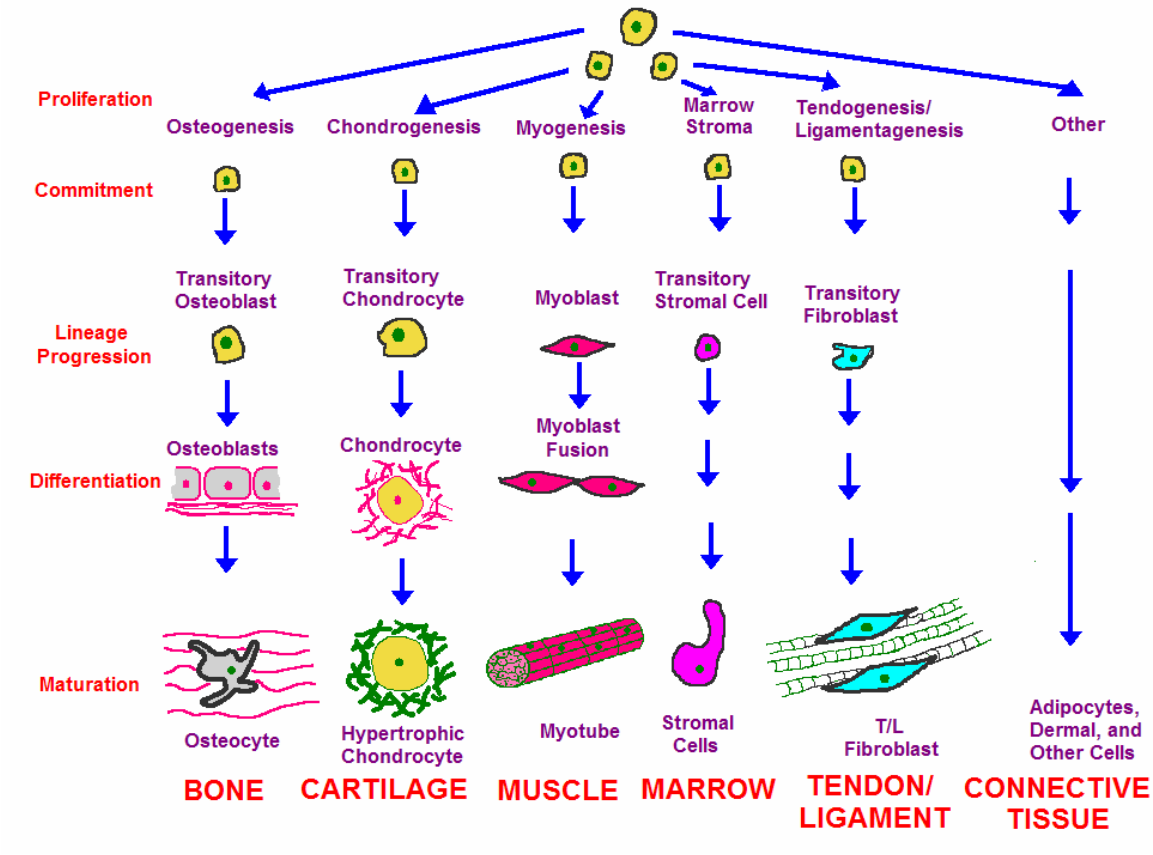

Figure 2.2 Summary of Solid Free Form Fabrications Systems. SFF systems are categorized by processing methods: (a) and (b) are laser stereolithography systems that photo-polymerize a liquid resin; (c) and (d) are printing-based systems; (e) and (f) are nozzle-based methods that extrude heated materials or printed materials that can be thermally or chemically altered [36].

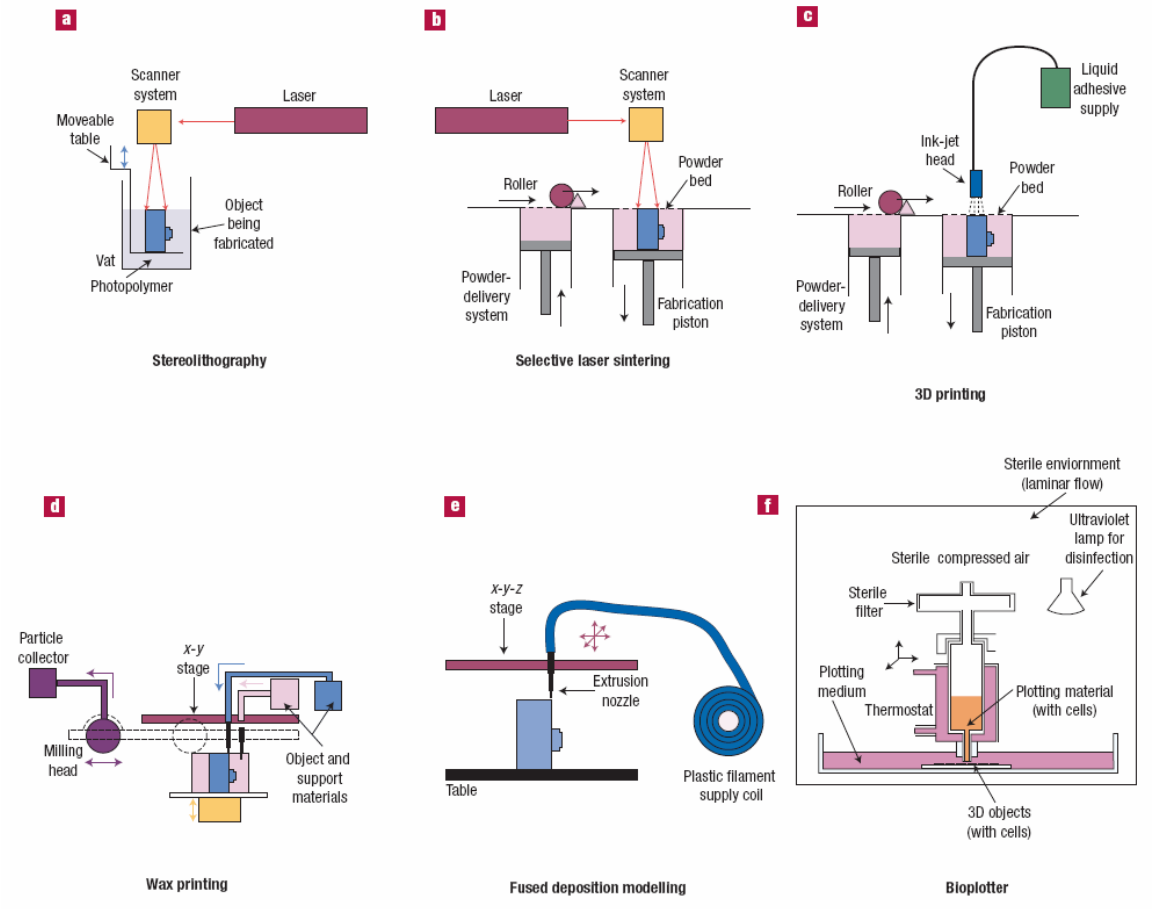

2.8 REFERENCES

1. Vacanti, J.P. and R. Langer, *Tissue engineering: the design and fabrication of living replacement devices for surgical reconstruction and transplantation.* Lancet, 1999. **354 Suppl 1**: p. SI32-4.
2. Yarlagadda, P.K., M. Chandrasekharan, and J.Y. Shyan, *Recent advances and current developments in tissue scaffolding.* Biomed Mater Eng, 2005. **15**(3): p. 159-77.
3. Ahsan, T. and R.M. Nerem, *Bioengineered tissues: the science, the technology, and the industry.* Orthod Craniofac Res, 2005. **8**(3): p. 134-40.
4. Rahaman, M.N. and J.J. Mao, *Stem cell-based composite tissue constructs for regenerative medicine.* Biotechnol Bioeng, 2005. **91**(3): p. 261-84.
5. Elisseeff, J., et al., *Advances in skeletal tissue engineering with hydrogels.* Orthod Craniofac Res, 2005. **8**(3): p. 150-61.
6. Williams, J.T., et al., *Cells isolated from adult human skeletal muscle capable of differentiating into multiple mesodermal phenotypes.* Am Surg, 1999. **65**(1): p. 22-6.
7. Romanov, Y.A., et al., *Mesenchymal stem cells from human bone marrow and adipose tissue: isolation, characterization, and differentiation potentialities.* Bull Exp Biol Med, 2005. **140**(1): p. 138-43.
8. Musina, R.A., E.S. Bekchanova, and G.T. Sukhikh, *Comparison of mesenchymal stem cells obtained from different human tissues.* Bull Exp Biol Med, 2005. **139**(4): p. 504-9.
9. Kuznetsov, S.A., et al., *Circulating skeletal stem cells.* J Cell Biol, 2001. **153**(5): p. 1133-40.

10. Caplan, A.I. and S.P. Bruder, *Mesenchymal stem cells: building blocks for molecular medicine in the 21st century.* Trends Mol Med, 2001. **7**(6): p. 259-64.

11. Simmons, P.J., et al., *Isolation, characterization and functional activity of human marrow stromal progenitors in hemopoiesis.* Prog Clin Biol Res, 1994. **389**: p. 271-80.

12. Simmons, P.J. and B. Torok-Storb, *Identification of stromal cell precursors in human bone marrow by a novel monoclonal antibody, STRO-1.* Blood, 1991. **78**(1): p. 55-62.

13. Walsh, S., et al., *Expression of the developmental markers STRO-1 and alkaline phosphatase in cultures of human marrow stromal cells: regulation by fibroblast growth factor (FGF)-2 and relationship to the expression of FGF receptors 1-4.* Bone, 2000. **27**(2): p. 185-95.

14. Bruder, S.P., et al., *Monoclonal antibodies reactive with human osteogenic cell surface antigens.* Bone, 1997. **21**(3): p. 225-35.

15. Bruder, S.P., et al., *Mesenchymal stem cell surface antigen SB-10 corresponds to activated leukocyte cell adhesion molecule and is involved in osteogenic differentiation.* J Bone Miner Res, 1998. **13**(4): p. 655-63.

16. Barry, F.P., et al., *The monoclonal antibody SH-2, raised against human mesenchymal stem cells, recognizes an epitope on endoglin (CD105).* Biochem Biophys Res Commun, 1999. **265**(1): p. 134-9.

17. Barry, F., et al., *The SH-3 and SH-4 antibodies recognize distinct epitopes on CD73 from human mesenchymal stem cells.* Biochem Biophys Res Commun, 2001. **289**(2): p. 519-24.

18. Rickard, D.J., et al., *Isolation and characterization of osteoblast precursor cells from human bone marrow.* J Bone Miner Res, 1996. **11**(3): p. 312-24.

19. Jaiswal, R.K., et al., *Adult human mesenchymal stem cell differentiation to the osteogenic or adipogenic lineage is regulated by mitogen-activated protein kinase.* J Biol Chem, 2000. **275**(13): p. 9645-52.

20. Pittenger, M.F., et al., *Multilineage potential of adult human mesenchymal stem cells.* Science, 1999. **284**(5411): p. 143-7.

21. Pittenger, M.F., J.D. Mosca, and K.R. McIntosh, *Human mesenchymal stem cells: progenitor cells for cartilage, bone, fat and stroma.* Curr Top Microbiol Immunol, 2000. **251**: p. 3-11.

22. Johnstone, B., et al., *In vitro chondrogenesis of bone marrow-derived mesenchymal progenitor cells.* Exp Cell Res, 1998. **238**(1): p. 265-72.

23. Wakitani, S., T. Saito, and A.I. Caplan, *Myogenic cells derived from rat bone marrow mesenchymal stem cells exposed to 5-azacytidine.* Muscle Nerve, 1995. **18**(12): p. 1417-26.

24. Noth, U., et al., *Anterior cruciate ligament constructs fabricated from human mesenchymal stem cells in a collagen type I hydrogel.* Cytotherapy, 2005. **7**(5): p. 447-55.

25. McBeath, R., et al., *Cell shape, cytoskeletal tension, and RhoA regulate stem cell lineage commitment.* Dev Cell, 2004. **6**(4): p. 483-95.

26. Martin, I., et al., *Fibroblast growth factor-2 supports ex vivo expansion and maintenance of osteogenic precursors from human bone marrow.* Endocrinology, 1997. **138**(10): p. 4456-62.

27. Worster, A.A., et al., *Chondrocytic differentiation of mesenchymal stem cells sequentially exposed to transforming growth factor-beta1 in monolayer and insulin-like growth factor-I in a three-dimensional matrix.* J Orthop Res, 2001. **19**(4): p. 738-49.

28. Goessler, U.R., et al., *In-vitro analysis of the expression of TGFbeta -superfamily-members during chondrogenic differentiation of mesenchymal stem cells and chondrocytes during dedifferentiation in cell culture.* Cell Mol Biol Lett, 2005. **10**(2): p. 345-62.

29. Williams, C.G., et al., *In vitro chondrogenesis of bone marrow-derived mesenchymal stem cells in a photopolymerizing hydrogel.* Tissue Eng, 2003. **9**(4): p. 679-88.

30. Sanchez-Ramos, J., et al., *Adult bone marrow stromal cells differentiate into neural cells in vitro.* Exp Neurol, 2000. **164**(2): p. 247-56.

31. Woodbury, D., et al., *Adult rat and human bone marrow stromal cells differentiate into neurons.* J Neurosci Res, 2000. **61**(4): p. 364-70.

32. Deng, W., et al., *In vitro differentiation of human marrow stromal cells into early progenitors of neural cells by conditions that increase intracellular cyclic AMP.* Biochem Biophys Res Commun, 2001. **282**(1): p. 148-52.

33. Gojo, S., et al., *In vivo cardiovasculogenesis by direct injection of isolated adult mesenchymal stem cells.* Exp Cell Res, 2003. **288**(1): p. 51-9.

34. Orlic, D., et al., *Bone marrow cells regenerate infarcted myocardium.* Nature, 2001. **410**(6829): p. 701-5.

35. Nagaya, N., et al., *Transplantation of mesenchymal stem cells improves cardiac function in a rat model of dilated cardiomyopathy.* Circulation, 2005. **112**(8): p. 1128-35.

36. Hollister, S.J., *Porous scaffold design for tissue engineering.* Nat Mater, 2005. **4**(7): p. 518-24.

37. Tsang, V.L. and S.N. Bhatia, *Three-dimensional tissue fabrication.* Adv Drug Deliv Rev, 2004. **56**(11): p. 1635-47.

38. Boland, T., et al., *Cell and organ printing 2: fusion of cell aggregates in three-dimensional gels.* Anat Rec A Discov Mol Cell Evol Biol, 2003. **272**(2): p. 497-502.

39. Ringeisen, B.R., et al., *Jet-based methods to print living cells.* Biotechnol J, 2006. **1**(9): p. 930-48.

40. Zein, I., et al., *Fused deposition modeling of novel scaffold architectures for tissue engineering applications.* Biomaterials, 2002. **23**(4): p. 1169-85.

41. Hutmacher, D.W., M. Sittinger, and M.V. Risbud, *Scaffold-based tissue engineering: rationale for computer-aided design and solid free-form fabrication systems.* Trends Biotechnol, 2004. **22**(7): p. 354-62.

42. Lo, H., M.S. Ponticiello, and K.W. Leong, *Fabrication of controlled release biodegradable foams by phase separation.* Tissue Engineering, 1995. **1**(1): p. 15-28.

43. Brun, P., et al., *Chondrocyte aggregation and reorganization into three-dimensional scaffolds.* J Biomed Mater Res, 1999. **46**(3): p. 337-46.

44. Nazarov, R., H.J. Jin, and D.L. Kaplan, *Porous 3-D scaffolds from regenerated silk fibroin.* Biomacromolecules, 2004. **5**(3): p. 718-26.

45. Wang, Y., et al., *In vitro cartilage tissue engineering with 3D porous aqueous-derived silk scaffolds and mesenchymal stem cells.* Biomaterials, 2005. **26**(34): p. 7082-94.

46. Gravel, M., et al., *Responses of mesenchymal stem cell to chitosan-coralline composites microstructured using coralline as gas forming agent.* Biomaterials, 2006. **27**(9): p. 1899-906.

47. Zhao, F., et al., *Effects of hydroxyapatite in 3-D chitosan-gelatin polymer network on human mesenchymal stem cell construct development.* Biomaterials, 2006. **27**(9): p. 1859-67.

48. Young, C.S., et al., *Tissue-engineered hybrid tooth and bone.* Tissue Eng, 2005. **11**(9-10): p. 1599-610.

49. Mondrinos, M.J., et al., *Engineering Three-Dimensional Pulmonary Tissue Constructs.* Tissue Eng, 2005.

50. Lin, A.S., et al., *Microarchitectural and mechanical characterization of oriented porous polymer scaffolds.* Biomaterials, 2003. **24**(3): p. 481-9.

51. Borden, M., M. Attawia, and C.T. Laurencin, *The sintered microsphere matrix for bone tissue engineering: in vitro osteoconductivity studies.* J Biomed Mater Res, 2002. **61**(3): p. 421-9.

52. Grayson, W.L., T. Ma, and B. Bunnell, *Human mesenchymal stem cells tissue development in 3D PET matrices.* Biotechnol Prog, 2004. **20**(3): p. 905-12.

53. Takahashi, Y. and Y. Tabata, *Homogeneous seeding of mesenchymal stem cells into nonwoven fabric for tissue engineering.* Tissue Eng, 2003. **9**(5): p. 931-8.

54. Shin, M., H. Yoshimoto, and J.P. Vacanti, *In vivo bone tissue engineering using mesenchymal stem cells on a novel electrospun nanofibrous scaffold.* Tissue Eng, 2004. **10**(1-2): p. 33-41.

55. Li, W.J., et al., *Multilineage differentiation of human mesenchymal stem cells in a three-dimensional nanofibrous scaffold.* Biomaterials, 2005. **26**(25): p. 5158-66.

56. Nuttelman, C.R., M.C. Tripodi, and K.S. Anseth, *In vitro osteogenic differentiation of human mesenchymal stem cells photoencapsulated in PEG hydrogels.* J Biomed Mater Res, 2004. **68A**(4): p. 773-82.

57. Li, Q., et al., *Biodegradable and photocrosslinkable polyphosphoester hydrogel.* Biomaterials, 2006. **27**(7): p. 1027-34.

58. Subramanian, A. and H.Y. Lin, *Crosslinked chitosan: its physical properties and the effects of matrix stiffness on chondrocyte cell morphology and proliferation.* J Biomed Mater Res A, 2005. **75**(3): p. 742-53.

59. Zaleskas, J.M., et al., *Contractile forces generated by articular chondrocytes in collagen-glycosaminoglycan matrices.* Biomaterials, 2004. **25**(7-8): p. 1299-308.

60. Wang, F.S., et al., *Superoxide mediates shock wave induction of ERK-dependent osteogenic transcription factor (CBFA1) and mesenchymal cell differentiation toward osteoprogenitors.* J Biol Chem, 2002. **277**(13): p. 10931-7.

61. Altman, G.H., et al., *Cell differentiation by mechanical stress.* Faseb J, 2002. **16**(2): p. 270-2.

62. Simmons, C.A., et al., *Cyclic strain enhances matrix mineralization by adult human mesenchymal stem cells via the extracellular signal-regulated kinase (ERK1/2) signaling pathway.* J Biomech, 2003. **36**(8): p. 1087-96.

63. Liu, L., et al., *Preparation and characterization of collagen-hydroxyapatite composite used for bone tissue engineering scaffold.* Artif Cells Blood Substit Immobil Biotechnol, 2003. **31**(4): p. 435-48.

64. Li, X., et al., *Chemical characteristics and cytocompatibility of collagen-based scaffold reinforced by chitin fibers for bone tissue engineering.* J Biomed Mater Res B Appl Biomater, 2005.

65. Meinel, L., et al., *Silk implants for the healing of critical size bone defects.* Bone, 2005. **37**(5): p. 688-98.

66. Meinel, L., et al., *Engineering cartilage-like tissue using human mesenchymal stem cells and silk protein scaffolds.* Biotechnol Bioeng, 2004. **88**(3): p. 379-91.

67. Meinel, L., et al., *Engineering bone-like tissue in vitro using human bone marrow stem cells and silk scaffolds.* J Biomed Mater Res A, 2004. **71**(1): p. 25-34.

68. Gomes, M.E., et al., *In Vitro Localization of Bone Growth Factors in Constructs of Biodegradable Scaffolds Seeded with Marrow Stromal Cells and Cultured in a Flow Perfusion Bioreactor.* Tissue Eng, 2006. **12**(1): p. 177-188.

69. Holtorf, H.L., et al., *Scaffold mesh size affects the osteoblastic differentiation of seeded marrow stromal cells cultured in a flow perfusion bioreactor.* J Biomed Mater Res A, 2005. **74**(2): p. 171-80.

70. Holtorf, H.L., J.A. Jansen, and A.G. Mikos, *Flow perfusion culture induces the osteoblastic differentiation of marrow stroma cell-scaffold constructs in the absence of dexamethasone.* J Biomed Mater Res A, 2005. **72**(3): p. 326-34.

71. Datta, N., et al., *In vitro generated extracellular matrix and fluid shear stress synergistically enhance 3D osteoblastic differentiation.* Proc Natl Acad Sci U S A, 2006.

72. Tsutsumi, S., et al., *Retention of multilineage differentiation potential of mesenchymal cells during proliferation in response to FGF.* Biochem Biophys Res Commun, 2001. **288**(2): p. 413-9.

73. Solchaga, L.A., et al., *FGF-2 enhances the mitotic and chondrogenic potentials of human adult bone marrow-derived mesenchymal stem cells.* J Cell Physiol, 2005. **203**(2): p. 398-409.

74. Bianchi, G., et al., *Ex vivo enrichment of mesenchymal cell progenitors by fibroblast growth factor 2.* Exp Cell Res, 2003. **287**(1): p. 98-105.

75. Reddi, A.H. and N.S. Cunningham, *Initiation and promotion of bone differentiation by bone morphogenetic proteins.* J Bone Miner Res, 1993. **8 Suppl 2**: p. S499-502.

76. Wozney, J.M., *The bone morphogenetic protein family and osteogenesis.* Molecular Reproduction and Development, 1992. **32**(1): p. 160-7.

77. Richardson, T.P., et al., *Polymeric system for dual growth factor delivery.* Nat Biotechnol, 2001. **19**(11): p. 1029-34.

78. Jansen, J.A., et al., *Growth factor-loaded scaffolds for bone engineering.* J Control Release, 2005. **101**(1-3): p. 127-36.

79. Mapili, G., et al., *Laser-layered microfabrication of spatially patterned functionalized tissue-engineering scaffolds.* J Biomed Mater Res B Appl Biomater, 2005. **75**(2): p. 414-24.

80. Carstens, M.H., M. Chin, and X.J. Li, *In situ osteogenesis: regeneration of 10-cm mandibular defect in porcine model using recombinant human bone morphogenetic protein-2 (rhBMP-2) and Helistat absorbable collagen sponge.* J Craniofac Surg, 2005. **16**(6): p. 1033-42.

81. Holtorf, H.L., J.A. Jansen, and A.G. Mikos, *Ectopic bone formation in rat marrow stromal cell/titanium fiber mesh scaffold constructs: effect of initial cell phenotype.* Biomaterials, 2005. **26**(31): p. 6208-16.

82. Takahashi, Y., M. Yamamoto, and Y. Tabata, *Enhanced osteoinduction by controlled release of bone morphogenetic protein-2 from biodegradable sponge composed of gelatin and beta-tricalcium phosphate.* Biomaterials, 2005. **26**(23): p. 4856-65.

83. Yang, X.B., et al., *Human osteoprogenitor growth and differentiation on synthetic biodegradable structures after surface modification.* Bone, 2001. **29**(6): p. 523-31.

84. Lu, Y., et al., *A digital micro-mirror device-based system for the microfabrication of complex, spatially patterned tissue engineering scaffolds.* J Biomed Mater Res A, 2006.

85. Hern, D.L. and J.A. Hubbell, *Incorporation of adhesion peptides into nonadhesive hydrogels useful for tissue resurfacing.* J Biomed Mater Res, 1998. **39**(2): p. 266-76.

86. Hersel, U., C. Dahmen, and H. Kessler, *RGD modified polymers: biomaterials for stimulated cell adhesion and beyond.* Biomaterials, 2003. **24**(24): p. 4385-415.

87. Schnaar, R.L., B.G. Langer, and B.K. Brandley, *Reversible covalent immobilization of ligands and proteins on polyacrylamide gels.* Anal Biochem, 1985. **151**(2): p. 268-81.

88. Brandley, B.K. and R.L. Schnaar, *Covalent attachment of an Arg-Gly-Asp sequence peptide to derivatizable polyacrylamide surfaces: support of fibroblast adhesion and long-term growth.* Anal Biochem, 1988. **172**(1): p. 270-8.

89. Nuttelman, C.R., M.C. Tripodi, and K.S. Anseth, *Synthetic hydrogel niches that promote hMSC viability.* Matrix Biol, 2005. **24**(3): p. 208-18.

90. Shin, H., et al., *Osteogenic differentiation of rat bone marrow stromal cells cultured on Arg-Gly-Asp modified hydrogels without dexamethasone and beta-glycerol phosphate.* Biomaterials, 2005. **26**(17): p. 3645-54.

91. Shin, H., et al., *Attachment, proliferation, and migration of marrow stromal osteoblasts cultured on biomimetic hydrogels modified with an osteopontin-derived peptide.* Biomaterials, 2004. **25**(5): p. 895-906.

92. Nuttelman, C.R., M.C. Tripodi, and K.S. Anseth, *Dexamethasone-functionalized gels induce osteogenic differentiation of encapsulated hMSCs.* J Biomed Mater Res A, 2006. **76**(1): p. 183-95.

93. Lalani, Z., et al., *Spatial and temporal localization of transforming growth factor-beta1, bone morphogenetic protein-2, and platelet-derived growth factor-A in healing tooth extraction sockets in a rabbit model.* J Oral Maxillofac Surg, 2003. **61**(9): p. 1061-72.

94. Wake, M.C., et al., *Effects of biodegradable polymer particles on rat marrow-derived stromal osteoblasts in vitro.* Biomaterials, 1998. **19**(14): p. 1255-68.

95. Park, H., et al., *Delivery of TGF-beta1 and chondrocytes via injectable, biodegradable hydrogels for cartilage tissue engineering applications.* Biomaterials, 2005. **26**(34): p. 7095-103.

96. Holland, T.A., Y. Tabata, and A.G. Mikos, *Dual growth factor delivery from degradable oligo(poly(ethylene glycol) fumarate) hydrogel scaffolds for cartilage tissue engineering.* J Control Release, 2005. **101**(1-3): p. 111-25.

97. Peter, S.J., et al., *Effects of transforming growth factor beta1 released from biodegradable polymer microparticles on marrow stromal osteoblasts cultured on poly(propylene fumarate) substrates.* J Biomed Mater Res, 2000. **50**(3): p. 452-62.

98. Wang, D.A., et al., *Bioresponsive phosphoester hydrogels for bone tissue engineering.* Tissue Eng, 2005. **11**(1-2): p. 201-13.

99. Wang, J., H.Q. Mao, and K.W. Leong, *A novel biodegradable gene carrier based on polyphosphoester.* J Am Chem Soc, 2001. **123**(38): p. 9480-1.

100. Nishimura, N., et al., *A new bioactive bone cement: its histological and mechanical characterization.* J Appl Biomater, 1991. **2**(4): p. 219-29.

101. Kokubo, T., *Bioactive glass ceramics: properties and applications.* Biomaterials, 1991. **12**(2): p. 155-63.

102. Ehara, A., et al., *Effects of alpha-TCP and TetCP on MC3T3-E1 proliferation, differentiation and mineralization.* Biomaterials, 2003. **24**(5): p. 831-6.

103. Sun, J.S., et al., *The effects of calcium phosphate particles on the growth of osteoblasts.* Journal of Biomedical Materials Research, 1997. **37**(3): p. 324-34.

104. Murphy, W.L., et al., *Effects of a bone-like mineral film on phenotype of adult human mesenchymal stem cells in vitro.* Biomaterials, 2005. **26**(3): p. 303-10.

105. Ong, J.L., et al., *Osteoblast precursor cell activity on HA surfaces of different treatments.* J Biomed Mater Res, 1998. **39**(2): p. 176-83.

106. Chang, Y.L., C.M. Stanford, and J.C. Keller, *Calcium and phosphate supplementation promotes bone cell mineralization: implications for hydroxyapatite (HA)-enhanced bone formation.* J Biomed Mater Res, 2000. **52**(2): p. 270-8.

107. Chou, L., B. Marek, and W.R. Wagner, *Effects of hydroxylapatite coating crystallinity on biosolubility, cell attachment efficiency and proliferation in vitro.* Biomaterials, 1999. **20**(10): p. 977-85.

108. Deligianni, D.D., et al., *Effect of surface roughness of hydroxyapatite on human bone marrow cell adhesion, proliferation, differentiation and detachment strength.* Biomaterials, 2001. **22**(1): p. 87-96.

109. Zhang, G., et al., *A PEGylated Fibrin Patch for Mesenchymal Stem Cell Delivery.* Tissue Eng, 2006. **12**(1-2): p. 9-19.

110. Cho, J.H., et al., *Chondrogenic differentiation of human mesenchymal stem cells using a thermosensitive poly(N-isopropylacrylamide) and water-soluble chitosan copolymer.* Biomaterials, 2004. **25**(26): p. 5743-51.

111. Ruel-Gariepy, E., et al., *A thermosensitive chitosan-based hydrogel for the local delivery of paclitaxel.* Eur J Pharm Biopharm, 2004. **57**(1): p. 53-63.

112. Dang, J.M., et al., *Temperature-responsive hydroxybutyl chitosan for the culture of mesenchymal stem cells and intervertebral disk cells.* Biomaterials, 2006. **27**(3): p. 406-18.

113. Temenoff, J.S., et al., *Thermally cross-linked oligo(poly(ethylene glycol) fumarate) hydrogels support osteogenic differentiation of encapsulated marrow stromal cells in vitro.* Biomacromolecules, 2004. **5**(1): p. 5-10.

114. Robey, P.G., *Bone Matrix Proteoglycans and Glycoproteins*, in *Principles of Bone Biology*, J.P. Bilezikian, L.G. Raisz, and G.A. Rodan, Editors. 1996, Academic Press: San Diego. p. 155-65.

115. Dennis, J.E. and A.I. Caplan, *Bone Marrow Mesenchymal Stem Cells*, in *Stem Cells Handbook*, S. Sell, Editor. 2004, Humana Press: Totowa. p. 107-18.

CHAPTER THREE

Laser-layered Micro-fabrication of Spatially Patterned Functionalized Tissue Engineering Scaffolds

3.1 INTRODUCTION

The field of tissue engineering, in recent years, has achieved significant milestones. One of the fundamental limitations in current efforts, however, has been our inability to produce multiple tissue types (e.g. bone, cartilage, ligaments, muscles etc.) in a pre-designed fashion inside a single scaffold structure [1, 2]. Although stem cells have been shown to differentiate into a variety of cell types, simultaneous construction of hybrid tissue structures within a single three-dimensional (3D) environment resembling the complex architecture of organs are yet to be reported. The basic barrier in creating such structures is our lack of knowledge on how stem cells behave and differentiate under spatio-temporally distributed biochemical and physical microenvironments, similar to those encountered during organ development.

Most patterning techniques to study cell behavior have been developed for two-dimensional (2D) surfaces [3-5]. Although these studies have provided tremendous insights into a variety of cellular processes and interactions, cell behavior within controlled 3D microenvironments have not been studied. Currently, most 3D scaffolding techniques only allow us to incorporate bio-factors "in bulk", i.e. the factors are distributed randomly all throughout the matrix. Even recent attempts in free-form fabricated scaffolds [6-9] or scaffolds with multiple sustained released factors [10] have only reported "bulk" incorporation. Complex spatial patterning along with temporal distribution of signaling molecules in the immediate microenvironment of stem cells, a hallmark of native tissue development, has yet to be engineered and studied.

The two fundamental steps towards achieving patterned microenvironments inside scaffold structures are (a) creating localized concentrations (or gradients) of multiple growth factors by controlled spatial incorporation while preventing their diffusion to surrounding areas and (b) creating a temporal gradient of growth factors (i.e., be able to precisely deliver several growth factors in a physiologically relevant time sequence). Here we present efforts in achieving micropatterned scaffold structures using a layer-by-layer microfabrication approach, with photo-polymerizable poly(ethylene glycol)- (PEG)-based hydrogels and polymer microparticles. Our goal is to create precise, pre-designed spatial distribution of multiple entities inside a single scaffold and mimic the physiological environment from which a single progenitor population can differentiate into multiple tissue lineages.

We have developed a laser-based, layer-by-layer, stereolithography approach for photo-crosslinking bio-functionalized, acrylated PEG monomers carrying soluble and entrapped particles to achieve spatial patterning. Photo-crosslinked hydrogel-based scaffolds, both degradable and non-degradable, have been widely investigated for musculoskeletal tissue engineering. Several researchers have demonstrated that PEG-based hydrogels can be successfully used to culture chondrocytes and osteocytes for bone and cartilage specific tissue regeneration [6, 11-15]. Others have developed hydrogels (using synthetic or natural polymers) having specific functionalities and degradation characteristics for similar purpose [16-18]. Chondrogenic differentiation of mesenchymal stem cells (MSCs) within PEG-based hydrogels has also been demonstrated by Elisseeff, Anseth and colleagues [19, 20]. However, most of these approaches use “bulk” encapsulation of cells and factors to create either bone or cartilage. Recent efforts to create hybrid structures have been reported using in-vitro derived osteocytes and chondrocytes (from MSCs) followed by incorporation of those precursor

cells in different layers prior to in-vivo implantation [21, 22]. Attempts to direct a single stem cell population into multiple lineages within a single scaffold structure by creating patterned growth factor distribution have not yet been reported. In addition, PEG-based scaffolds with designed internal structures and porosities for cell seeding and subsequent study of progenitor cells in complex microenvironments are yet to be demonstrated.

A key concept in creating localized patterning of bio-factors is the ability to prevent or control their diffusion into surrounding areas. In native tissue such spatial patterning is created by various extracellular matrix (ECM) components that bind to and sequester specific growth factors. We hypothesized that functionalizing the patterned scaffolds with ECM components (e.g. heparan sulfate) would allow us to sequester the entrapped growth factors in specific regions, thereby maintaining the spatial patterning. Components of the ECM not only play significant role in cell adhesion and migration but also supports optimal cell differentiation through molecular signaling by creating local concentration gradients of growth factors [reviewed by Taipale and Keski-Oja] [23]. Hollinger et al. [2] discussed the need of tissue engineering scaffolds to incorporate factor-immobilization concepts since local concentrations of growth factors play key role in directing lineage specific differentiation of progenitor cells. Highly charged glycosaminoglycans (GAG) e.g. heparan sulfates in the ECM, bind to soluble signaling molecules thereby preventing diffusion, creating local concentrations and optimal signaling, especially for basic fibroblast growth factor, FGF-2 [24-30]. Here we show that heparin incorporation into PEG scaffolds can create localized concentrations of growth factors thereby producing pre-designed spatial patterning.

We further demonstrate that polymer microparticles can be spatially incorporated within the scaffolds, thereby providing evidence that eventually controlled-release carriers with various release kinetics can be used to create temporal patterns along with

spatial distributions. Murine marrow stromal cells were successfully incorporated within these patterned structures by direct seeding on arginine-glycine-aspartic acid (RGD)-functionalized scaffolds. Such pre-designed structures could provide us, in the short term, with a valuable tool to study stem cell differentiation in complex microenvironments and might eventually enable us to fabricate complex tissue structures from a single progenitor population.

3.2 MATERIALS AND METHODS

3.2.1 PEGDMA Solutions and Photoinitiators

Poly(ethylene glycol) dimethacrylate (PEGDMA, Mw 1000, Polysciences Inc.), was dissolved in phosphate-buffered saline (PBS) to form either 10-20% (w/v) or 100% (w/v) solutions. The photoinitiator, 2-hydroxy-1-[4(hydroxyethoxy)phenyl]-2-methyl-1-propanone (Irgacure 2959, Ciba Geigy, USA), was used to generate free radicals for the induction of chain polymerization, with a concentration of 0.05 wt% for the lower concentration PEGDMA solutions (10-20% w/v) or 0.07 wt% for the 100% (w/v) PEG solution. The photoinitiator was first dissolved in PBS at a maximum concentration of 0.7 wt% to ensure complete solubility, and subsequently added to the PEGDMA solutions [31]. Prepared macromer solutions were kept in a dark environment to inhibit the pre-crosslinking of the polymer by incidental exposure to ambient light.

3.2.2 Pre-treatment of Glass Coverslips

Surfaces of glass coverslips were modified with an organosilane to covalently bond the hydrogel upon polymerization, thereby promoting a strong adhesion with the

hydrogels when rinsed with PBS or placed in buffered solutions/cell medium [32]. Surface-tethered methacrylate groups, which covalently attach to the acrylate groups of PEGDMA upon photo-polymerization, were created on the surface of glass coverslips by first immersing the slides in a solution of 3:1 ratio of 30% (w/v) H_2O_2 in distilled water and H_2SO_4. The hydroxylated slides were then immersed in 1 mM solution of 3-(trichlorosily)propyl methacrylate in a 4:1 solution of heptane and carbon tetrachloride. All chemicals were purchased from Sigma-Aldrich, unless otherwise noted.

3.2.3 Microfabrication of PEG Scaffolds Using a Frequency-Tripled Nd:YAG Laser

Using a 100% (w/v) PEGDMA solution with photoinitiator, 3D scaffolds were fabricated using an experimental set-up with the third harmonic wave of an Nd:YAG laser (λ = 355 nm, Surelite from Continuum, **Figure 3.1**), which generated nanosecond pulses. The laser energy was measured to be ~10 mJ/pulse. Macromer solutions were placed on a manually operated 3D micromanipulator stage. The stage carrying the liquid macromer solutions was translated in the x-y direction at a scanning speed of approximately 50 μm/sec in order to create pre-designed patterns within a single layer of a tissue engineering scaffold. The un-polymerized solution was washed off with PBS. This process is repeated for each different macromer solution composition to create single or multilayered patterned scaffolds.

Fluorescently-labeled latex microparticles (5.47 μm Cy5, 0.93 μm FITC, and 1.0 μm TRITC, Bangs Laboratories Inc.) were added to the macromer solutions at varying concentrations (ranging from 1% to 10% v/v) prior to crosslinking in order to show the

capabilities of this laser set-up to not only encapsulate the particles during polymer crosslinking, but to pattern them in a pre-designed fashion. Vertical patterning i.e. in the z-direction, was achieved by creating two-layered scaffolds. Macromer solution containing Cy5-labeled particles was selectively polymerized in a grid-type geometry. The un-polymerized solution was washed off extensively, and a second macromer solution containing FITC-labeled particles was polymerized over the first layer in the same geometry. These constructs were analyzed using either a confocal microscope (Leica SP2 AOBS) or by scanning electron microscopy (Phillips 515 SEM). Z-slices obtained using confocal fluorescence microscopy were reconstructed to create 3D images of the entire scaffolds.

3.2.4 RGD and Heparin Conjugation to PEG

Figure 3.2 shows the reaction scheme for functionalizing the scaffold material. A well-characterized fibronectin-derived peptide, YRGDS (tyrosine-arginine-glycine-aspartic acid-serine, Bachem Biosciences Inc., Torrance, CA), was reacted in equimolar amounts with acryloyl-PEG-*N*-hydroxysuccinimide (acryl-PEG-NHS, Mw 3400, Nektar Therapeutics Inc.) [14, 18]. 200 μL sodium bicarbonate buffer (pH 8.2) was added to acryl-PEG-NHS, which in a drop-wise fashion, was added to the YRGDS solution (1 mg/mL in sodium bicarbonate buffer). Conjugation was completed in a dark environment for 3 hours at room temperature. Peptide-modified PEG-acryl was frozen in liquid nitrogen, lyophilized for 24-hours, and stored in a desiccator at -20°C until further use.

To create a heparin moiety onto PEG-acrylates, ethylenediamine (EDA) was first reacted in excess with acryl-PEG-NHS at a 5:1 molar ratio to yield acryl-PEG-NH_2, similar to the method for RGD conjugation. The reaction was completed for 3 hours at

room temperature in a dark environment followed by extensive dialysis (Tube-o-dialyzer, MWCO 1000, Geno Technologies, St. Louis, MO) of unreacted EDA. Samples were frozen and lyophilized for 24 hours. Matrix-assisted laser desorption/ionization spectrometry (Applied Biosystems Voyager DE-PRO MALDI TOF-MS) was performed after this reaction to ensure that ethylenediamine did not create acryl-PEG dimers.

Periodated heparin (Mw 10,000 Celsus Laboratories Inc., USA) was reacted in equimolar amounts for 3 hours in a dark environment with acryl-PEG-NH_2 to yield acryl-PEG-heparin in the presence of 50 mM $NaBH_3CN$ as the reducing agent. Heparin, containing aldehyde moieties, undergoes Schiff-base reactions with organic amines, and if treated with $NaBH_3CN$, the Schiff-base intermediate is reduced to its corresponding amine, forming an irreversible bond. Centrifugation (Pall Macrosep®, MWCO 10,000) was performed to eliminate the reducing agent and unreacted components, and the product was lyophilized and stored in a dessicator at -20°C until further use. Proton-NMR was used to analyze the acryl-PEG-heparin reaction.

3.2.5 Cell Culture

Murine OP9 marrow stromal cells (a gift from T. Reid, University of Toronto) were cultured in Minimum Essential Medium-Alpha (Gibco Invitrogen Corp.) supplemented with 20% fetal bovine serum, 30 mM sodium bicarbonate (Sigma-Aldrich Co.), 2 mM L-glutamine (Gibco Invitrogen Corp.), 50 μg/mL penicillin-streptomycin (Gibco Invitrogen Corp.), and 100 mM of β-mercaptoethanol (Sigma-Aldrich Co.). Cells were passaged every 2-3 days.

An amine-reactive fluorescent dye, CellTrace™ Far Red DDAO-SE (Molecular Probes, Eugene OR) was used as a cell tracer to study cell attachment onto RGD-modified scaffolds. The succinimidyl ester reactive group of the dye forms a covalent

attachment to primary amines that occur in proteins and other bio-molecules on the inside and outside of cells. Because the fluorescent tag is inherited by daughter cells even after multiple divisions, cells were labeled in culture before their use in cell attachment studies. Additionally DAPI (Molecular Probes, Eugene OR) was also used to stain for cell nuclei. All cell staining were performed according to manufacturer's protocol.

3.2.6 Cell Attachment to RGD-modified Hydrogels

Acryl-PEG-RGD at a concentration of 5.0 mM was added to a 100% (w/v) PEGDMA solution with I2959 as the photoinitiator. Single-layered scaffolds (2 mm x 2 mm x 0.5 mm, L x W x H) with defined porosities were fabricated. The scaffolds were UV sterilized overnight in a cell culture hood prior to cell seeding. Parafilm was placed in a non-treated cell culture plate in order to form a hydrophobic surface when seeding the cells, and the scaffolds were placed on top of the film. Fluorescently-labeled murine bone-marrow stromal cells (OP9) were seeded on both the unmodified and RGD-modified constructs at a density of $2x10^4$/scaffold using 200 μl of medium. Medium was added to the culture plate after a 4 hr seeding period. The scaffold-cell constructs were cultured for 24 hours, and then rinsed with pre-warmed PBS to remove non-immobilized cells. Cells were fixed onto the scaffolds using 4% paraformaldeyde (pH 7.3) solution for 4 hours at 37°C. DAPI was used to stain for cell nuclei upon fixation. The scaffolds were imaged with confocal fluorescence microscopy and critical-point dried for SEM (Phillips 515) analysis.

3.2.7 FGF-2 binding to Heparin-modified PEG

On separate methacrylate-treated coverslips, thin-layered hydrogels were fabricated using 10% (w/v) PEGDMA with photoinitiator and 10% acryl-PEG-heparin. Each thin-layered hydrogel encapsulated 2 μg of FGF-2 (R&D Systems). Unbound FGF-2 was allowed to diffuse out of the hydrogels overnight while incubating in PBS at 37°C. The PBS solution in which the substrates were submersed was replaced three times during a period of 24 hours incubation to remove released FGF-2. To evaluate for FGF-2 binding to heparin-modified hydrogels, immunostaining was performed using primary anti-FGF antibody, biotinylated-secondary antibody, and streptavidin-FITC. The binding time for the antibodies and streptavidin-FITC were one hour each. Fluorescence microscopy was used to detect for FGF-2 immobilization within the hydrogels.

To test for FGF-2 binding in the multi-layered models, a two-layered hydrogel construct was polymerized using a UV lamp (365 nm, intensity ~4 mW/cm^2) and a 3 x 3 x 1 mm^3 plastic molding. The first layer, with 20% (w/v) PEGDMA and 0.05 wt% I2959 solution, was partially polymerized by exposing to the UV light for 4 minutes. The second macromer solution, which had 5.0 mM acryl-PEG-heparin and 2 μg of FGF-2 in addition to the 20% PEGDMA solution, was polymerized over the first layer by exposing it to UV light for 10 minutes. The hydrogel construct was then placed in PBS buffer (pH 7.4) for a period of 3 days. The construct was transversely sliced, and immunostaining was completed, as described previously, to evaluate for FGF-2 binding. A control group to this study was formulated in a similar way, except that the layer that did not contain acryl-PEG-heparin also encapsulated 2 μg of FGF-2.

3.3 RESULTS

3.3.1 Microfabrication of Single and Multi-layered Scaffolds with Precise Internal Features

The laser-based stereolithography method was used to create polymer scaffold structures with specific pore/channel dimensions. FITC-labeled latex microparticles were incorporated into the macromer solution prior to laser exposure in order to demonstrate the ability to incorporate controlled-release carriers or biomolecules within the scaffold as well as for easy visualization using confocal fluorescence microscopy. Porous scaffolds were fabricated with line spacings (center to center) of 300, 400 and 500 μm respectively. As shown in **Figure 3.3(A-C)** precise and highly controlled internal architectures can be generated during scaffold fabrication. Pores (channels) of sizes ~175 μm, 300 μm and 350-400 μm were achieved using the indicated line spacing within a single, 3D scaffold layer. As evident, highly uniform pore distribution was achieved using this technique. **Table 3.1** shows the detailed geometrical characterization of the scaffolds. The data also demonstrates that bio-factors and microparticles can be easily incorporated within the scaffold walls during the fabrication process. It is to be noted that the horizontal walls are slightly narrower than the vertical ones. This is due to the fact that the x-direction movement of the stage is computer-controlled at 50 μm/secs while the movement in the y direction is manually controlled to achieve an equivalent speed. Minor discrepancies in laser scanning speed could create such differences in wall thickness (a slower speed results in a thicker polymerized area).

Figure 3.3D shows a scanning electron micrograph of a representative, single-layer scaffold, while **Figure 3.3E** demonstrates the ability to create multiple layers. The

two-layer scaffold shown in **Figure 3.3E** also provides evidence that layers with various wall thickness and dimensions can be created using this approach.

3.3.2 Pre-designed Spatial Patterning of Scaffold Structures can be Achieved using Laser Fabrication

A key feature of this stereolithography method for scaffold fabrication is its ability to create pre-designed spatial patterns of single or multiple molecules and particles. We have demonstrated this ability and flexibility of this technique using both single layer (2D) and multi-layer (3D) structures as well as in structures with precise internal architectures. As shown in **Figure 3.4A**, TRITC-labeled latex particles can be spatially-patterned within a single polymer layer in a decreasing particle concentration (10%, 5% and 2.5% w/w). The line-graph indicates the fluorescence intensity (and hence a measure of particle concentration) across the polymer layer and demonstrates the feasibility of creating gradients of single growth factors as well as controlled-release particles within the scaffold. **Figure 3.4B** demonstrates patterning of multiple agents in a single layer. Cy5 or FITC-labeled particles were incorporated in the macromer solutions prior to laser exposure. Each pattern (line) was "written" using the laser and the un-polymerized polymer-particle solution was washed off prior to polymerizing the second line using a different polymer-particle solution. This shows the ability of this fabrication process to create precise and pre-determined distribution of multiple factors.

Figure 3.4C provides evidence on the feasibility of combining internal porosities and architectures along with spatial patterning inside a scaffold. A scaffold was fabricated using FITC-labeled particle-carrying polymer as well as polymer without the presence of any other agents. As shown, a pre-designed quadrant pattern was created using the stereolithography method in which the particles were specifically sequestered in

quadrants 1 and 4 while no factors were incorporated in quadrants 2 and 3. In addition channels of dimension 100 μm were created during the fabrication process.

Figures 3.4 (D-E) demonstrates the ability of this process to create multi-layered, 3D structures with spatially distributed factors. Either Cy5 or FITC-labeled polymer microparticles were incorporated within each layer during photopolymerization with the laser while creating uniform pores of dimension 400 μm. **Figure 3.4D** shows a stacked-confocal picture (3D reconstruction) while **Figure 3.4E** is a collage of confocal slices through vertical sections of the scaffold. This suggests that both lateral (**Figure 3.4C**) and vertical (**Figure 3.4 D-E**) patterning and can be achieved using this method of scaffold fabrication.

3.3.3 Heparin-functionalization Allows Effective Sequestration of FGF-2

In order to maintain spatial patterning of soluble growth factors inside a scaffold structure, it is critical to sequester the factors in their intended regions and control the diffusion of the growth factors within and across the spatial region. ECM components are known to participate in sequestration and localization of certain growth factors. Here we demonstrate that covalent conjugation of heparin to PEGDMA prior to scaffold fabrication provides efficient binding of basic fibroblast growth factor (FGF-2) and localization in both single and multi-layered scaffold models. MALDI-TOF ensured that no acryl-PEG dimers were formed with the addition of ethylenediamine during acryl-PEG-NH_2 synthesis, and only 3600 Mw peaks were found on the spectra (**Figure 3.5A**). ^{1}H-NMR confirmed the conjugation of heparin to acryl-PEG-NH_2, as illustrated in **Figure 3.5B-D**. ^{1}H-NMR showed peaks for both the presence of PEG (chemical shift 3.6 ppm) and heparin moieties (chemical shift range 3-5.5 ppm) when analyzing acryl-PEG-heparin. In the single-layered model (**Figure 3.6A-D**), polymer-layers containing

heparin-modified PEGDMA showed efficient FGF-2 binding and sequestration as demonstrated by immuno-fluorescence assays 72 hours after the addition of FGF-2. Matrices without heparin did not show FGF-2 immobilization. FGF-2 binding and localization was also illustrated in multi-layered hydrogels (**Figure 3.6E- H**). By observing immuno-stained hydrogels through confocal fluorescence microscopy, FGF-2 diffusion from the heparin-modified layer to the unmodified layer was not observed after a 72-hour incubation period in aqueous medium. These findings indicate that FGF-2 specifically binds to regions of PEG scaffolds that have been covalently modified with heparin. Furthermore, FGF-2 was encapsulated in both layers of the multi-layered scaffolds, (**Figure 3.6G-H**), and green fluorescence indicates that FGF-2 is more concentrated in the layer that contains acryl-PEG-heparin. Such functionalization concepts could provide effective means to maintain the spatial patterns created using the stereolithography method and allow one to control the rate of growth factor release from the scaffold walls.

3.3.4 Laser-microfabricated Scaffolds are Conducive of Cell Attachment when Functionalized with RGD

PEGDMA scaffolds containing 5 mM RGD-modified PEG resulted in efficient attachment and spreading of OP-9 stromal cells while scaffolds without the cell-adhesion peptide did not show any cell attachment. **Figure 3.7A-B** shows scanning electron micrograph of RGD-functionalized (**Figure 3.7B**) and non-functionalized laser-microfabricated scaffolds that were seeded with OP-9 cells. After 24 hours, no cell attachment was seen in the PEGDMA scaffolds while the RGD-containing scaffolds were filled with what appears to be ECM-like substances. Cell attachment on similar scaffolds was confirmed using confocal fluorescence microscopy. **Figure 3.7C** shows DAPI

staining on cells seeded on RGD-functionalized microfabricated scaffolds. It is evident that a large number of cells are attached to the scaffold walls. **Figure 3.7D** demonstrates cell seeding on a porous scaffold carrying FITC-labeled polymer particles. These cells were pre-labeled with CellTrace™. Red fluorescence specifies the attachment of cells to the surfaces of the scaffold, and the green fluorescence indicates that entrapped polymer. The data shows cells attach and spread efficiently on the scaffold wall.

3.4 DISCUSSION

One of the fundamental limitations of current efforts in the field of tissue engineering has been our inability to produce multiple tissue types in a pre-designed fashion within a single construct. Recent and past methods in fabricating tissue engineering scaffolds have only incorporated a random, bulk distribution of bio-factors that are conducive to the differentiation of a single tissue type inside a 3D structure. Because complex, patterned microenvironments are necessary to develop multiple cell-types within a single scaffold, spatial distribution of bio-factors, as well as their temporal release kinetics must be integrated to closely mimic the physiological environment. Furthermore simple, easy to fabricate 3D scaffolds that allow the study of cells within highly controlled geometrical features as well as within pre-designed patterns of biochemical and physical factors, could provide significant insights into complex cellular processes.

We have developed a laser-based SL system that can build complex scaffold structures using a layer-by-layer photopolymerization process. PEGDMA was used as a model polymer because of its easy availability as well as the ability to conjugate ECM to the polymer using well-defined chemistry. However, any polymer or resins that undergo

photo-initiated free-radical polymerization can be used as long as they are cyto-compatible. In addition, degradable scaffolds can also be fabricated using this process by introducing hydrolytically or enzymatically degradable segments within the photopolymer as described by Anseth and colleagues [13, 33, 34] and Hubbell and colleagues [18].

The point-by-point polymerization process is similar to a raster scanning device that could eventually be completely automated. Such automated stereolithography systems are commercially available and can be computer-guided. However, it must be noted that the resolution of most commercial stereolithography system remains approximately 200-250 μm. Although some commercial systems have a theoretical feature size of 75 μm, they failed to create open pores and channels when provided with a scaffold design, similar to those presented here (data not shown). Eventually such a fabrication system can be coupled to computer aided design and manufacturing (CAD/CAM)-driven automation and can use CT or MRI-based data as the input for designing complex scaffolds. Such systems have been described by Hollister et al. [6, 35-37] albeit at much larger feature sizes. The attraction of a simple laser-based system is that it can be a benchtop, research-scale system with high resolution. Although we have used an UV laser because of existing data showing cyto-compatibility of the photoinitiator [13], it is conceivable that other lasers can be substituted as long as a corresponding cell compatible photoinitiator is available.

The cross-linking of the macromer solution induced by the focused UV pulsed laser (λ=355 nm), and the complexity of the scaffold's architecture is controlled by the translational motion of the stage in the x-y directions, as well as feature resolution. The laser beam can be modeled as a Gaussian distribution in which the beam's diameter at the focal waist governs the theoretical x-y resolution of the system, which in turn dictates the

smallest feature sizes attainable (e.g. porosities or wall thickness of the scaffold). The focal waist of a Gaussian beam with a circular cross section is given by:

$$w_o=(2\lambda / \pi) * f^{\#}, \text{ [Equation 1]}$$

where w_o is the laser beam radius at the focal waist, λ is the wavelength, $f^{\#}$ (f number) is given by

$$f^{\#} = f / 2w_1$$

where f is the focal length of the lens, and w_1 is the beam radius at the lens. Using this equation, in our case, the theoretical resolution is calculated to be 5.8 μm (λ=355 nm, f= 25.4 mm, and beam w_1= 1 mm). Similarly, the depth of focus equation for a Gaussian beam with a circular cross section provides the theoretical resolution in the z-axis which in turn dictates the thickness of each layer. This can be solved by:

$$dof = (\pi w_o^2/\lambda)*(\zeta 2-1)^{1/2}, \text{ [Equation 2]}$$

where dof is the depth of focus, and $\zeta$is the acceptable focus within 2% or 1.02. For the current setup the theoretical depth of focus calculated from Equation 2 is 15 μm. These values demonstrate that the laser-based system has the potential to be a high resolution instrument. However, the experimental x-y resolution as well the z resolution of our system was measured to be ~100 μm which was governed by the amount of macromer solution placed on the translational stage. These significant deviations between the theoretical and experimental values can be due to laser diffraction, heat conduction, photoinitiator diffusion, and scattering due to polymer particles. We believe that through careful selection of photoinitiator, particle concentration and optimal laser-optics, this resolution can be significantly improved. However, even at its current resolution, the

feature sizes of the setup are conducive of studying cell differentiation and tissue formation in a highly controlled, pre-designed manner. An ideal wall thickness of a scaffold should be sufficient enough to not only encapsulate 5 to 10 μm-sized controlled-release particles and other bio-molecules, but should provide enough surface area for stem cells to attach and spread for optimal cell-to-cell communication and differentiation. The scaffold-fabrication system developed here allows us to study the effects of channel wall thickness, pores size, polymer crosslink density (all leading to the issues of nutrient diffusivity) in a controlled and detailed manner.

The laser-layered stereolithography process has the capability of spatially patterning growth factors and ECM components by their addition into the macromer solution prior to photo-polymerization. Instead of bulk photo-crosslinking PEG, as reported by other groups [11, 13], laser SL provides a controlled point-by-point polymerization method of creating a pre-designed scaffold. This unique capability specific to SL enables multiple types of growth factors to be spatially patterned within a single structure, overcoming a major roadblock in current efforts with creating more complex tissue-like structures. Another advantage for using this method is that microparticles have been effectively encapsulated during the crosslinking of PEGDMA solution. In our experimental applications both degradable poly(lactide-co-glycolide) microparticles (data not shown) and non-degradable polystyrene particles were used to show patterning of controlled-release carriers. Spatial incorporation of controlled-release particles having pre-designed release profiles would allow effective temporal patterning of the growth factors necessary for the signaling of progenitor cell differentiation (e.g. growth factor A could be early release while growth factor B could be a late release).

Surfaces of these micro-fabricated scaffolds must also be functionalized for cell recognition, providing a more biomimetic environment for stem cell proliferation and

behavior. Therefore ECM components were integrated within scaffolds by covalent-conjugation to the scaffolding biomaterial. Fibronectin-derived RGD is a commonly employed amino acid sequence for functionalizing PEG. Scaffolds were functionalized with RGD to be more biomimetic, thereby mediating adhesion to the seeded OP-9 cells. Micrographs show both protein and cellular attachment to the scaffolds that were modified with RGD. Cells that were seeded onto 100% PEG scaffolds without the presence of RGD did not remain viable.

In addition, one of the key factors in creating hybrid tissue structures is the ability to effectively sequester growth factors and maintain spatial patterning by controlling their diffusion in the scaffold. We hypothesized that appropriate modifications of the scaffold polymer with ECM components would allow for efficient binding and effective localization of growth factors. To demonstrate spatial patterning as well as localization of specific bio-factors, FGF-2 was chosen as model growth factor. The PEGDMA macromer was pre-modified with heparin prior to scaffold fabrication in order to regulate activity of the growth factor, FGF-2, and control its diffusion from the prescribed regions. By localizing growth factors into their specific compartments within a single scaffold, molecular signaling for hybrid stem cell differentiation can be further optimized. Heparin for growth factor binding was evaluated in both thin-layered and multi-layered systems. The immunostaining results show that FGF-2 remained sequestered in a heparin-containing matrix rather than diffusing away, indicating feasibility for successful patterning in a scaffold structure.

Integration of cells within PEG-based scaffolds can be mediated in two different ways: (a) direct cell encapsulation during the crosslinking polymerization and (b) cell seeding into fabricated scaffolds in which diffusion as well as surface chemistry governs cell distribution. We chose the latter method for integrating cells within our micro-

fabricated scaffolds since the pre-defined channels serve as porosities. It should be noted that the structural material of the scaffold is also a hydrogel that allows for intrinsic diffusivity throughout the scaffold in addition to the presence of channels. We hypothesize that combining the hydrogel material with a porous macrostructure will allow significantly improved diffusion of oxygen and nutrients to the interior of the scaffold, a major limitation of current scaffolding techniques.

There are however some key limitations to this fabrication process in its current form. First, the fabrication process is slow and if not automated could be tedious, especially for larger scaffold sizes. Thus, cell encapsulation within the hydrogel material, as has been the norm by other researchers using similar materials [14, 19, 20] is not possible. We have instead chosen to seed cells within the structures as an alternative. Direct cell encapsulation, however, in combination with laser-SL, could prove to be a promising method since multiple progenitor cells could ultimately be used, mimicking a more complex physiological tissue/organ. It would be helpful to have both options (encapsulation as well as seeding) available. We are working on increasing the speed of the layer-by-layer fabrication process using more advanced optical techniques that would allow both direct encapsulation as well as seeding of cells. Secondly, staggered layers (to ensure later interconnectivity of pores and channels) have not been achieved. Since in traditional stereolithography such staggering and overhanging structures are quite common and generally achieved using a sacrificial filler material, we believe that the current technique can be further enhanced using such approaches. We are continuing to further enhance the capabilities of this technique to incorporate such features. Although it should be noted that since the walls of the scaffold are hydrogels there is actually lateral diffusion of oxygen and nutrients possible. Thirdly the concept of "washing off" one solution prior to polymerizing another (for spatial patterning) could lead to some

cross-contamination between patterns. Although our results indicate that we can successfully pattern several components, it remains to be seen how complex the patterning can be before mixing becomes a problem. However, we believe that even simple 3D spatial patterns can provide us with unique insights on cell behavior under complex microenvironments.

Another important issue that needs to be addressed in future work is to determine differences photo-polymerization kinetics and mechanical integrity of scaffolds upon functionalizing with ECM components. Functionalization of scaffolds with RGD and heparin moieties decreases the rate of photo-polymerization due to their mono-functional acrylated macromer groups. We also observed that scaffolds modified with either acryl-PEG-heparin or acryl-PEG-RGD were less stiff in mechanical integrity than scaffolds fabricated using plain PEG macromer solution. Insight into how varying concentrations of these ECM components affect overall scaffold compressive modulus or stiffness as well as rate of photo-polymerization will be further investigated. These key factors could potentially affect stem cell behavior in such a precisely controlled microenvironment.

In conclusion we have developed a laser-based layer-by-layer photopolymerization process for microfabricating porous polymer scaffolds. This process allows for precise, pre-designed spatial distribution of single or multiple molecules within the scaffold as well as the fabrication of pre-determined internal architectures. We also demonstrate that functionalizing the scaffold material with RGD and heparin ensures efficient cell attachment and allows for spatial sequestration of patterned growth factors (FGF-2). Such microfabricated scaffold structures could provide tools to study progenitor cell populations under patterned, complex microenvironments and ultimately aid in creating pre-designed, hybrid tissue structures from a single stem cell population.

Table 3.1 Geometric Characteristics of the Microfabricated Scaffolds Depicted in Figure 3.3(A-C)

	Distance between center of lines			
	Theoretical	***Measured***	***Measured pore size***	***Measured wall thickness***
Scaffold A	300 μm	~350 μm	~175 μm x 175 μm	~140 μm, 200 μm
Scaffold B	400 μm	~450 μm	~300 μm x 350 μm	~90 μm, 120 μm
Scaffold C	500 μm	~565 μm	~350 μm x 425 μm	~100 μm, 200 μm

Figure 3.1 Experimental setup of the laser-based layer-by-layer stereolithography process for fabrication of patterned scaffolds.

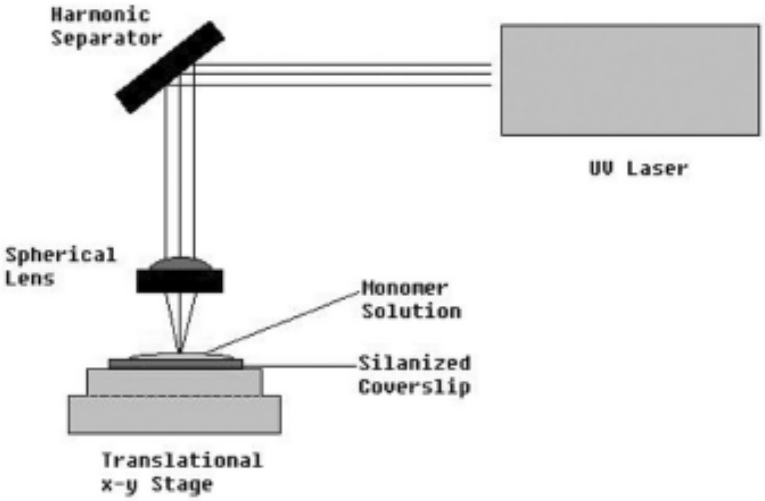

Figure 3.2 Reaction schemes detailing the conjugation of heparin and RGD to acrylated polyethylene glycols.

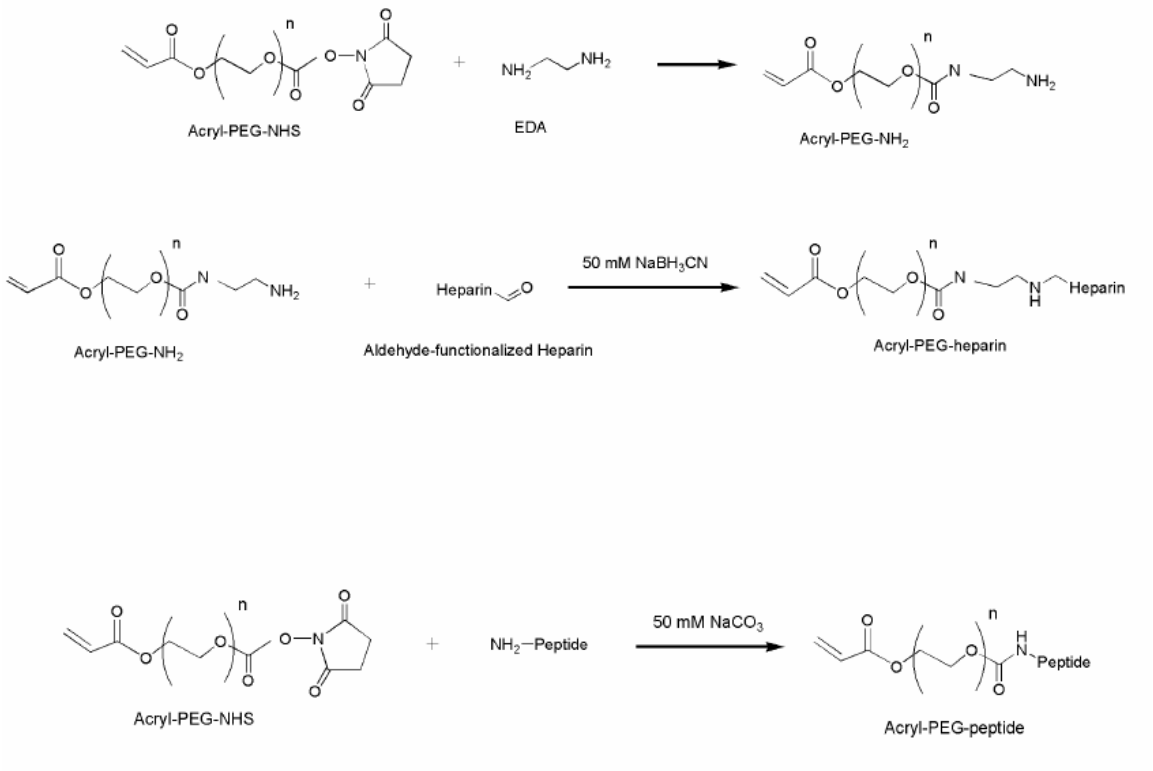

Figure 3.3. Confocal fluorescence and SEM micrographs show scaffolds with precise internal geometries can be fabricated using the stereolithography method. Fluorescence micrographs in figures (A-C) show scaffolds formulated with 100% (w/v) PEGDMA, 0.07 wt% Irgacure 2959, and 1% (w/w) FITC-labeled latex particles. Size bar shown is equal to 200 μm. Scaffold dimensions for each scaffold (A-C) are listed in Table 3.1, and the white scale bar equals 200 μm. SEM micrographs in figures (D and E), formulated in the same concentrations of PEGDMA and I2959, represent a single layer scaffold and a multi-layered scaffold, respectively. To differentiate the layers within a single scaffold when analyzing with SEM, the first layer of figure E was polymerized to have a thicker wall dimension then the second layer.

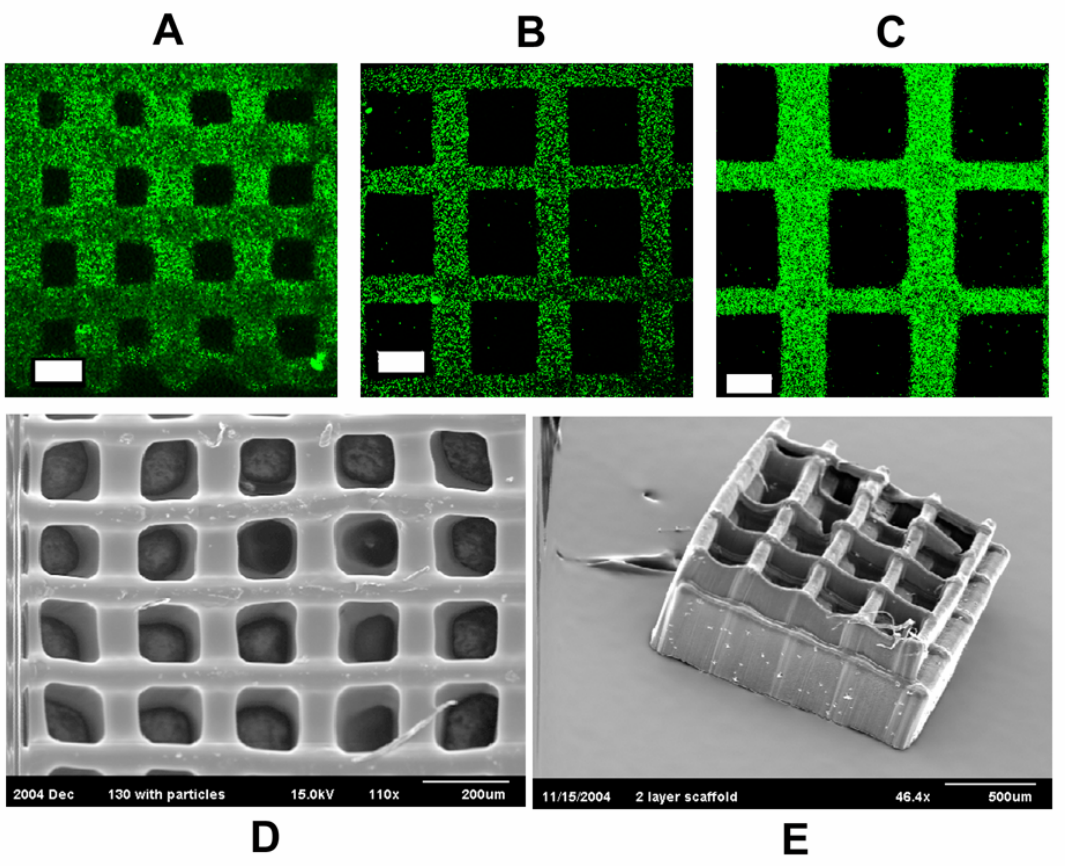

Figure 3.4 **Laser-based SL can create pre-designed, spatially patterned scaffold structures. Scaffolds shown here are formulated using 100% (w/v) PEGDMA and 0.07 wt% I2959. Figure A illustrates decreasing amounts of TRITC-labeled latex particles that are linearly patterned in a gradient form. The concentrations from L-R are 10%, 5%, and 2.5% (w/w) of particles in macromer solution. The graph below shows the intensity profile indicating decreasing fluorescence (and hence particle concentration) from left to right. Figures B & C illustrate spatial patterning using either FITC- or Cy5-labeled latex particles, as well as the capability of the laser SL to create uniform, precise, channels (pores) within a scaffold (white bar = 200 μm). Figure D illustrates a 3D reconstruction of a multi-layered scaffold using confocal z-slices. The individual slices through the scaffold are shown in figure E as a composite picture. The channel porosity within this particular multi-layered scaffold was measured to be approximately 400 μm.**

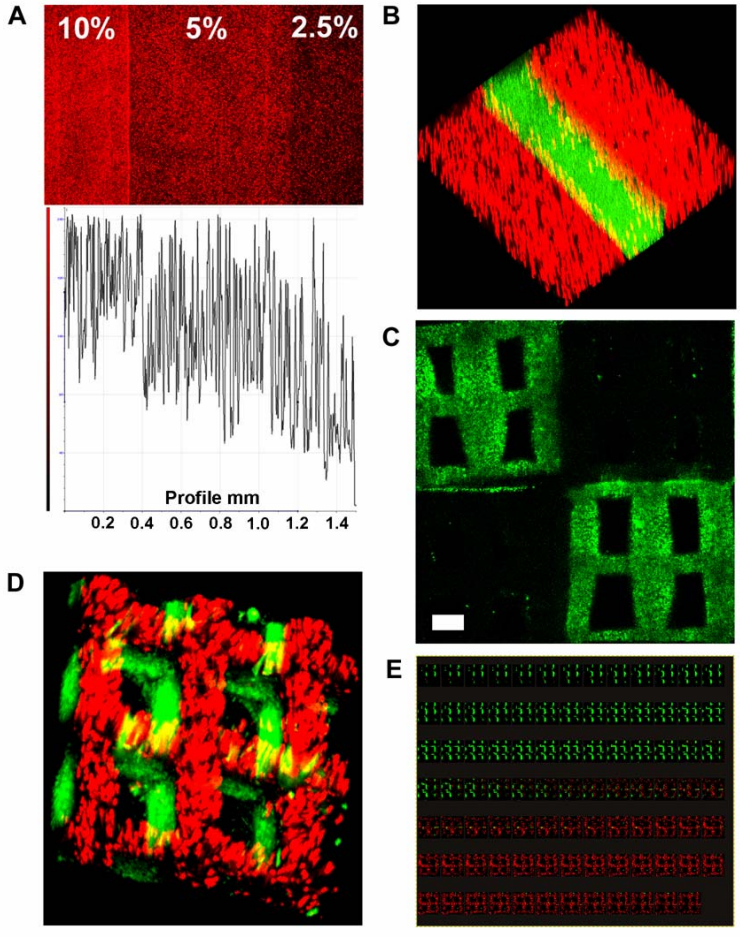

Figure 3.5 **MALDI-TOF in (A) confirmed that no acryl-PEG dimers were formed during when EDA was reacted with acryl-PEG-NHS. Only ~3600 Mw peaks were formed after this reaction (and not 7200 Mw peaks). ^{1}H-NMR spectra for unreacted components of acryl-PEG-NHS and periodated heparin in (B) and (C) respectively. The arrow in (B) and (D) depict the peak for acryl-PEG-NHS that occurs at a chemical shift of 3.6. The striped bar seen in (C) and (D) depict the presence of heparin moieties, and the chemical shift ranges from 3-5.5 ppm. After conjugation of these compounds and the filtration of unreacted compounds, ^{1}H-NMR shows that both heparin and PEG peaks were still present in (D). Figure (D) is also a zoomed-out view, and therefore the heparin peaks appear to be shorter.**

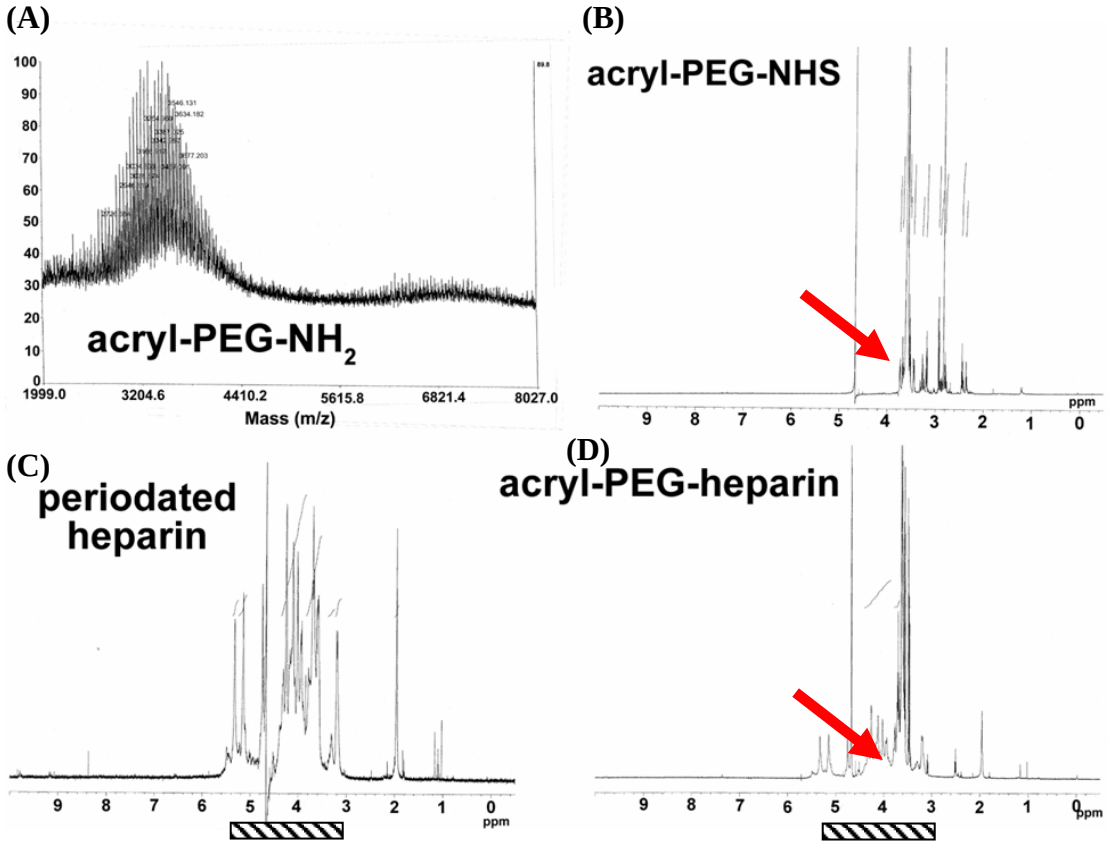

Figure 3.6 Incorporation of heparin mediates FGF-2 sequestration. This was demonstrated using both thin-layered polymer matrices (A-D) as well as multi-layered scaffolds (E, F). Localization of FGF-2 was evaluated via immuno-histochemistry and fluorescence microscopy (10X objective). Green fluorescence is due to the presence of FGF-2. FGF-2 (2 μg) was encapsulated in the thin-layered hydrogels. Brightfield images (A, C) and fluorescence images (B, D) were captured to determine FGF-2 immobilization. Hydrogels without acryl-PEG-heparin (A, B) do not show FGF-2 binding, whereas hydrogels modified with acryl-PEG-heparin (C, D) show FGF-2 sequestration.

Figure E is a schematic of the multi-layered scaffold depicted in F. Both layers were constructed using 20% (w/v) PEGDMA, 0.05% Irgacure 2959, and UV light. The top layer has 5.0 mM acryl-PEG-heparin and encapsulates 2 μg of FGF-2. Figure F illustrates that FGF-2 is effectively localized only within the layer that contains heparin.

Figure G is another schematic of a multi-layered scaffold depicted in H, formulated in the same way as explained above, except FGF-2 is encapsulated in both layers. After 72 hours in PBS, and removing soluble FGF-2 in the supernatant solution, fluorescence microscopy confirms that FGF-2 is more localized in the layer that contains acryl-PEG-heparin.

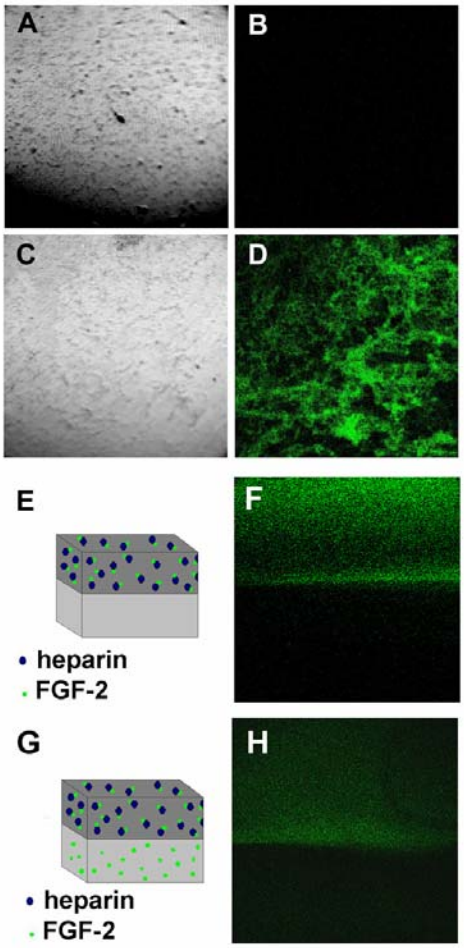

Figure 3.7 **Incorporation of RGD in the scaffold material mediates efficient cell attachment and spreading. SEM micrographs show top views of a 2 mm x 2 mm scaffold without RGD-modification (wall thickness is ~100μm) (A) and of a 2 mm x 2 mm scaffold containing 5.0 mM RGD-PEG-acryl (wall thickness ~200 μm) (B). Black scale bars in (A) and (B) equal 200μm. It appears that the attached OP-9 cells in (B) have secreted ECM-like materials on the scaffold. Confocal fluorescence microscopy (C, D) indicated that cells only attached to RGD-functionalized scaffolds. Figure C shows DAPI nuclei staining (scale bar = 200 μm), and figure D shows cells pre-stained with CellTracer™. The green staining seen in figure D is fluorescence from FITC-labeled particles that were encapsulated during photo-polymerization.**

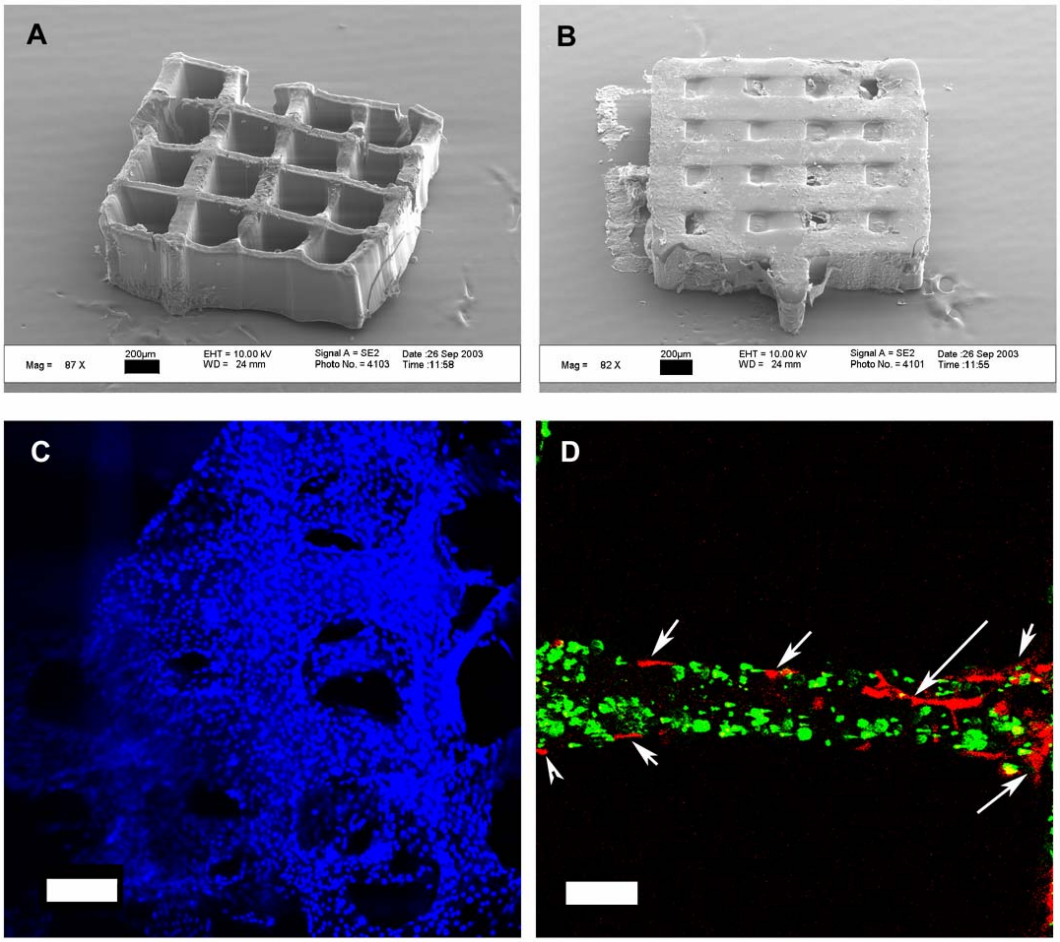

3.5 REFERENCES

1. Griffith, L.G., *Emerging design principles in biomaterials and scaffolds for tissue engineering.* Ann N Y Acad Sci, 2002. **961**: p. 83-95.
2. Orban, J.M., K.G. Marra, and J.O. Hollinger, *Composition options for tissue-engineered bone.* Tissue Eng, 2002. **8**(4): p. 529-39.
3. Tan, J.L., et al., *Simple approach to micropattern cells on common culture substrates by tuning substrate wettability.* Tissue Eng, 2004. **10**(5-6): p. 865-72.
4. Chen, C.S., et al., *Cell shape provides global control of focal adhesion assembly.* Biochem Biophys Res Commun, 2003. **307**(2): p. 355-61.
5. Chen, C.S., et al., *Micropatterned surfaces for control of cell shape, position, and function.* Biotechnol Prog, 1998. **14**(3): p. 356-63.
6. Feinberg, S.E., et al., *Image-based biomimetic approach to reconstruction of the temporomandibular joint.* Cells Tissues Organs, 2001. **169**(3): p. 309-21.
7. Hollister, S.J., R.D. Maddox, and J.M. Taboas, *Optimal design and fabrication of scaffolds to mimic tissue properties and satisfy biological constraints.* Biomaterials, 2002. **23**(20): p. 4095-103.
8. Park, A., B. Wu, and L.G. Griffith, *Integration of surface modification and 3D fabrication techniques to prepare patterned poly(L-lactide) substrates allowing regionally selective cell adhesion.* J Biomater Sci Polym Ed, 1998. **9**(2): p. 89-110.
9. Sachlos, E. and J.T. Czernuszka, *Making tissue engineering scaffolds work. Review: the application of solid freeform fabrication technology to the production of tissue engineering scaffolds.* Eur Cell Mater, 2003. **5**: p. 29-39; discussion 39-40.

10. Richardson, T.P., et al., *Polymeric system for dual growth factor delivery.* Nat Biotechnol, 2001. **19**(11): p. 1029-34.

11. Elisseeff, J., et al., *Photoencapsulation of chondrocytes in poly(ethylene oxide)-based semi-interpenetrating networks.* J Biomed Mater Res, 2000. **51**(2): p. 164-71.

12. Elisseeff, J., et al., *Controlled-release of IGF-I and TGF-beta1 in a photopolymerizing hydrogel for cartilage tissue engineering.* J Orthop Res, 2001. **19**(6): p. 1098-104.

13. Bryant, S.J. and K.S. Anseth, *Hydrogel properties influence ECM production by chondrocytes photoencapsulated in poly(ethylene glycol) hydrogels.* J Biomed Mater Res, 2002. **59**(1): p. 63-72.

14. Burdick, J.A. and K.S. Anseth, *Photoencapsulation of osteoblasts in injectable RGD-modified PEG hydrogels for bone tissue engineering.* Biomaterials, 2002. **23**(22): p. 4315-23.

15. Hedberg, E.L., et al., *Controlled release of an osteogenic peptide from injectable biodegradable polymeric composites.* J Control Release, 2002. **84**(3): p. 137-50.

16. Burkoth, A.K. and K.S. Anseth, *A review of photocrosslinked polyanhydrides: in situ forming degradable networks.* Biomaterials, 2000. **21**(23): p. 2395-404.

17. Anseth, K.S., V.R. Shastri, and R. Langer, *Photopolymerizable degradable polyanhydrides with osteocompatibility.* Nat Biotechnol, 1999. **17**(2): p. 156-9.

18. Halstenberg, S., et al., *Biologically engineered protein-graft-poly(ethylene glycol) hydrogels: a cell adhesive and plasmin-degradable biosynthetic material for tissue repair.* Biomacromolecules, 2002. **3**(4): p. 710-23.

19. Nuttelman, C.R., M.C. Tripodi, and K.S. Anseth, *In vitro osteogenic differentiation of human mesenchymal stem cells photoencapsulated in PEG hydrogels.* J Biomed Mater Res, 2004. **68A**(4): p. 773-82.

20. Williams, C.G., et al., *In vitro chondrogenesis of bone marrow-derived mesenchymal stem cells in a photopolymerizing hydrogel.* Tissue Eng, 2003. **9**(4): p. 679-88.

21. Kim, T.K., et al., *Experimental model for cartilage tissue engineering to regenerate the zonal organization of articular cartilage.* Osteoarthritis Cartilage, 2003. **11**(9): p. 653-64.

22. Alhadlaq, A. and J.J. Mao, *Tissue-engineered osteochondral constructs in the shape of an articular condyle.* J Bone Joint Surg Am, 2005. **87**(5): p. 936-44.

23. Taipale, J. and J. Keski-Oja, *Growth factors in the extracellular matrix.* Faseb J, 1997. **11**(1): p. 51-9.

24. Allen, B.L., M.S. Filla, and A.C. Rapraeger, *Role of heparan sulfate as a tissue-specific regulator of FGF-4 and FGF receptor recognition.* J Cell Biol, 2001. **155**(5): p. 845-58.

25. Pye, D.A., et al., *Regulation of FGF-1 mitogenic activity by heparan sulfate oligosaccharides is dependent on specific structural features: differential requirements for the modulation of FGF-1 and FGF-2.* Glycobiology, 2000. **10**(11): p. 1183-92.

26. Richard, C., M. Roghani, and D. Moscatelli, *Fibroblast growth factor (FGF)-2 mediates cell attachment through interactions with two FGF receptor-1 isoforms and extracellular matrix or cell-associated heparan sulfate proteoglycans.* Biochem Biophys Res Commun, 2000. **276**(2): p. 399-405.

27. Lin, X., et al., *Heparan sulfate proteoglycans are essential for FGF receptor signaling during Drosophila embryonic development.* Development, 1999. **126**(17): p. 3715-23.

28. Rahmoune, H., et al., *Interaction of heparan sulfate from mammary cells with acidic fibroblast growth factor (FGF) and basic FGF. Regulation of the activity of basic FGF by high and low affinity binding sites in heparan sulfate.* J Biol Chem, 1998. **273**(13): p. 7303-10.

29. Quarto, N. and F. Amalric, *Heparan sulfate proteoglycans as transducers of FGF-2 signalling.* J Cell Sci, 1994. **107 (Pt 11)**: p. 3201-12.

30. Gleizes, P.E., et al., *Basic fibroblast growth factor (FGF-2) internalization through the heparan sulfate proteoglycans-mediated pathway: an ultrastructural approach.* Eur J Cell Biol, 1995. **66**(1): p. 47-59.

31. Bryant, S.J., C.R. Nuttelman, and K.S. Anseth, *Cytocompatibility of UV and visible light photoinitiating systems on cultured NIH/3T3 fibroblasts in vitro.* J Biomater Sci Polym Ed, 2000. **11**(5): p. 439-57.

32. Koh, W.G., A. Revzin, and M.V. Pishko, *Poly(ethylene glycol) hydrogel microstructures encapsulating living cells.* Langmuir, 2002. **18**(7): p. 2459-62.

33. Davis, K.A. and K.S. Anseth, *Controlled release from crosslinked degradable networks.* Crit Rev Ther Drug Carrier Syst, 2002. **19**(4-5): p. 385-423.

34. Metters, A.T., K.S. Anseth, and C.N. Bowman, *Fundamental studies of biodegradable hydrogels as cartilage replacement materials.* Biomed Sci Instrum, 1999. **35**: p. 33-8.

35. Taboas, J.M., et al., *Indirect solid free form fabrication of local and global porous, biomimetic and composite 3D polymer-ceramic scaffolds.* Biomaterials, 2003. **24**(1): p. 181-94.

36. Lin, C.Y., N. Kikuchi, and S.J. Hollister, *A novel method for biomaterial scaffold internal architecture design to match bone elastic properties with desired porosity.* J Biomech, 2004. **37**(5): p. 623-36.

37. Hollister, S.J., et al., *An image-based approach for designing and manufacturing craniofacial scaffolds.* Int J Oral Maxillofac Surg, 2000. **29**(1): p. 67-71.

CHAPTER FOUR

A Digital Micro-Mirror Device (DMD)-based System for the Microfabrication of Complex, Spatially Patterned Tissue Engineering Scaffolds

4.1 INTRODUCTION

Recent advances in fabricating scaffolds for tissue engineering applications have yet to report methods in creating three-dimensional (3D) constructs that incorporate complex spatial-patterning of extracellular matrix components (ECM) and growth factors, which could provide biomimetic complex microenvironments for studying cell behavior and differentiation [1-3]. Most 3D scaffolding systems are only capable of differentiating a single progenitor cell population into one particular cell lineage due to either (a) bulk incorporation of bio-factors within the scaffolding matrix [4] or (b) exogenous delivery of hormones, chemicals, or growth factors in culture medium [5-7]. From a tissue engineering perspective, a significant advancement could be attained by creating precise, spatially distributed microenvironments within a single scaffold that would allow us to study simultaneous, patterned differentiation of stem and progenitor cells into multiple lineages and develop concepts to ultimately engineer complex, hybrid organ structures. A key step towards achieving such patterned 3D structures is the development of novel scaffold-manufacturing techniques by which distributed environments can be incorporated in a simple yet precise, reproducible fashion.

Laser micro-stereolithography (μSL) has become an accepted rapid prototyping method that allows the 3D microfabrication of solid models from images created by computer-aided design (CAD) programs [8-10]. We have recently reported a layer-by-layer laser microfabrication method for creating spatially patterned scaffolds using photo-

crosslinkable polymers. In this method a motorized x-y-z platform immersed in a liquid photopolymer is selectively exposed to a focused ultra-violet (UV) laser light. The polymer cures and becomes solid only at the focal point whereas non-irradiated areas remain liquid. After the first layer is formed the platform moves downward and a new layer of polymer is solidified according to the design. This layer-by-layer micro-manufacturing method enables complex internal features such as patterning of growth factors and ECM proteins. Bhatia and colleagues [11] have also provided an innovative soft lithography and a microsyringe method to fabricate biodegradable PLGA-based scaffolds with complex architectures. Multilayered structures were fabricated by thermally laminating each layer, and a classical salt leaching approach was used to create random porosities in the scaffold.

Although fine structures can be produced by a laser-based μSL technique, the process is usually slow due to the nature of point-by-point laser scanning. This prevents the incorporation of cells within the scaffold walls during the fabrication process and could also lead to denaturation and inactivation of biological molecules during the prolonged fabrication period. Here we report a novel, digital micro-mirror device (DMD)-based scaffold fabrication technique that allows precise, pre-designed patterning of multiple molecules and allows generation of complex architectures in a high-throughput, layer-by-layer fashion.

Bertsch and colleagues reported a μSL process employing a liquid crystal display (LCD) as a dynamic mask to photopolymerize an entire layer simultaneously and demonstrated fabrication of small mechanical parts such as a turbine and spring [12, 13]. Itoga and colleagues [14] have also explored LCD projectors to study two-dimensional (2D) cellular behavior through the micro-patterning of non-cytoadhesive polymers onto plasma-treated glass surfaces. However, LCD as a dynamic mask has limited optical

efficiency [15]. A new technology, Digital Micro-mirror Device™ (DMD, Texas Instruments, Dallas, TX), offers better performance in terms of optical fill factor (85% with DMD versus 64% with LCD) and light transmission (71% with DMD versus 21% with LCD). Furthermore, computer projectors, like the ones widely used for PowerPoint presentations, are commercially available for utilizing DMD technology in image transferring.

Rather than writing the 3D microstructure point-by-point (as previously reported in our laser scanning system [16]), or using a molded structure with thermal lamination [11], we have developed a DMD-based dynamic mask for the simultaneous photo-polymerization of partial and/or entire layers of a scaffold via projection. By changing bio-factors or controlled-released particles within the polymerizable resin, each layer or even partial layers were made up of a variety of controlled-release microparticles, thereby creating spatially distributed environments with micron-size resolution. Heparan sulfate was also conjugated to poly(ethylene glycol) acryloyl, and patterned-polymerized within the scaffold. This glycosaminoglycan (GAG) binds and protects growth factors, specifically FGF-2, an important biochemical cue for the differentiation of progenitor cells. In addition, precise and complex internal architectures (e.g. pore size and shape) were created using DMD. Cells were efficiently incorporated inside the scaffold walls during fabrication or seeded on the scaffolds following covalent modification of the surface with fibronectin. Murine marrow-derived stromal cells seeded in these DMD μSL-fabricated patterned scaffolds efficiently differentiated into osteoblasts and produced scaffold mineralization thereby demonstrating the ability of such structures to support cell proliferation and differentiation.

4.2 MATERIALS AND METHODS

4.2.1 PEGDA Solutions and Photoinitiator

Macromer solutions used to fabricate hydrogel scaffolds were formulated using 100% (w/v) poly(ethylene diacrylate) (PEGDA, Mw 3400, Nektar Therapeutics, AL) dissolved in phosphate buffered saline (PBS). To induce chain polymerization through the generation of free radicals, an ultra-violet photoinitiator, 2-hydroxy-1-[4(hydroxyethoxy)phenyl]-2-methyl-1-propanone (Irgacure 2959, Ciba Geigy, USA), was used at a concentration of 0.1 wt%. The photoinitiator was first dissolved in PBS at a concentration of 0.7 wt% in order to ensure complete solubility before adding to the PEGDA solution. Prepared macromer solutions were kept in a dark environment to prevent pre-crosslinking of the polymer by incidental exposure to ambient light.

4.2.2 DMD Micro-stereolithography (μSL) and Scaffold Fabrication

The micro-stereolithographic system was developed based on a commercial projector (PB2120, BenQ, Taiwan) coupled with a digital micro-mirror device (DMD™, Texas Instruments). Similar to a conventional stereolithography process, the DMD μSL created 3D microstructures in a layer-by-layer fashion. The shapes of the constructed layers were determined by slicing the desired 3D scaffold design into a series of evenly spaced planes. Patterns of each layer were drawn in a series of PowerPoint slides, which were then executed on the DMD chip to generate a dynamic mask. The illuminated light is modulated according to the defined mask on the DMD chip and then goes through a reduction-projection lens assembly to form an image on the surface of the resin or macromer solution. The illuminated area was solidified simultaneously under one

exposure, while the dark regions remained in liquid. After one layer was patterned, the substrate was lowered and the as-patterned layer was then covered by fresh macromer solution. Microstructures with complex geometries were created by sequentially polymerizing the layers. To fabricate scaffolds with multiple material compositions, solidified areas were rinsed thoroughly before immersing with a different macromer composition. To demonstrate the ability of this system to create spatially-patterned, multi-layered scaffolds, fluorescently-labeled polystyrene microparticles (1.0 μm Cy5-labeled and 1.0 μm FITC-labeled, Molecular Probes, Eugene, OR) were added separately to PEGDA solutions at a final concentration of 0.03 wt% prior to irradiation. These constructs were analyzed using either a confocal microscope for fluorescence patterning (Leica SP2 AOBS) or by scanning electron microscopy (Phillips 515 SEM) for multi-layered scaffolds.

The DMD μSL system is schematically shown in **Figure 4.1**. The system consists of five major components: a DMD chip embedded in the projector as a dynamic mask, a light source, a projection lens assembly, a translation stage with a micrometer, and a container containing macromer solution. All the components cooperate to ensure correct exposure, resolution, and layer thickness. To ensure cell viability through the use of a biocompatible UV photoinitiator, the original high intensity white light source was replaced with a UV light source with timer (Green Spot, UV Source Inc., CA). The light was guided through a ¼ inch (6.35 mm) liquid-filled fiber optics. Two bi-convex lenses (18 mm diameter, 40 mm focal length) with 5 mm spacing were used to converge the light emanating from the fiber optics. The projection lens assembly with adjustable aperture and focus consisted of two equal plano-convex lenses (25 mm diameter, 25 mm focal length). Each lens was oriented with the convex surface towards the longer conjugate distance. The aperture was placed in-between two lenses. All lenses were

made of UV grade fused silica (Edmund Optics, Barrington, NJ). The average exposure intensity was determined to be 2 mW/cm^2. Throughout the experiments, the magnification (size of the scaffold/size of the pattern) was fixed at 1/90.

The working principle of the DMD chip is also detailed in **Figure 4.1**. The DMD chip serves as an array of reflective aluminum micro-mirrors, which can be tilted with two bias electrodes to form angles of either +10° or -10° with respect to the surface. Illumination from the light source reflects into the projection lens only when the micro-mirror is in its +10° state. In the -10° state, the pixel appears dark because the illuminated light is not reflected into the projection lens. The reflected light from the -10° micro-mirror is collected by a light absorber. When the micro-mirror is in +10° state, it is classified as "tilt on" or ON. Conversely, when the micro-mirror is in -10° state, it is classified as "tilt off" or OFF.

Though the schematic in **Figure 4.1** depicts only three micro-mirrors for illustrative purposes, the actual DMD chip contains more than 442,000 switchable mirrors on a 5/8-in (15.875 mm) wide surface. For instance, in **Figure 4.1**, there are 3 pixels of white, black, white color respectively on the screen. The DMD chip is signaled by the computer to tilt the first micro-mirror to +10° state, the second micro-mirror to -10° state, and the third micro-mirror to +10° state. The first and third micro-mirror, which is in ON condition, reflects the illuminated light to the projection lens. Subsequently, the light reflected by the DMD into the projection lens is directed into the resin to cure the macromer solution. Conversely, the second mirror, which is in OFF condition, reflects the illuminated light to the light absorber.

4.2.3 Heparin Conjugation and FGF-2 Sequestration

As previously reported [16], heparin was conjugated to acryl-PEG by first reacting ethylenediamine (EDA) in excess with acryloyl-PEG-*N*-hydroxysuccinimide (acryl-PEG-NHS, Nektar Therapeutics) at a 5:1 molar ratio to yield acryl-PEG-NH_2. The reaction was completed for 3 hours at room temperature in a dark environment followed by the dialysis (Tube-o-dialyzer, MWCO 1000, Geno Technologies, St. Louis, MO) of unreacted EDA. Samples were frozen and lyophilized for 24 hours. Periodated heparin (Mw 10,000 Celsus Laboratories Inc., USA) was reacted in equimolar amounts for 3 hours in a dark environment with acryl-PEG-NH_2 to yield acryl-PEG-heparin in the presence of 50 mM $NaBH_3CN$ as the reducing agent. Filtration through centrifugation (Pall Macrosep®, MWCO 10,000) was performed to eliminate the reducing agent and unreacted components. The product was lyophilized and stored in a dessicator at -20°C until further use.

Acryl-PEG-heparin was added to the PEGDA macromer solution at a 5.0mM concentration, and patterned-polymerization was performed also using PEGDA macromer solution without acryl-PEG-heparin. Prior to polymerization, FGF-2 (Cell Sciences) was added to each of the macromer solutions at a concentration of 10 μg/mL. Patterned-polymerization was performed similarly to how the fluorescently-labeled particles were patterned as described above with the DMD-μSL. Scaffolds were rinsed extensively with PBS for a 48 hour period to remove unbound FGF-2, and immuno-histochemistry was performed to evaluate for binding. Immunostaining was performed using primary anti-FGF-2 antibody (Cell Sciences) and a secondary antibody bound with Alexa Fluor dye (Molecular Probes). The binding time for the antibodies were one hour each, with PBS and 0.05% Tween-20 washings in between and an initial 1% BSA blocking incubation. Fluorescence microscopy was used to detect for FGF-2

immobilization within the patterned hydrogels. Furthermore heparin was stained blue with 1% alcian blue in 3% acetic acid to visualize the localization of the GAGs within the patterned scaffolds.

4.2.4 DMD μSL Cell Encapsulation and Viability

Murine OP-9 marrow stromal cells (a gift from T. Reid, University of Toronto) were cultured in Minimum Essential Medium-Alpha (MEM, Gibco Invitrogen Corp., Carlsbad, CA) supplemented with 20% fetal bovine serum, 30 mM sodium bicarbonate (Sigma-Aldrich Co.), and 1% (v/v) penicillin-streptomycin (Gibco Invitrogen Corp.). Cell passaging and medium exchange were carried out every 2-3 days.

Before the 10th passage, OP9 cells were trypsinized and centrifuged to a pellet. PEGDA solution (formulated as described above) was filter sterilized and added to the cell pellet at concentration of 5 x 10^6 OP9 cells/mL macromer. A 15 μL suspension of cell-macromer solution was then pattern-polymerized using DMD-μSL for ~8 minutes. Unpolymerized solution was rinsed away extensively with sterile PBS, and scaffolds were transferred into tissue culture plates with medium and placed into an incubator. Cell encapsulation efficiency was determined in triplicate by counting cells in the unpolymerized solution using a hemocytometer. After a 24 hour incubation (5% CO_2, 37°C) period, 2 μM calcein AM (Molecular Probes, Eugene, OR) in PBS was added to the hydrogel-cell constructs, following the manufacturer's protocol, which stains viable cells green through intracellular esterase activity. Scaffolds were observed using fluorescence microscopy, and images were captured.

4.2.5 Surface Modification of Scaffolds for Cellular Attachment

Surfaces of hydrogels were modified to be cyto-adhesive by covalently conjugating fibronectin (from Bovine serum, Sigma Aldrich, St. Louis, MO) to patterned scaffolds. Prior to photo-polymerization, methacrylic acid (Sigma Aldrich, St. Louis, MO) was added to the macromer (PEGDA) solutions, as described above, at a molar ratio of 1:4 (methacrylic acid:PEGDA). Upon vortexing to ensure thorough mixing, solutions were irradiated with DMD μSL for the patterned polymerization of a 3D scaffold. The carboxylate groups tethering from the surfaces of the scaffolds (due to the presence of methacrylic acid) was activated through 1-ethyl-3-(3-dimethylaminopropyl)/N-hydroxysulfosuccinimide chemistry (EDC/sulfo-NHS, Pierce Biotechnology Inc., Rockfold, IL) in order to form stable amide bonds with fibronectin [17]. Briefly, a 500 μL solution consisting of 0.1 M MES buffer [2-(N-morpholino) ethane sulfonic acid), pH 6.5], 30 molar excess of Sulfo-NHS and 30 molar excess of EDC were added to each scaffold. The conversion of the carboxyl groups to amine-reactive sulfo-NHS esters was performed for 2 hours at room temperature on a plate rotator before the addition of 1.5 mL fibronectin (10μg/mL) using low-adhesion protein binding microtubes (Fisher Scientific). Fibronectin conjugation to the surfaces of the scaffolds was performed for a 24 hour period at room temperature. The negative control scaffolds did not contain methacrylic acid, but were treated in the same method as the experimental scaffolds. X-ray photoelectron spectroscopy (XPS, PHI 5700) was used to determine the presence of nitrogen (N) elements due to amide linkages of the conjugated fibronectin. Scaffolds were rinsed extensively with sterile PBS before cell seeding experiments.

To detect surface-conjugated fibronectin, immunostaining was performed using biotinylated anti-fibronectin antibody (Abcam Inc., Cambridge, MA) and streptavidin-FITC (Southern Biotechnology Associates, Inc., Birmingham, AL). The incubation time

for the antibody was 1 hour and for the streptavidin-FITC was 30 minutes at room temperature using a plate rotator. For a 24 hr period, scaffolds were incubated and rinsed several times with sterile PBS at room temperature. Fluorescence microscopy was used to detect surface-conjugated fibronectin. Furthermore, enzyme-linked immunosorbent assay (ELISA) was used to determine the amount of fibronectin conjugated to surfaces of the scaffolds. Biotinylated anti-fibronectin, streptavidin horseradish peroxidase, and tetramethylbenzidine (R&D Systems, Minneapolis, MN) were used to detect for unconjugated protein in the reaction supernatant of four different scaffolds. Absorbance was determined at 450 nm using a microplate reader (Opsys MR, Thermo Labsystems, Chantilly, VA) and plotted against a known standard curve.

4.2.6 Mesenchymal Stem Cell Isolation and Osteogenic Induction

Bone marrow was obtained from BALB/c mice (7-30 weeks old, Charles River Laboratories, Inc., Wilmington, MA). Upon sacrificing mice through carbon dioxide asphyxiation, bone marrow was flushed out of the tibias and femurs using a 27½-gauge needle and barrel with basal medium. Basal medium consisted of Dulbecco's modified Eagle's medium supplemented with 10% (v/v) fetal bovine serum and 1% (v/v) penicillin-streptomycin (Gibco Invitrogen Corp., Carlsbad, CA). After washing cells via centrifugation (1000 rpm, 5 minutes), viable cells were counted using trypan blue and a hemocytometer. To initiate murine mesenchymal stem cell culture (mMSC), cells were plated at a density of 2×10^6 cells/cm^2. The culture was placed in a humidified incubator (5% CO_2, 37°C) for 72 hours when non-adherent cells were removed via medium exchange. Cell passaging upon plate confluence and medium exchange were performed every 2-3 days [18].

Primary mMSCs, two weeks in culture, were trypsinized for 10 minutes at 37°C, centrifuged, counted, and seeded onto fibronectin-modified scaffolds at a density of 50,000 cells per scaffold. Sterile parafilm was placed in a non-treated cell culture plate in order to form a hydrophobic surface when seeding the cells, and the scaffolds were placed on top of the film. Cell attachment onto scaffolds was performed by suspending the cells in 100 μL of medium onto the constructs, thereby forming a "ball" due to an increased contact angle with the parafilm surface. Medium was added to the culture plate after a 4-hour incubation period. Cell attachment was quantified in triplicate by washing the cell-scaffold structures with sterile PBS and counting unattached cells with a hemacytometer. Osteogenic differentiation was initiated by culturing seeded mMSCs onto scaffolds for up to 4 weeks in basal medium supplemented with 10 mmol/L β-glycerophosphate, 10^{-8} mol/L dexamethasone, and 5 μg/mL ascorbic acid 2-phosphate.

4.2.7 Histology

At two-week and four-week time points, scaffolds were removed from in vitro culture and fixed overnight in 4% paraformaldehyde at 4°C. Scaffolds were dehydrated by adding 80% ethanol, 90% ethanol, 95% ethanol, 100% ethanol, 100% ethanol, 50% ethanol/50% Citrisolve (Fisher Scientific), 100% Citrisolve, 100% Citrisolve, and molten paraffin at 60°C in 1-hour sequential steps [6]. The scaffolds were then left overnight in molten paraffin at 60°C. Paraffin embedded samples were allowed to harden for a 24-hour period, sectioned at 10 μm using a microtome (American Optical Spencer Rotary Microtome Model 820), and then placed on glass slides. The slides were warmed for 5 minutes at 60°C and dried overnight at room temperature. Slides were dried an additional 30 minutes at 60°C, rehydrated, and stained. Nuclear fast red and von Kossa staining were used to visualize cell nuclei and scaffold calcification, respectively.

Scaffolds that did not contain cells were also von Kossa stained to determine if the PEG scaffolds alone stained black. Brightfield microscopy was used to observe the samples (Olympus IX70, Olympus America, Melville, NY; Optronics MagnaFire digital camera, Goleta, CA).

4.3 RESULTS

4.3.1 Single and Multi-layered Scaffolds with Defined Architectures Created by DMD μSL

The DMD μSL method was used to create polymer scaffolds with pores and channels having wide variety of shapes and dimensions. The configuration of the scaffold pores was dictated simply by altering the "mask" drawn on a PowerPoint slide, thus illustrating the powerful capability of this system to design features of any shape or form. As shown in the scanning electron microscopic (SEM) micrographs of **Figures 4.2(A-D)**, different pore geometries (hexagons, triangles, honeycombs with triangles, and squares) can be included within a single scaffold (pore size dimensions range from ~165μm to ~650μm, scale bars shown). Precise internal features of the scaffolds were fabricated with one single 90 sec exposure to the UV light of the DMD μSL. Additionally controlled internal architectures can be generated in parallel. **Figure 4.2D** shows scaffolds fabricated in a multi-layered fashion. The pore dimensions used in this scaffold are 250μm by 250μm with a measured wall thickness of 100μm. Construct edges appeared to be slightly rounded, due to swelling of the hydrogel structure. Keeping the light intensity (2 mW/cm^2) and exposure time constant, the smallest feature size attainable with DMD μSL was measured to be approximately 20 μm (data not shown).

This system is fundamentally limited by optical diffraction and diffusion of free radicals in the polymer solutions.

4.3.2 Single- and Multi-layered Scaffolds can be Spatially Patterned using DMD μSL

The DMD μSL system can fabricate both single layer and multi-layered scaffolds with pre-designed, spatially-patterned molecules and particles. The feasibility of such precise spatial patterning was demonstrated using PEGDA solutions containing either Cy-5 or FITC-labeled polystyrene particles that were encapsulated in a pre-designed pattern during the polymerization process. As shown in **Figure 4.3A**, solutions containing different particles can be patterned in a quadrant-specific geometry, in which the solution with Cy-5 particles were polymerized in the upper left and lower right regions, and the solution with FITC particles were polymerized in the upper right and lower left regions. This figure demonstrates the ability of the DMD μSL system to pattern multiple agents within a single layer through sequential steps of polymerization and rinsing of unpolymerized solutions. We also demonstrated spatial patterning in multi-layered scaffolds, as shown in **Figures 4.3(B-C)**, by creating constructs that specifically consisted of two layers, each containing either Cy-5 or FITC-labeled particles. The bottom layer was pattern-polymerized with a single 90-second exposure using Cy-5 particle-polymer solution, and then rinsed extensively to remove unpolymerized polymer and particles. The second layer, containing FITC particle-polymer solution, was then polymerized in the same method on top of the first layer using the same patterning mask.

4.3.3 FGF-2 Sequestration in Heparin-modified Scaffolds

Acryl-PEG-heparin was added to PEGDA macromer solution and patterned polymerized on one half of an entire scaffold. The unpolymerized heparin-modified solution was then rinsed away with PBS, and PEGDA solution, without acryl-PEG-heparin was polymerized on the other half of the scaffold. Alcian blue staining in **Figure 4.4A** shows that heparin-modified PEG was effectively patterned within the pre-determined area of the single-layered scaffolds. FGF-2 was also sequestered in the areas of the patterned scaffold that only contained heparin, as illustrated with fluorescence microscopy in **Figure 4.4B**.

4.3.4 Covalent Modification of Scaffold Surfaces with Fibronectin

Since PEG polymers have hydrophilic and non-ionic properties, the scaffold surface must be modified to mediate efficient cell seeding. Here we demonstrate the covalent conjugation of fibronectin, an extracellular matrix component that signals for cell anchorage and spreading, to scaffolds via EDC/sulfo-NHS chemistries. **Figure 4.5** shows fluorescence images of immuno-stained scaffolds. Scaffolds containing methacrylic acid in the macromer solution (left) fluoresce green, indicating the successful covalent conjugation of the fibronectin, whereas the scaffold without methacrylic acid (right) did not show any adsorption or conjugation of fibronectin. ELISA studies indicated that fibronectin attached to scaffold surfaces at a concentration of approximately 9.2 $\mu g/cm^2$ ($\pm$ 0.3 $\mu g/cm^2$) or 48.9 $\mu mol/cm^2$ ($\pm$ 0.03 $\mu mol/cm^2$).

4.3.5 OP-9 Cell Encapsulation and Viability

Patterned encapsulation of cells within the scaffold walls was achieved by the addition of OP-9 cells to the macromer solution prior to DMD μSL UV irradiation. **Figure 4.6A** shows a fluorescence micrograph of cells overlaid onto a transmitted micrograph of the scaffold, and demonstrates the viability of encapsulated cells within a single-layered scaffold (~150 μm thick layer). Most of the encapsulated cells within the hydrogel structures remained viable after a 24 hour incubation period as indicated by calcein staining, indicating a cytocompatible fabrication process. Cell encapsulation efficiency for this particular patterned-scaffold was determined to be approximately 73% (± 9.6%). Encapsulation efficiency is, however, dependent, on scaffold channel or pore dimensions, the volume of cell-macromer solution used, and the presence of a container to hold the cell-macromer solution during the photo-polymerization process to prevent solution spreading.

4.3.6 Osteogenic Differentiation of mMSCs in DMD μSL-fabricated Scaffolds

Seeded mMSCs successfully attached onto patterned fibronectin-conjugated scaffolds created by DMD μSL, with a 70% (±3%) attachment efficiency, and were then exposed to osteogenic medium. **Figures 4.6(B-C)** show nuclear fast red and von Kossa staining in constructs cultured for two and four weeks. **Figure 4.6B** shows von Kossa staining on scaffolds removed at 2-week time period (10X objective), and **Figure 4.6C** shows nuclear fast red and von Kossa staining of scaffolds removed at 4-week time period (40X objective). Cell cytoplasm stains pink and the nuclei stain bright red. Mineralized areas of the constructs stained black. These histological data show high levels of mineralization throughout the microfabricated scaffold matrix, indicating that seeded mMSCs transform into osteoblasts with the presence of osteogenic medium.

Additionally, as a negative control, PEG scaffolds alone did not stain black when von Kossa was applied (data not shown). PEG-based scaffolds incorporating MSCs cultured only in basal medium do not show any mineralization when stained via von Kossa, as presented by Nuttelman et. al. [6].

4.4 DISCUSSION

A key limitation in tissue engineering is the fabrication of pre-designed, spatially-patterned microenvironments that physiologically mimic what is observed by stem and progenitor cells during organ development. Creating such complex microenvironments inside scaffold constructs would allow us to better study cell behavior and differentiation under controlled, biomimetic settings. The ability to develop such constructs that combine both spatial and temporal-patterning of physical and biochemical factors could ultimately lead to creating multiple tissue types from a single stem cell population inside a 3D structure. We have developed a versatile layer-by-layer microfabrication system consisting of a DMD-based dynamic masking technology to create polymer scaffolds that integrate complex micro-architectures and spatially patterned bio-factors for studies in progenitor cell differentiation.

Similar to the laser-based stereolithography method we have previously reported [16], DMD μSL can also build 3D scaffold structures through a layer-by-layer photo-polymerization technique. In addition, the key features achieved using the laser-based system, for example, creation of precise gradients of bio-factors or fabrication of specific, pre-designed pore sizes can be easily obtained using the DMD system (data not shown). The main advantage of using this novel scaffold fabrication system over the laser-based system or other stereolithography methods is that the photo-polymerization of an entire single layer is achieved simultaneously, and ultimately a 3D construct is achieved by

"building" subsequent layers in the same fashion by exchanging polymer solution in between. In addition, more complex internal architectures as well as efficient cell encapsulation can be achieved using DMD. Although PEGDA was used in this present study, because the DMD μSL system is based on a photo-initiated, free-radical chain polymerization process, any polymer-photoinitiator solution undergoing such a reaction can be used. To achieve degradable scaffold structures, enzymatically or hydrolytically degradable moieties, as reported by Anseth and colleagues and Hubbell and colleagues [19-22] could also be used in the DMD μSL system.

The DMD-μSL system has the powerful capability of (a) generating complex internal architectures and (b) entrapping multiple biochemical factors (soluble or in controlled-release particles) in precise, pre-designed spatial patterns by their addition into the macromer solution prior to photo-polymerization. Since the masks used for polymerization were designed to take on any shape or size using PowerPoint, the geometries of the porosities, as well as the scaffold, can virtually be of any pattern. Entrapped degradable particles, carrying biological or chemical factors and having various release kinetics, could also allow for temporal patterning necessary for the prolonged and sequential signaling of progenitor cell differentiation. This stereolithography process could eventually lead to developing elaborate scaffolds conducive of creating more complex tissue-like structures, a major obstacle in current tissue engineering efforts.

The effects of exposure time, light intensity, polymer, and photoinitiator concentrations were investigated to optimize the resolution and patterning of the scaffold structures. A crucial task in the optical set-up of DMD μSL is ensuring that the masking pattern irradiates uniformly by utilizing the appropriate light source. Though optical fibers could potentially provide uniform light, its intensity profile could result in a quasi-

Gaussian distribution. Another option that would provide a uniform light source is the use of an optical homogenizer, which simply homogenizes the intensity profile. Instead of using either of these methods, we took advantage of the versatility of DMD μSL by simply adjusting the gray scale of the masking patterns that were irradiated onto the macromer solutions. This process was achieved by darkening the gray scale of the pixels that received the highest intensity from the light source to balance the non-uniformity. Throughout our experiments, we observed that the required exposure time to photo-polymerize the macromer solution decreased as the light intensity increased.

Generally, in fabricating photo-polymerized tissue engineering scaffolds, a short exposure time is desired for two critical reasons: (a) viability of encapsulated cells decreases as exposure time increases and (b) increased diffusion of free radicals from the photo-initiator causes distorted patterns with longer exposure times. Exposure time could be reduced by increasing light intensity to avoid such issues. Decreasing exposure time, however, simultaneously enhances diffraction, thereby reducing pattern resolution. Furthermore, both diffraction from the masking pattern and diffusion of the free radicals could limit scaffold resolution. Increasing both polymer and photoinitiator concentrations resulted in more resolved patterning of the scaffolds, only under an optimum light intensity and a decreased exposure time. Otherwise, as reported by Bhatia and colleagues, keeping the parameters of exposure time and light intensity constant, polymer and photoinitiator concentration does not affect patterning resolution [23]. We limited the photoinitiator concentration in the macromer solutions to no more than 0.1wt% with our experiments based on previous photo-initiator cyto-toxicity studies done by Bryant et. al. [24].

The addition of GAGs, such as heparan sulfates, provides a more complex microenvironment that closely mimics the stem cell niche. Since heparin is characterized

to not only bind, but protect certain growth factors, this biochemical factor can be localized within certain regions of single scaffold. FGF-2 is an important mitogenic factor for the osteogenic differentiation of marrow-derived progenitor cells, and its localization within a structure could help mediate bone formation. Creating a region within a complex architecture that is conducive of bone formation only could lead to a tissue-engineered structure that closely mimics physiological tissue/organ.

Cell viability during encapsulation within 3D constructs is dependent upon the biocompatibility of the materials used and their by-products, scaffold fabrication process, and nutrient/waste diffusion throughout the porous matrix. DMD μSL was shown to be a bio-compatible scaffold fabrication technique when encapsulating cells during the photo-polymerization of the PEGDA macromer solution. UV light intensity, exposure time for scaffold polymerization, and free radicals generated from the photo-initiator did not affect the viability of the encapsulated cells even after 24 hours in culture. Because of its cross-linking nature from a liquid to a solid phase and the ability to imbibe water up to more than 90% [25], PEGDA is an ideal polymer to encapsulate cells and sustain their viability. The cross-linking network of PEG-based hydrogels also provides efficient transport of nutrient and waste delivery, thus contributing to the sustainability of encapsulated cells. We hypothesize that the channels serving as macro-structural pores of the scaffolds created by DMD-μSL further act to increase nutrient/waste diffusion of cells as opposed to the "bulk" polymerization of cell and PEG-based polymer solutions as reported by others [5, 6]. Cell viability would vary along the cross-sections (x-y-z directions) of thicker hydrogels that were bulk-polymerized due to inefficient nutrient/waste diffusion within the interior of the matrix (i.e. only surfaces of the gels would get optimum diffusion). Because DMD-μSL has the capability of patterning channels as pores all throughout the hydrogel scaffolds, the viability of encapsulated cells

only depends on wall thickness (x-y directions) and not the entire thickness (height or z-direction) of the 3D construct. Scaffold wall thickness is easily controlled through the design of the masking patterns irradiated by DMD-μSL and would only have to be a certain thickness to encapsulate a sufficient amount of cells. Furthermore because unpolymerized solutions can be washed away in between UV irradiations, multiple cell types could also be patterned within a single construct, leading to a more intricate tissue engineering construct.

In addition to cell encapsulation, scaffold surfaces can be functionalized to conjugate fibronectin, thus allowing efficient cell seeding, attachment, and proliferation. Because fibronectin is covalently-conjugated post-fabrication, the possibility of denaturation due to UV exposure is eliminated. Seeded murine MSCs attached efficiently to fibronectin functionalized scaffolds. The differentiation of MSCs on patterned scaffolds was achieved through the addition of osteogenic culture medium and confirmed through standard histological staining for matrix calcification. Mineralization of the scaffold over a 4-week period in culture illustrates that these DMD micro-fabricated, patterned scaffolds are capable of allowing mMSCs to adhere, proliferate, and transform into osteoblasts.

In conclusion, we have demonstrated DMD-μSL to be a powerful technology in creating pre-designed, spatially patterned scaffolds for applications in cell and tissue engineering. This novel stereolithography system has the capability of creating precise distributions of chemical and biological factors within a 3D scaffolding structure. The scaffolds are also suitable for the encapsulation of single or multiple cell types in a spatially distributed fashion. Functionalizing the patterned scaffolds with fibronectin creates a microenvironment suitable for the attachment, proliferation, and differentiation of mMSCs. These micro-fabricated, spatially patterned scaffolds could ultimately consist

of intricate architectures that combine both spatial and controlled-release kinetics of biochemical factors, creating a suitable environment for studying hybrid tissue formation from a single stem cell population.

Figure 4.1 Schematic of the Digital Micro-mirror Device Micro-stereolithography (DMD μSL) set-up

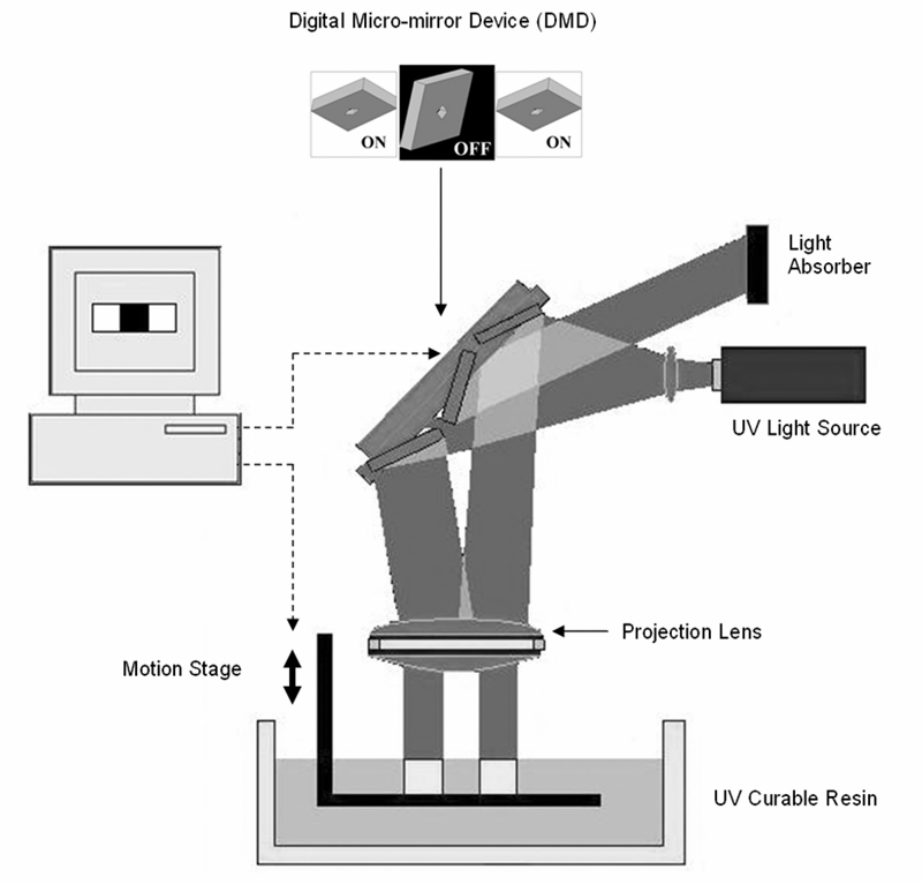

Figure 4.2 Scanning electron microscopy (SEM) illustrate that DMD μSL can create scaffolds with intricate pore geometries. Hexagons (honeycomb), triangles, triangles inside hexagons, and squares shaped pores were created by directly drawing in PowerPoint files and using the DMD as a dynamic "mask". Geometrical side dimensions of the pores range from approximately 165 μm to 650 μm (scale bars shown). Scaffolds depicted in figure D specifically show a two-layered scaffold. All scaffolds were irradiated for 90 seconds per layer and formulated using 100% (w/v) PEGDA in PBS and 0.1wt% Irgacure 2959.

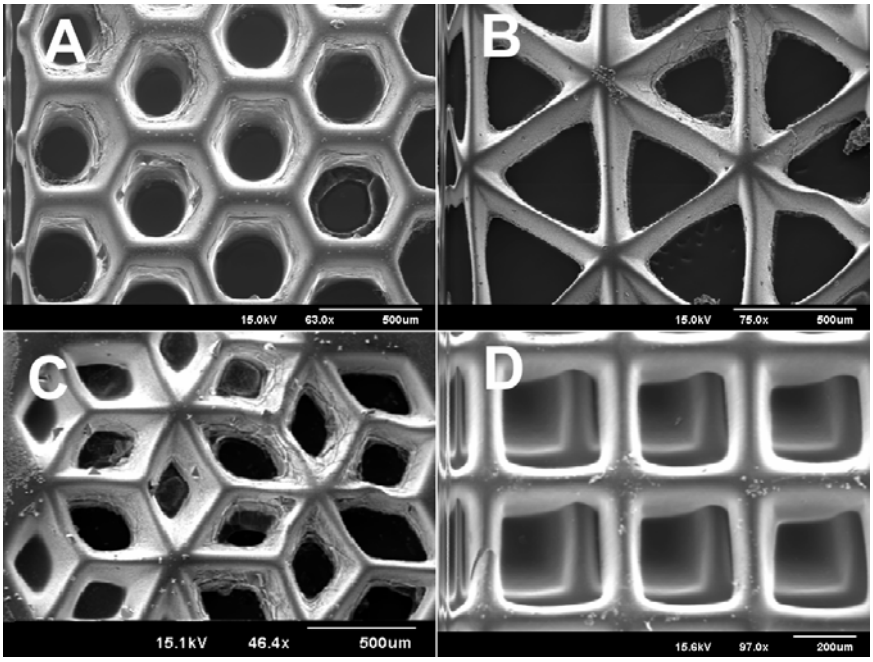

Figure 4.3. DMD-μSL can create pre-designed, spatially-patterning inside scaffold structures. Fluorescence confocal microscopy of scaffolds formulated with 100% (w/v) PEGDA in PBS, 0.1 wt% Irgacure 2959, and 0.03 wt% carrying either FITC- or Cy5- labeled polystyrene particles (taken with a 10X objective). Figure A shows spatial patterning of a single-layer in a "quadrant" specific pattern. Figures B and C show spatial patterning within multi-layered scaffolds. White scale bar represents 200 μm.

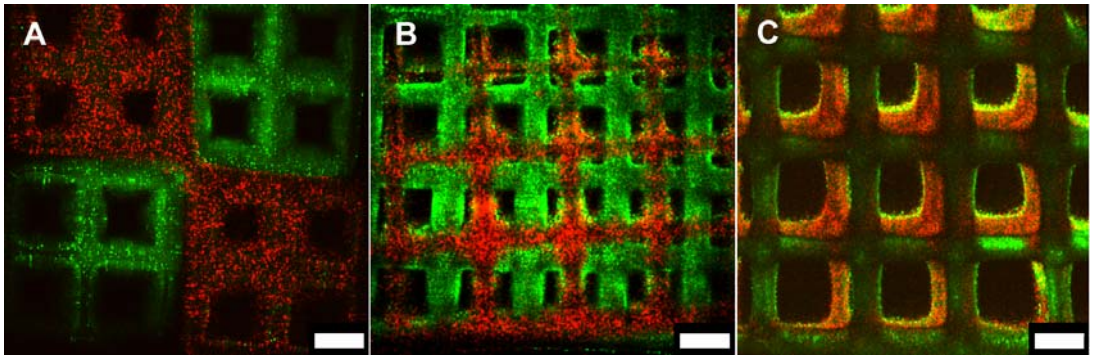

Figure 4.4 **Acryl-PEG-heparin was added to the PEGDA macromer solution at a concentration of 5.0 mM, and patterned-polymerized with the DMD μSL on one half of an entire scaffold, followed by extensive washing with PBS. Plain PEGDA macromer solution was then patterned-polymerized on the other half of the scaffold. Both solutions also encapsulated 10 μg/mL of FGF-2. Scaffolds were then placed in a 37°C incubator to allow any unbound FGF-2 to diffuse out of the scaffolds, while washing several times with PBS. Heparin moieties were stained blue using alcian blue staining as depicted in (A) through brightfield microscopy (10X objective). Immuno-histochemistry was performed to detect for bound FGF-2 and fluorescence microscopic images (B) shows that FGF-2 (red fluorescence) was only sequestered in areas that contained heparin (10X objective).**

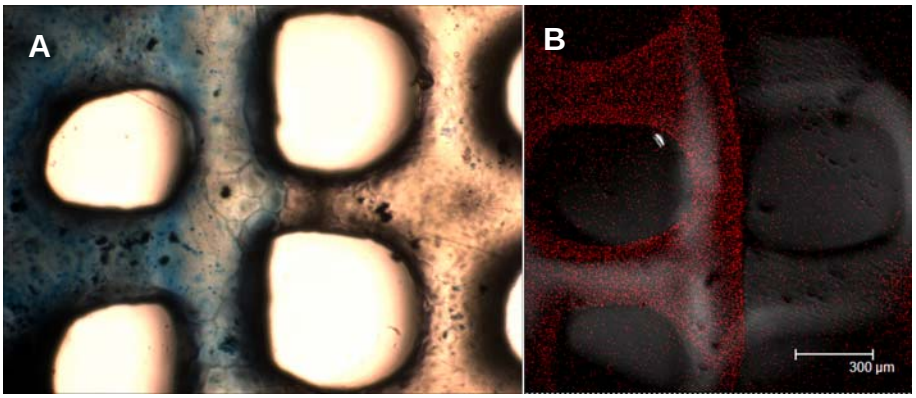

Figure 4.5 **Immuno-histochemistry of Conjugated Fibronectin. Fibronectin was covalently conjugated to scaffolds surfaces. Fluorescence micrographs show scaffolds immuno-stained for fibronectin. Biotinylated anti-fibronectin antibody and streptavidin-FITC were used to stain the microfabricated scaffolds following fibronectin conjugation. Figure A shows the successful covalent conjugation of fibronectin through the methacrylic acid macromer added during the fabrication process. The scaffold illustrated in figure B does not contain methacrylic acid and shows no conjugation (negative control). White scale bar represents 200 μm.**

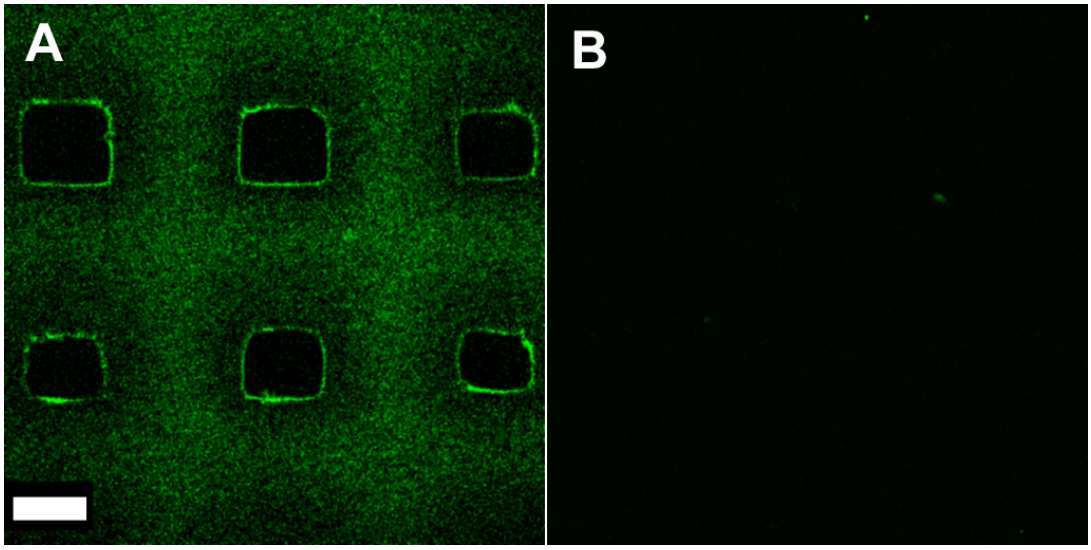

Figure 4.6. Viable Cell Encapsulation and Differentiation of Marrow-derived Cells. (A) Marrow-derived stromal cells remain viable following encapsulation in DMD μSL fabricated scaffolds. Scaffolds depicted in this figure were formulated with 100% (w/v) PEGDA in PBS and 0.1wt% Irgacure 2959. Prior to photo-polymerization, OP-9 marrow stromal cells were added to the macromer solution at a concentration of 5 x 10^6 cells/mL. After a 24 hour incubation period, 2μM calcein was added to cell-scaffold constructs, which stains viable cells green. Transmitted and fluorescent images captured from confocal microscopy were overlaid and shown in Figure A. Patterned scaffolds are capable of osteogenic differentiation of bone-marrow derived progenitor cells. White scale bar represents 200 μm. Figures (B-C) show fibronectin-conjugated scaffolds seeded with primary mMSCs at a density of 50,000 cells per scaffold. At 2-week and 4-week time points, scaffolds were removed from culture, paraffin embedded, and sectioned. These sections were stained with nuclear fast red and von Kossa. Brightfield micrographs (figure B with a 10X objective at 2-week time point and figure C with a 40X objective at 4-week time point) show extensive scaffold mineralization indicating osteogenic differentiation (von Kossa stain: black).

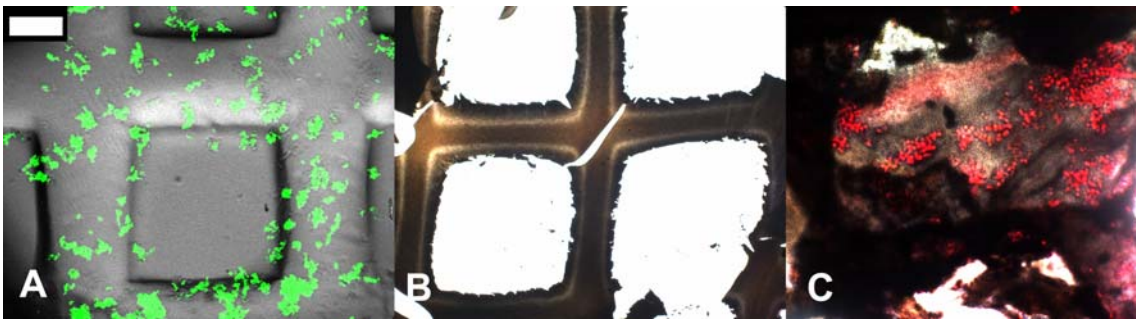

4.5 REFERENCES

1. Griffith, L.G., *Emerging design principles in biomaterials and scaffolds for tissue engineering.* Ann N Y Acad Sci, 2002. **961**: p. 83-95.
2. Sharma, B. and J.H. Elisseeff, *Engineering structurally organized cartilage and bone tissues.* Ann Biomed Eng, 2004. **32**(1): p. 148-59.
3. Orban, J.M., K.G. Marra, and J.O. Hollinger, *Composition options for tissue-engineered bone.* Tissue Eng, 2002. **8**(4): p. 529-39.
4. Richardson, T.P., et al., *Polymeric system for dual growth factor delivery.* Nat Biotechnol, 2001. **19**(11): p. 1029-34.
5. Williams, C.G., et al., *In vitro chondrogenesis of bone marrow-derived mesenchymal stem cells in a photopolymerizing hydrogel.* Tissue Eng, 2003. **9**(4): p. 679-88.
6. Nuttelman, C.R., M.C. Tripodi, and K.S. Anseth, *In vitro osteogenic differentiation of human mesenchymal stem cells photoencapsulated in PEG hydrogels.* J Biomed Mater Res, 2004. **68A**(4): p. 773-82.
7. Johnstone, B., et al., *In vitro chondrogenesis of bone marrow-derived mesenchymal progenitor cells.* Exp Cell Res, 1998. **238**(1): p. 265-72.
8. Maruo, S. and K. Ikuta, *New microstereolithography (Super-IH process) to create 3D freely movable micromechanism without sacrificial layer technique*, in *MHS'98: Proceedings of the 1998 International Symposium on Micromechatronics and Human Science*. 1998. p. 115.
9. Sachlos, E. and J.T. Czernuszka, *Making tissue engineering scaffolds work. Review: the application of solid freeform fabrication technology to the production*

of tissue engineering scaffolds. Eur Cell Mater, 2003. **5**: p. 29-39; discussion 39-40.

10. Zhang, X., X.N. Jiang, and C. Sun, *Micro-stereolithography of polymeric and ceramic microstructures.* Sensors and Actuators A, 1999. **77**: p. 149-156.
11. Vozzi, G., et al., *Fabrication of PLGA scaffolds using soft lithography and microsyringe deposition.* Biomaterials, 2003. **24**(14): p. 2533-40.
12. Bertsch, A., Lorenz, H., Renaud, P., *3D microfabrication by combining microstereolithography and thick resist UV lithography.* Sensors and Actuators A, 1999. **73**: p. 14-23.
13. Bertsch, A., Bernhard, P., Vogt, C., and Renaud, P., *Rapid Prototyping of Small Size Objects.* Rapid Prototyping Journal, 2000. **6**(4): p. 259-266.
14. Itoga, K., et al., *Cell micropatterning using photopolymerization with a liquid crystal device commercial projector.* Biomaterials, 2004. **25**(11): p. 2047-53.
15. Sun, C., Fang, N., Wu, D.M., and Zhang, X., *Projection micro-stereolithography using digital micro-mirror dynamic mask.* Sensors and Acutuators A-Physical, 2005. **121**(1): p. 113-120.
16. Mapili, G., et al., *Laser-layered microfabrication of spatially patterned functionalized tissue-engineering scaffolds.* J Biomed Mater Res B Appl Biomater, 2005. **75**(2): p. 414-24.
17. Kasturi, S.P., K. Sachaphibulkij, and K. Roy, *Covalent conjugation of polyethyleneimine on biodegradable microparticles for delivery of plasmid DNA vaccines.* Biomaterials, 2005. **26**(32): p. 6375-85.
18. Meirelles Lda, S. and N.B. Nardi, *Murine marrow-derived mesenchymal stem cell: isolation, in vitro expansion, and characterization.* Br J Haematol, 2003. **123**(4): p. 702-11.

19. Bryant, S.J. and K.S. Anseth, *Hydrogel properties influence ECM production by chondrocytes photoencapsulated in poly(ethylene glycol) hydrogels.* J Biomed Mater Res, 2002. **59**(1): p. 63-72.

20. Davis, K.A. and K.S. Anseth, *Controlled release from crosslinked degradable networks.* Crit Rev Ther Drug Carrier Syst, 2002. **19**(4-5): p. 385-423.

21. Metters, A.T., K.S. Anseth, and C.N. Bowman, *Fundamental studies of biodegradable hydrogels as cartilage replacement materials.* Biomed Sci Instrum, 1999. **35**: p. 33-8.

22. Halstenberg, S., et al., *Biologically engineered protein-graft-poly(ethylene glycol) hydrogels: a cell adhesive and plasmin-degradable biosynthetic material for tissue repair.* Biomacromolecules, 2002. **3**(4): p. 710-23.

23. Liu, V.A. and S.N. Bhatia, *Three-dimensional photopatterning of hydrogels containing living cells.* Biomedical Microdevices, 2002. **4**(4): p. 257-266.

24. Bryant, S.J., C.R. Nuttelman, and K.S. Anseth, *Cytocompatibility of UV and visible light photoinitiating systems on cultured NIH/3T3 fibroblasts in vitro.* J Biomater Sci Polym Ed, 2000. **11**(5): p. 439-57.

25. Peppas, N.A., *Hydrogels*, in *Biomaterials Science*, A.S.H. Buddy D. Ratner, Frederick J. Schoen, and Jack E. Lemons, Editor. 1996, Academic Press: San Diego. p. 60-64.

CHAPTER FIVE

Osteogenic Differentiation of Mesenchymal Stem Cells on DMD-fabricated Tissue Engineering Scaffolds

5.1 INTRODUCTION

Pioneered from micromachining and rapid prototyping technologies [1, 2], stereolithography (SL) has emerged as a widespread approach for studying cellular function at the microscale level and for creating tissue engineering scaffolds [2-5]. Traditional methods of studying cellular behavior involve homogenous conditions across planar, two-dimensional (2D) surfaces or porous polymer scaffolds that serve as three-dimensional (3D) platforms for stem cells to attach, proliferate, and differentiate [6, 7]. Studies in planar conditions or in bulk-fabricated scaffolds lack the complexity of cell-cell and cell-matrix interactions found *in vivo*. Pre-designed, intricate architectures, with micro-scale features closely mimicking the tissue defect, would better orchestrate stem cell differentiation within *in vitro* conditions.

A tissue-engineered construct responds to local stimuli found in their 3D environment, and micro-SL (μSL) can create scaffolds that closely mimic structural and biochemical cues present in native tissue. Micro-SL has the powerful capability of building 3D complex structures with specific pore sizes and shapes in a layer-by-layer fashion using photo-crosslinkable monomers. We have recently reported layer-by-layer micro-SL methods, laser- and digital micromirror-based, for creating intricate 3D scaffolds that spatially pattern multiple, biochemical agents within pre-determined regions [8, 9]. Specifically, the digital-micromirror device (DMD) based-SL system was shown to fabricate scaffolds in which mesenchymal stem cells (MSCs) efficiently

attached and differentiated into osteoblasts. A key advantage to this system is that intricate architectures could combine both spatial and controlled-release kinetics of biochemical factors, thus producing an ideal environment in which a single stem cell population could simultaneously differentiate into multiple cell types. Current stem cell engineering methods of creating hybrid tissues, as studied by Mao and colleagues [10, 11], involve pre-differentiating precursor cells into multiple cells types, such as osteoblasts and chondrocytes, and then encapsulating these cells within a single, compartmentalized scaffold. Although this method of creating composite tissues has proven to be successful, the homing of stem cells to a defect site *in vivo* and then simultaneously differentiating into various cell types have yet to be understood.

DMD μSL creates scaffolds in which stem cell behavior can be analyzed in a more complex form. Here we show how specific channel size and geometry of scaffolds can directly effect MSCs osteoblast differentiation. During *in vitro* osteogenesis low scaffold porosity size suppresses cell proliferation and induces cell aggregation, whereas *in vivo* bone in-growth is increased with structures that have higher porosity and pore dimensions. Pore size for bone formation is dependent upon the material used to fabricate the scaffold, and an excellent review of these materials and porosity studies is written by Karageorgiou and Kaplan [12]. Furthermore pore geometry has played a role in MSCs differentiation within *in vivo* cultures due to variations in vasculature and the delivery of oxygen [13].

Using poly(ethylene glycol) diacrylate (PEGDA) as the biomaterial, patterned scaffolds were created with various architectures, and changes in osteoblast gene expression levels were measured. PEGDA is a prevalent macromer used to develop tissue engineering scaffolds because, when crosslinked, this hydrophilic polymer network can imbibe a large volume of water while efficiently transporting cell nutrient and waste

throughout the structure [14, 15]. Because PEG is a non-fouling material, several chemical modifications to PEG-based polymers have been utilized to enable cell and extracellular matrix component (ECM) adherence for use as a biomimetic tissue engineering scaffold [16, 17]. Fibronectin was conjugated to the PEGDA scaffolds upon fabrication to allow MSCs to attach and then undergo differentiation. Furthermore we demonstrate how PEGDA mesh size alters gene expression levels of differentiated MSCs.

5.2 MATERIALS AND METHODS

5.2.1 Setup of the DMD-based Micro-stereolithography (DMD μSL) System

As previously reported, the micro-stereolithographic system was constructed by coupling a commercial projector (PB2120, BenQ, Taiwan) to a digital micro-mirror device (DMD™, Texas Instruments) with a modification to the lens component [9]. This stereolithography system created 3D scaffolds in a layer-by-layer fashion, in which the patterns of each scaffold layer were designed using Microsoft PowerPoint slides. These patterns were then translated to the DMD chip, acting as a dynamic photomask by illuminating the image onto the photo-curable macromer solution. The white regions of the pattern polymerized the macromer solution simultaneously while the black regions remained liquid. The photo-crosslinkable macromer solution was in a container placed on a motorized x-y-z stage.

The light as well as intensity was adjusted by the DMD chip, as defined by the pattern and pixel luminance, and went through a reduction-projection lens component to form a mask on the resin or macromer solution. The lens component was a fixed UV

focal lens (Edmunds Optics) that provided an increased focal length of the optical path, thereby providing a larger irradiation area as previously reported [9].

5.2.2 Photocurable PEGDA Polymer and Scaffold Fabrication

Poly(ethylene glycol) diacrylate (PEGDA Mw 3400, Nektar Therapeutics, Huntsville, AL) was used at a concentration of 100% (w/v) in phosphate buffered saline (PBS) and 0.1 wt% 2-hydroxy-1-[4(hydroxyethoxy)phenyl]-2-methyl-1-propanone (Irgacure 2959, Ciba Technologies) as the photo-crosslinkable macromer to fabricate the scaffolds. Prior to cell encapsulation and solution formulation, PEGDA was sterilized in a UV hood for a 12-hour period. Irgacure 2959 was initially made at concentration of 0.7% (w/v) in PBS and sterilized using a 0.2μm filter syringe before adding to PEGDA solution. Specific channel geometry and sizes used to create the 300 μm thick scaffolds are listed in **Table 5.1**. Dimension of scaffold wall thickness was kept constant at 400 μm for all scaffolds. When creating scaffolds with varying channel geometry, the channel volumes were also kept constant at 0.048 mm^3.

When encapsulating cells, acryl-PEG-RGD was added to the 100% (w/v) PEGDA macromer solution prior to cell addition and scaffold fabrication at concentrations of 0 mM, 0.5 mM, and 5.0 mM. Another method of incorporating cells within the scaffolds was through cell seeding after scaffold fabrication. This process involved adding methacrylic acid (MAA, Sigma Aldrich) to the PEGDA macromer solution at a molar ratio of 1:4 (MAA:PEGDA) prior to patterned UV irradiation, as illustrated in **Figure 5.1**. Scaffolds were rinsed several times with PBS to remove unreacted MAA. The carboxyl functional groups from MAA were used to form a stable amide bond with fibronectin and activated through 1-ethyl-3-(3-dimethylaminopropyl)/N-hydroxysulfosuccinimide chemistry (EDC/sulfo-NHS, Pierce Biotechnology Inc.,

Rockford, IL). Both EDC and sulfo-NHS were added to the scaffolds at 30*X* molar excess of MAA using 500 μL of 0.1 M MES buffer (pH 6.5). Carboxyl conversion to amine-reactive sulfo-NHS esters was performed for 2 hour at room temperature on a rotator before the addition of 1.5 mL fibronectin (10μg/mL), using low-adhesion protein binding microcentrifuge tubes (Fisher Scientific) to complete the reactions. Fibronectin conjugation was performed for a 24 hour period at room temperature. Scaffolds were sterilized in 70% ethanol for 30 minutes and rinsed several times with PBS prior to cell seeding to remove unreacted fibronectin and ethanol. Calcein AM staining (Molecular Probes, Eugene, OR), at a concentration of 2 μM was used to stain attached, viable D1 cells to scaffolds after a 4 hour seeding period. Digital images were captured of the scaffolds through fluorescence microscopy.

5.2.3 Cell Culture

D1 ORL UVA (ATCC, Manassas, VA) bone marrow progenitor cell line was used to study the tissue engineering properties of the scaffolds created by the DMD μSL system. D1 cells are characterized to differentiate into osteocytes, chondrocytes and adipocytes in the presence of appropriate stimuli and environment [18, 19]. Primary medium was composed of 10% (w/v) fetal bovine serum (ATCC) and 1% (w/v) penicillin streptomyocin (Gibco) in Dulbecco's Modified Eagle's Medium (ATCC). Osteogenic medium was formulated with the addition of 10 mM β-glycerophosphate, 10 mM ascorbic acid, and 10^{-8} M dexamethasone in primary medium (all chemicals from Sigma Aldrich, St. Louis, MO). D1 cells were passaged no more than 10 times during the course of the differentiation studies.

D1 cells were added to the photo-curable macromer solution at a density of 20 x 10^6 cells/mL. A total volume of 20 μL cell-macromer solution was placed on the stage of

the DMD μSL system and irradiated for 8 minutes (n=4). Unpolymerized cell-macromer solution that remained in liquid phase was rinsed off with sterile PBS. Scaffolds were placed in osteogenic medium and kept in a humidified incubator (37°C, 5% CO_2) for a 2 week culture period. Medium exchange was performed every 2-3 days.

In addition to using D1 mesenchymal stem cell line, the osteogenic potential of primary bone marrow-derived cells from mice was also analyzed. NIH guidelines for the care and use of laboratory animals were observed and all animal protocols were approved by the Institutional Animal Care and Use Committee (IACUC) at the University of Texas at Austin. BALB/c mice (7-30 wk old, Charles River Laboratories, Wilmington, MA) were sacrificed using carbon dioxide asphyxiation, and marrow from tibias and femurs were flushed out using a 27½- gauge needle and barrel with primary medium. Cells were washed via centrifugation, and viable cells were counted using trypan blue and a hemocytometer. MSCs culture was initiated by plating the cells at a density of 2×10^6 cells/cm^2 and cultured in a humidified incubator for 72 hour, at which point non-adherent cell were removed through medium exchange. Cell passaging upon plate confluency and medium exchange were performed every 2-3 days.

Primary MSCs, 2 weeks in culture, were trypsinized for 10 minutes at 37°C, centrifuged, counted, and seeded onto fibronectin-modified scaffolds at a density of 200,000 cells per scaffold (n=4). Sterile parafilm was placed in a non-treated cell culture plate to form a hydrophobic surface when seeding the cells, and the scaffolds were placed on top of the film. Cell attachment onto scaffolds was performed by suspending the cells in 50μL of medium on the constructs, thereby forming a "ball" due to an increased contact angle with the hydrophobic parafilm surface. Osteogenic medium was added to the culture plate after a 4 hour incubation period, and the parafilm was removed from culture.

5.2.4 PEG Hydrogel Mesh Size

Solid scaffold constructs (i.e. no channels) were photo-polymerized using the DMD μSL to determine polymer mesh size. Mesh size of DMD fabricated hydrogels was then compared to hydrogels polymerized using a long wave UV lamp. The Flory-Rehner theory, modified by Peppas and Merrill, was used to determine the number average molecular weight, M_c, of the polymer chain between two cross-links:

$$\frac{1}{Mc} = \frac{2}{Mn} - \frac{\frac{v}{V_1}\left(\ln\left(1 - v_{2,s}\right) + v_{2,s} + \chi_1 v_{2,s}^2\right)}{v_{2,r}\left(\left(\frac{v_{2,s}}{v_{2,r}}\right)^{1/3} - \left(\frac{v_{2,s}}{2v_{2,r}}\right)\right)},$$

in which M_n is the number average molecular weight of the uncrosslinked PEGDA, V_1 is the molar volume of the water, $v_{2,s}$ is the polymer volume fraction in the equilibrium swollen gel, v is the specific volume of the polymer, χ is the polymer-solvent interaction parameter, and $v_{2,r}$ is the polymer volume fraction in the relaxed state. The hydrogels were weighed in air and heptane immediately after crosslinking, after reaching swollen equilibrium, and after lyophilizing to obtain values for $v_{2,s}$ and $v_{2,r}$. Mesh size, ξ, was calculated using the following equation:

$$\xi = v_{2,s}^{-1/3}\left(\frac{2C_n Mc}{Mr}\right)^{1/2} l,$$

where C_n is the Flory characteristic ratio (4.0 for PEGs), l is the length of the bond along the polymer backbone (1.47 Å for PEGs), and M_r is the monomer molecular weight. PEGDA hydrogels are large hydrophilic polymer networks that can imbibe a large

volume of water. This inherent property of PEG provided the micro-porosity feature of these DMD μSL fabricated scaffolds, while the channel features created through patterning provided a macro-level of nutrient/waste transport, as illustrated in **Figure 5.2**.

5.2.5 Compression Strength Analysis of PEGDA Hydrogels

Poly(ethylene glycol) dimethacrylate (PEGDMA, Mw 1000, Polysciences Inc., Warrington, PA) at 10% and 100% w/v in PBS was used to determine compression moduli of bulk-polymerized scaffolds. The photoinitiator, Irgacure 2959, at 0.05 wt% concentration was added to the macromer solution, and a long wave UV lamp was used to initiate crosslinking for a 10 minute irradiation period. PEGDMA has similar properties to PEGDA, but was used in these preliminary experiments due to the inexpensive cost of the macromer. An Instron® In-Spec 2200 benchtop instrument was used at a rate of 0.001mm/s up to a maximum force of 100N to determine compression modulus data. Each PEGDA hydrogel was allowed to reach swollen equilibrium and measured for exact construct dimensions before analysis. Compressive moduli of the hydrogel scaffolds without cells were determined by computing the slope of the linear region of a stress/strain plot.

5.2.6 Cell Viability

Viability of D1 cells encapsulated in PEGDA hydrogels was compared using both the DMD μSL and UV lamp. The concentrations used when polymerizing with the UV lamp were 10% and 100% (w/v) PEGDA in PBS with 0.05 wt% Irgacure 2959. The only concentration formulated with the DMD μSL was 100% (w/v) PEGDA and 0.1 wt% Irgacure 2959. A total of 20 μL of macromer solution was used to create solid hydrogels

with a cell density of 20 x 10^6 D1/mL. Irradiation time for both systems was 8 minutes. Scaffolds were rinsed extensively with sterile PBS and incubated in primary medium for a 24 hour period. Methyl thiazolyl tetrazolium (MTT) assay was performed on these scaffolds and compared to a monolayer culture of D1 cells to calculate relative survival.

5.2.7 RNA Isolation and RT-PCR

Total RNA was isolated from the scaffolds through homogenization using TRIzol (Invitrogen), following the manufacturer's protocol. After drying the RNA pellet, it was re-suspended in nuclease-free water, and genomic DNA was removed using Abmion Turbo DNA-free™ kit. First strand cDNA was synthesized by reverse transcription (RT) using Superscript™ III kit (Invitrogen), following the manufacturer's protocol. The RT reaction was performed at 25°C for 10 minutes, 50°C for 50 minutes, and terminated at 85°C for at 5 minutes. Quantitative polymerase chain reaction (PCR) was performed using an ABI Prism® 7900 Real Time thermal cycler and HotStart DNA Taq polymerase with SYBR green/ROX PCR master mix (Superarray, Fredrick, Maryland). Primers for the housekeeping gene, or β-actin, collagen I, cbfα-1, and alkaline phosphatase, were used (Superarray, proprietary primers, sequences not disclosed). Collagen I, cbfα-1, and alkaline phosphatase were all specific to the osteoblast phenotype. β-actin was expressed in both differentiated and undifferentiated MSCs and therefore used as the housekeeping gene.

The PCR reactions were performed at 95°C for 10 minutes to activate the HotStart DNA Taq polymerase and then 40 cycles of 15 seconds at 95°C for denaturation, 60 seconds at 60°C for elongation, and 60 seconds at 72°C for elongation. Threshold cycle (C_T) values, as determined by the ABI PRISM® 7700 Sequence Detection System software, were used to analyze total product, and β-actin was used to

normalize relative gene expression for all the genes through the $2^{-\Delta\Delta CT}$ method [20]. Briefly, the normalized C_T value for the negative control (undifferentiated D1 cells in monolayer) was subtracted from the normalized C_T value for each of the samples, to obtain $\Delta\Delta C_T$, as illustrated in the following equation:

$$\Delta\Delta C_T = \Delta C_T \text{(sample)} - \Delta C_T \text{(negative control)},$$

where ΔC_T values for the samples and negative control are determined by:

$$\Delta C_T \text{(sample or negative control)} = C_T \text{ (gene of interest)} - C_T \text{(}\beta\text{-actin)}.$$

The latter equation normalizes the genes of interest (cbfα-1, collagen I, and alkaline phosphatase) using β-actin since this gene remains proportional to the amount of starting total RNA that was initially isolated from each sample. Gene expression fold differences were then determined via $2^{-\Delta\Delta CT}$ method, and the derivation of this analysis is described in detail by Livak and Schmittgen [20].

Negative controls to assess the quality of the primers and total RNA were also assessed, which consisted of running samples without template and synthesizing cDNA without reverse transcriptase, respectively. All samples were run in triplicate within the assay. End-point RT-PCR was completed by fractionating DNA amplicon on a 2% agarose gel containing ethidium bromide, and images were captured with a Molecular Imager FX (Bio-Rad Laboratories).

5.2.8 Statistical Analysis

All experiments were at least performed in triplicate. Results were reported as mean ± standard error. Statistical significance was determined by analysis of variance (ANOVA single factor) and set as $P < 0.05$.

5.3 RESULTS

5.3.1 Cell Viability

Cell viability of encapsulated D1 cells were evaluated with bulk hydrogels polymerized with either the UV lamp or DMD μSL system. These absorbance results show that after a 24 hour incubation period, cell viability was similar within all the PEGDA parameters tested (**Figure 5.3**). Viability was similar between the DMD μSL and UV lamp fabricated scaffolds at 100% (w/v) PEGDA. Because 10% (w/v) concentration of PEGDA in PBS is generally used in literature for encapsulating cells, we wanted to determine if cell viability is affected when using a higher PEGDA concentration. These optical density (OD) results indicated that there is approximately a 22% relative survival difference between 10% and 100% PEGDA concentrations, with 10% PEGDA having the higher survival rate. Ideally, relative survival (%) would be determined by comparing the OD values to a monolayer culture of D1 cells; however MTT metabolism would not be comparable since MTT crystals require diffusion through PEGDA hydrogels. In this case, absolute OD values were used to compare cell viability between the PEGDA concentrations.

5.3.2 Differentiation of D1-encapsulated Scaffolds

After a 2 week time point, monolayer D1 cells in osteogenic culture expressed all of the osteoblast genes studied as shown through end-point RT-PCR in **Figure 5.4**. All bands were present for the bone marker genes analyzed: alkaline phosphatase, cbfα-1, and collagen I. Because these osteoblast-specific genes were observed for this particular

immortalized cell line in monolayer culture, cell differentiation within 3D polymer scaffolds using the DMD μSL system were investigated. Gene expression was analyzed for DMD-fabricated scaffolds encapsulating D1 cells after 2 weeks in osteogenic medium, and these results are depicted in **Figure 5.5**. No specific gene expression trend was observed between the samples studied. Gene expression analysis was also performed on undifferentiated D1 cells (data not shown). Basal amounts of collagen I and cbfα-1 mRNA were observed, but no alkaline phosphatase activity was found; therefore relative gene expression of the scaffolds when compared to undifferentiated D1 cells was observed (except for the triangle channel), as illustrated in **Figure 5.5C**. However the absolute amount of alkaline phosphatase amplicon was not abundant to show the presences of bands in end point RT-PCR (**Figure 5.5D**).

Based on previous studies found in literature, the high PEGDA concentration used in these DMD μSL studies was speculated to be the underlying disadvantage to the design of the scaffolding system. To investigate this hypothesis, osteoblast gene expression was studied for D1 cells encapsulated in hydrogels of increasing PEGDA concentration. Mesh sizes of bulk-polymerized scaffolds were calculated and illustrated in **Table 5.2**. As expected, the PEGDA concentration with the highest mesh size was determined to be 10% (w/v), and the one with the lowest mesh was determined to be 100% (w/v). Furthermore, the mesh sizes for scaffolds created with the DMD μSL were determined to be similar to mesh sizes of scaffolds created with the UV lamp. Because PEGDA scaffolds take in a large amount of water in aqueous environments, it was imperative to calculate the mesh sizes of these scaffolds and to determine how much they varied at different polymer concentrations. This intrinsic property of PEG-based scaffolds was used as the micro-level porosity of DMD μSL fabricated scaffolds.

Bulk-polymerized scaffolds were fabricated using a long wave UV lamp, and after a 2 week culture in osteogenic medium, total RNA was isolated and real time RT-PCR was performed to determine the presence of the bone-specific markers. **Figure 5.6** illustrates real time RT-PCR and end-point gel electrophoresis results achieved with these bulk-polymerized PEGDA scaffolds. As PEGDA concentration increased from 10% to 100% (w/v), collagen I and cbfα-1 fold changes also increased, when compared to undifferentiated D1 cells (**Figures 5.6A and 5.6B**). On the contrary, alkaline phosphatase expression fold change decreased with increasing PEGDA concentration (**Figure 5.6C**). Gel electrophoresis of the generated amplicons for each gene was performed (**Figure 5.6D**) and compared to 100bp DNA ladder. All of the genes analyzed were present for all PEGDA concentrations, except for alkaline phosphatase in the 50, 80, and 100% (w/v) PEGDA concentrations. Based on these end point gel electrophoresis results, it was concluded that encapsulating D1 cells at a high PEGDA concentration greater than 30% (w/v) could inhibit the osteogenic differentiation capacity of D1 cells, and therefore a different method of cell integration within the micro-fabricated scaffolds had to be used.

5.3.3 Compression Moduli for PEGDA Hydrogels

Young's moduli were determined to be 33 kPa and 655 kPa for 10% and 100% w/v PEGDMA in PBS hydrogels, respectively, as depicted in **Figure 5.7**. The 100% w/v PEGDMA hydrogels were observed to be significantly higher than 10% w/v PEGDMA hydrogels. The higher PEGDMA concentration was determined to be 20 times more than the lowest PEGDMA bulk-polymerized scaffolds evaluated in our studies, which could contribute to the variations in differentiation potential of encapsulated MSCs.

5.3.4 Differentiation of D1-seeded Cells onto DMD-fabricated Scaffolds

D1 cells successfully attached to PEGDA:MAA scaffolds modified with fibronectin, as depicted in **Figure 5.8**. Green fluorescence due to calcein AM staining showed that cells adhered to scaffold surfaces and remain viable upon seeding. To ensure that the immortalized D1 cell line still maintained stem cell functionality in 3D cultures, this cell line was compared to marrow-derived progenitor cells, a more commonly used source of MSCs found in literature. D1 cells and marrow-derived cells were seeded at the same density to separate, fibronectin-modified, DMD-fabricated scaffolds and cultured in osteogenic medium for 2 weeks. **Figure 5.9A** shows end point RT-PCR results obtained from the D1 and marrow-derived seeded scaffolds; bands for all osteoblasts genes were present. Real time RT-PCR was performed, and the ΔC_T value for each MSCs population was used to determine that D1 cells had a higher osteoblast gene expression than primary marrow-derived MSCs. D1 ΔC_T values were then compared to the ΔC_T values of marrow-derived MSCs, as illustrated in **Figure 5.9B**. Gene expression fold changes for D1 showed that collagen I, cbfα-1, and alkaline phosphatase were expressed 2, 8, and 10 times more than marrow-derived MSCs, respectively.

Because D1 cells demonstrated increased osteoblast expression over marrow-derived MSCs, this cell population was therefore selected to study osteogenic differentiation of seeded cells onto DMD-fabricated scaffolds. Both real time (**Figures 5.10A-C**) and end-point (**Figure 5.10D**) RT-PCR results depict positive osteoblast gene expression results when D1 cells were seeded onto DMD-fabricated scaffolds and cultured in osteogenic medium for 2 weeks. From the channel parameters studied and listed in **Table 5.1**, the optimum channel size was determined to be 0.4 mm by 0.4 mm and with a square geometry. These particular channel parameters had the highest gene

expression fold changes for all of the genes analyzed than the other groups studied, when compared to undifferentiated D1 cells. Furthermore D1 cells seeded onto DMD μSL patterned scaffolds showed higher gene expression levels than D1-encapsulated scaffolds.

5.4 DISCUSSION

Photolithographic patterning of hydrogel scaffolds is a popular fabrication method since cell placement can be done in a controlled manner when using photo-crosslinkable monomers and light to initiate the gelation reaction. These photolithographic patterning methods can be used to effectively create multi-layered cell-hydrogel structures, but require the use of spacers and physical photomasks, that take time and plotters to fabricate [21, 22]. As previously reported, DMD μSL can create scaffolds with precisely controlled channel size and geometry using a simple computer-aided process that can create dynamic photomasks through Microsoft PowerPoint. Multi-layered scaffolds with spatially distributed factors in the same layer and across different layers can be readily fabricated using this stereolithography technique [9]. Here we present a more intensive study of specific scaffold properties, easily fabricated using DMD μSL, that optimize the osteogenic differentiation of MSCs.

Osteoprogenitor cells have predominantly been isolated from the bone marrow. Immortalized D1 cell line, cloned from a multipotent mouse bone marrow stromal precursor, was used to study channel parameters of DMD-fabricated scaffolds. These D1 cells, like marrow-derived precursor cells, have osteogenic, chondrogenic, and adipogenic differentiation potential. RT-PCR results illustrated osteogenic gene expression in 2D culture and proved this particular cell type can commit exclusively into the bone pathway.

Previous studies found in literature have successfully encapsulated MSCs within photo-polymerizable PEGDA at low concentrations (i.e., 10 to 30% w/v) and confirmed either osteogenic or chondrogenic differentiation [17, 23, 24]. We show that increased PEGDA concentrations, specifically macromer concentrations over 30%, show decreased alkaline phosphatase expression, an enzymatic activity responsible for bone matrix calcification by osteoblasts. Because alkaline phosphatases are concentrated within the cell surfaces, high binding affinities to positively charged calcium molecules occur, causing matrix calcification. Since lower PEGDA concentrations have larger mesh sizes due to decreased polymer crosslinking, nutrient and waste diffusion can occur more easily. Transport of β-glycerophosphate, ascorbic acid, and other proteins necessary for bone matrix deposition is more readily available with 10% and 30% (w/v) PEGDA hydrogels, thus increasing alkaline phosphatase activity. β-glycerophosphate acts as an organic phosphate around cells, thus triggering increased alkaline phosphatase activity and matrix calcification within *in vitro* cultures. Additionally ascorbic acid also acts to increase collagen secretion within the bone matrix.

Contrary to what is seen with alkaline phosphatase, both collagen I and cbfα-1 gene expression, also specific to osteoblasts, decrease with decreasing PEGDA concentration. Collagen I is the major extracellular matrix protein of bone, making up ~90% of the total organic bone matrix; therefore this protein is the most common marker for the osteoblast phenotype [25]. Cbfα-1 is a transcription factor that regulates osteocalcin production and marks the early development of osteoblasts precursors [26, 27]. Interestingly, scaffolds with the higher PEGDA concentrations also appear to have increased expressions of collagen I and cbfα-1, another inconsistent result from what was expected. We speculate that this conflicting trend with collagen I and cbfα-1 gene expression could be due to that D1 cells in the lower concentrated PEGDA scaffolds are

at a more advanced stage of osteoblast differentiation; therefore mRNA production for collagen I and cbfα-1 decreased as these cells became more committed in phenotype. Future experiments involve looking at longer culture periods in osteogenic medium to determine if any of these osteoblast-specific genes would undergo a different trend.

In addition to mesh size differences, we also speculate that changes in hydrogel mechanical stiffness may also contribute to variations in the differentiation potential of encapsulated MSCs. Increasing PEG macromer concentrations from 10% to 100% (w/v) in PBS also increases Young's moduli within the hydrogels (from ~33 kPa to ~655 kPa), thus changing the local mechanical environment to which the encapsulated cells respond. Osteocytes *in vivo* are known to respond to local mechanical stimuli within the bone matrix, and signal to osteoblasts, based on these specific mechanical forces, for bone remodeling via gap junctions and mitogen-activated protein kinase pathway (MAPK) signaling pathway [28]. Increased mechanical stiffness of 50-100% (w/v) PEGDA hydrogels could have reduced the rate of osteoblast maturation, and future work would involve evaluating effects of local mechanical changes on the differentiation pathways of MSCs.

These initial studies with bulk-polymerized scaffolds and their effects on the osteogenesis of MSCs allowed us to recognize a drawback of the DMD μSL system. Differentiation capacity of MSCs into osteoblasts decreased when encapsulating D1 cells at high PEGDA concentrations. The current DMD μSL set-up can only encapsulate cells and photo-polymerize 100% (w/v) PEGDA scaffolds at this specific concentration without losing feature resolution. Longer curing times could allow photo-polymerization of PEGDA at lower concentrations without losing feature resolution; however, cell viability would decrease due to the amount of time exposed to a harsh, non-culture environment.

Although this drawback does exist with the DMD μSL system, another option for cell incorporation within the scaffolds is available and was demonstrated to be successful. Cell seeding after scaffold fabrication was used to integrate cells within the spatially patterned 3D scaffolds. After 2 weeks in osteogenic medium, D1 cells seeded within the 3D scaffolds successfully expressed all the osteoblast-specific genes analyzed. Keeping scaffold wall dimensions and thickness constant, the optimum channel parameters found to have the highest gene expression fold change, when compared to undifferentiated D1 cells, are with a square geometry and channel dimension of 0.4 mm by 0.4 mm. Optimum pore dimensions of scaffolds for the formation of bone have also been characterized in literature to range from 300-400 μm (or 0.3-0.4 mm) [29], and this is consistent with what we find within our micro-fabricated scaffolds. Pore dimension within tissue engineered constructs is a critical aspect to the types of tissues being generated as this important feature is also incorporated in physiological environments. Cancellous or trabecular bone, specifically, is known to have such similar pore geometries within their sponge-like matrix. Mimicking this micro-scale feature is essential to *in vitro* 3D cultures that aim to differentiate MSCs into osteoblasts.

Furthermore, effects of geometrical shape variations in scaffold porosities within *in vitro* systems have to be reported, but seem to alter MSCs differentiation behavior, as observed in our studies. Perhaps curved surfaces as seen with the circle channel geometry, when compared to flat surfaces (square and triangle channels), may cause differences in intracellular signaling due to changes in cell shape and attachment. Intracellular signaling can be influenced by the surfaces to which they are attached due to variations in fibronectin orientation. Curved surfaces could present fibronectin in a more clustered form, thus changing anchorage through the amount of cell focal adhesions created. Additional studies with scaffold pore geometry within *in vivo* systems found in

literature, demonstrate that pore shape, specifically honeycomb architectures, do affect bone formation due to vascularization of the tissue [13]. These studies, however, only discuss a single, scaffold geometry and shows that increased tissue formation was exclusively due to the length and continuity of the pores. Future work will focus on how channel and scaffold shape directly affects stem cell behavior within multi-layered constructs.

Though we did observe decreased osteoblast gene expression levels with D1-encapsulated scaffolds, we have demonstrated another promising method for integrating and differentiating stem cells into the patterned scaffolds by method of seeding. Other limitations to the DMD μSL are light scattering and increased curing depth during the photo-curing process of several layers. Problems with light scattering affects previous layers of multi-layered scaffolds, causing macromer crosslinking to decrease feature resolution within these existing layers; therefore intricate structures requiring many layers causes the initial layers to lose interconnective porosity. This drawback, however, can be resolved using a UV quencher dye that absorbs scattered light within the bottom regions of the polymer solution. Additionally a dye quencher can act to decrease the curing depth of the projected light at the focal plane, thereby providing thinner, or more resolved, layers. These multi-layered scaffolds are currently underway using MSCs to study differences in total porosity and interconnective pathways within the structures.

Furthermore, because RNA isolation and RT-PCR was performed on whole, homogenized scaffolds, undifferentiated MSCs could also be present within the constructs along with differentiated osteoblasts. Future experiments consist of *in situ* hybridization with these multi-layered, spatially patterned scaffolds to determine which regions had optimal differentiation or if a differentiation gradient can be observed throughout a multi-layered scaffold.

Table 5.1. DMD μSL Microfabricated Scaffold Channel Parameters

		Total Channel Volume
Geometry	square	0.048 mm^3
	circle	0.048 mm^3
	triangle	0.048 mm^3
Size	200μm x 200μm	0.012 mm^3
(surface area)	400μm x 400μm	0.048 mm^3
	600μm x 600μm	0.108 mm^3

Table 5.2 Mesh Size Calculations of PEGDA (3400) Hydrogels

PEGDA Concentration (w/v)	Mesh Size ± Error (Å)
10%; long wave lamp	46.7 ± 4.05 *
30%; long wave lamp	25.3 ± 1.1
50%; long wave lamp	26.4 ± 4.8
80%; long wave lamp	25.4 ± 2.1
100%; long wave lamp	22.0 ± 1.8
100%; DMD	28.4 ± 2.7

(n=4, *: $P < 0.02$)

Figure 5.1. Fibronectin Conjugation to MAA:PEGDA DMD-fabricated Scaffolds

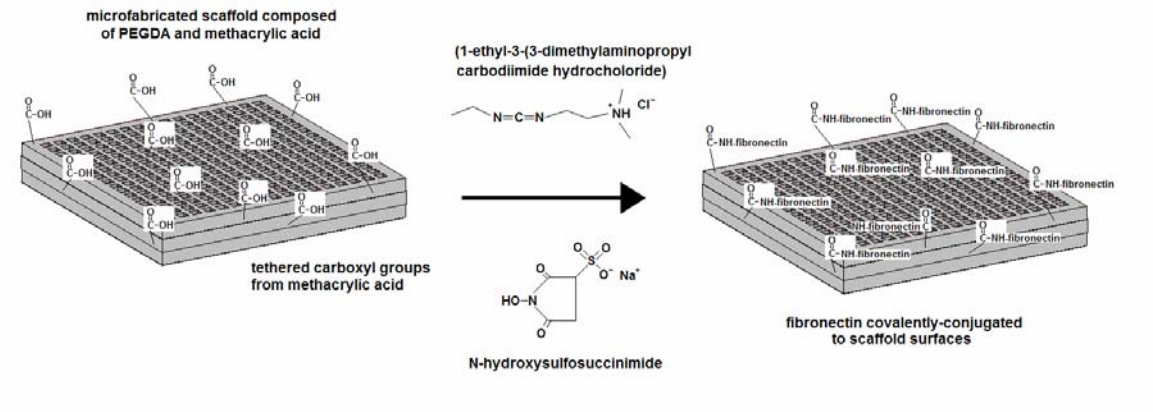

Figure 5.2 Schematic of Micro- and Macro-Porosities of DMD μSL Fabricated Scaffolds

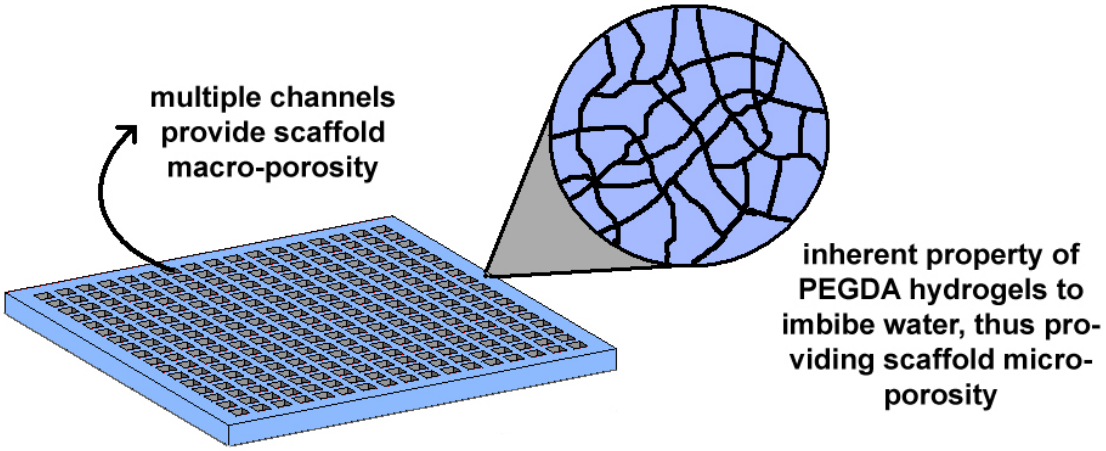

Figure 5.3 Cell Viability: UV Lamp versus DMD μSL Fabrication. Cell viability of D1-encapsulated scaffolds created by UV lamp or DMD μSL was determined through MTT assay. Scaffolds encapsulating D1 cells at a density of 20 x 10^6 cells/mL were bulk-polymerized using both methods, and optical density (OD) values were determined. The scaffolds were incubated in primary medium for a 24 hour period before the addition of MTT. At 100% (w/v) PEGDA concentration, cell viability was similar using both polymerization methods. The 10% (w/v) PEGDA scaffold photo-polymerized with the UV lamp had the highest cell viability. Bars represent standard error of n=4 samples, and significant difference was not observed between the sample conditions.

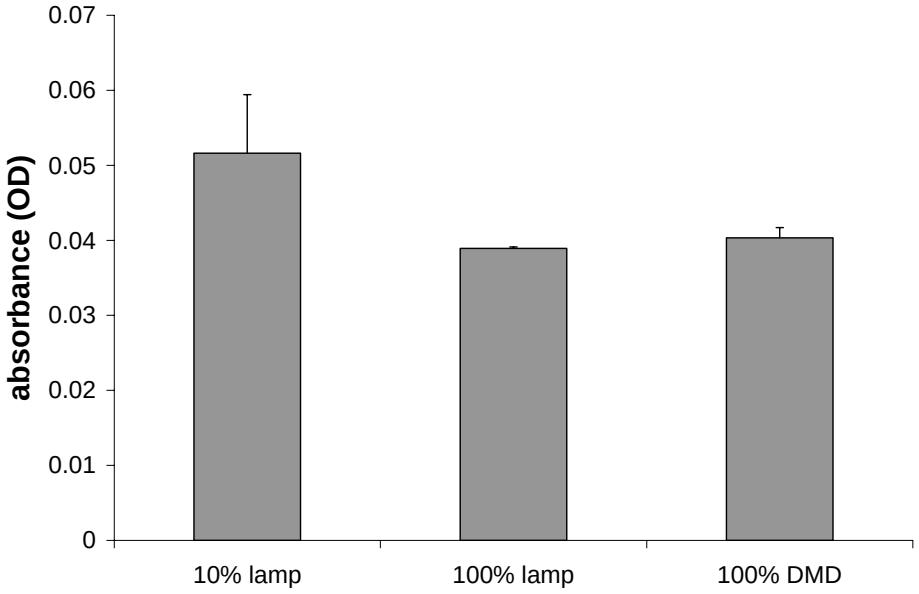

Figure 5.4. Gene expression analysis of differentiated D1 cells. End-point RT-PCR of D1 cells cultured in osteogenic medium for 2 weeks. Bands for osteogenic-specific genes (alkaline phosphatase, collagen I, and cbfα-1) as well as the β-actin housekeeping gene were present, indicating that D1 immortalized cell line effectively differentiated into osteoblasts. "No RT" lane showed that DNA contamination was not present during RT-PCR. Amplicon product sizes for β-actin, alkaline phosphatase, cbfα-1, and collagen I are 154, 150, 101, and 122, respectively.

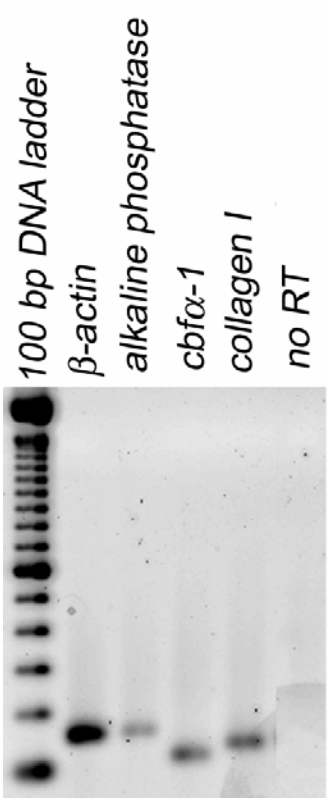

Figure 5.5 **Gene expression analysis of D1 cells encapsulated in patterned PEGDA scaffolds fabricated by DMD μSL. The channel parameters studied for these scaffolds are listed in Table 5.1. All osteoblast specific genes were expressed with no specific trend observed for each pattern. Collagen I is depicted in (A), cbfα-1 is depicted in (B) and alkaline phosphatase is depicted in (C). End point RT-PCR is depicted in (D). The end point RT-PCR results do not show alkaline phosphatase expression. Because there was no basal level of alkaline phosphatase activity in undifferentiated D1 cells, relative gene expression fold changes of scaffolds were still observed with real time PCR analysis. Alkaline phosphatase amplicon generation is not abundant to show the presence of bands when performing end point RT-PCR. Bars represent standard error of n=3 samples. Collagen I expression for channel dimension of 0.2 mm by 0.2 mm was found to be significantly lower than 0.6 mm by 0.6 mm channels dimensions (*: $P < 0.01$). Alkaline phosphatase expression for circle channel geometry was observed to be significantly higher than both the square and triangle channel geometries (#: $P < 0.01$).**

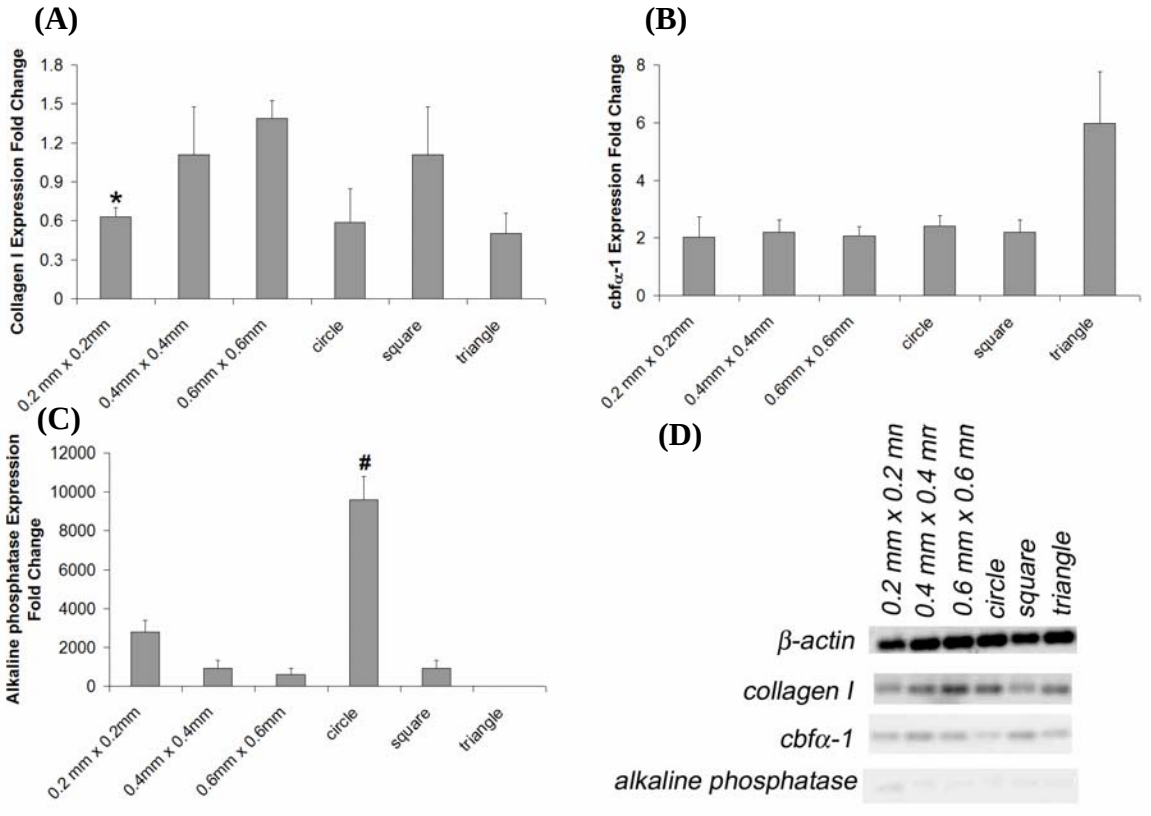

Figure 5.6 Gene expression analysis for D1 cells encapsulated in bulk-polymerized PEGDA scaffolds using a long UV lamp. Concentrations studied were 10, 30, 50, 80 and 100% PEGDA (w/v) in PBS with 0.05 wt% Irgarcure 2959 photoinitiator and 20 x 10^6 D1 cells/mL. Collagen I (figure A) and cbfα-1 (figure B) gene expressions increase with increasing PEGDA concentration, whereas alkaline phosphatase (figure C) is only seen in 10 and 30% PEGDA concentrations. Figure (D) depicts an image of end-point agarose gel illustrating the genes present for each PEGDA concentration. Bars represent standard error of n=3 samples. Collagen I expression for 100% w/v PEGDA hydrogels was significantly higher than all of the other concentrations (*: $P < 0.05$). The 10 and 30% PEGDA hydrogels were significantly lower than the 50 and 100% w/v PEGDA (#: $P < 0.05$) when comparing collagen I expression. Cbfα-1 expression from 10 and 30% w/v PEGDA concentrations was significantly lower than the 100% (&: $P < 0.03$). Alkaline phosphatase expression was significantly highest for 10% w/v PEGDA when compared to all of the other PEGDA concentrations (@: $P < 0.05$). Lastly 50% was significantly higher than 80% (! : $P < 0.03$), and 80% was significantly lower than 100% w/v PEGDA (^ : $P < 0.02$) when comparing alkaline phosphatase expression in (C).

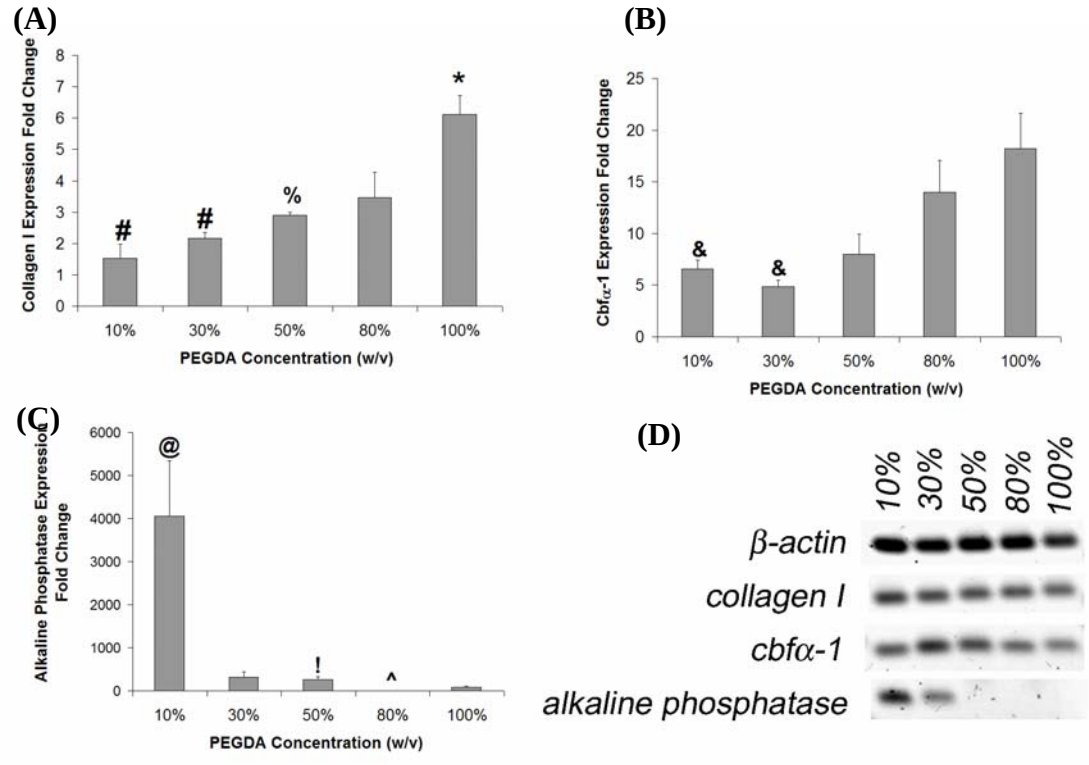

Figure 5.7 Compression strengths of 10% and 100% w/v PEGDMA bulk-polymerized hydrogel scaffolds. Young's moduli were determined for the lowest and highest PEG macromer solutions used in these experiments. The 10% and 100% (w/v) PEGDMA solutions were determined to be approximately 33 kPa and 655 kPa, respectively and found to be significantly different (* : $P < 0.01$). Bars indicate standard error of n=3 samples. This significant difference in compression modulus could affect the rate of MSCs differentiation into osteoblastic cells.

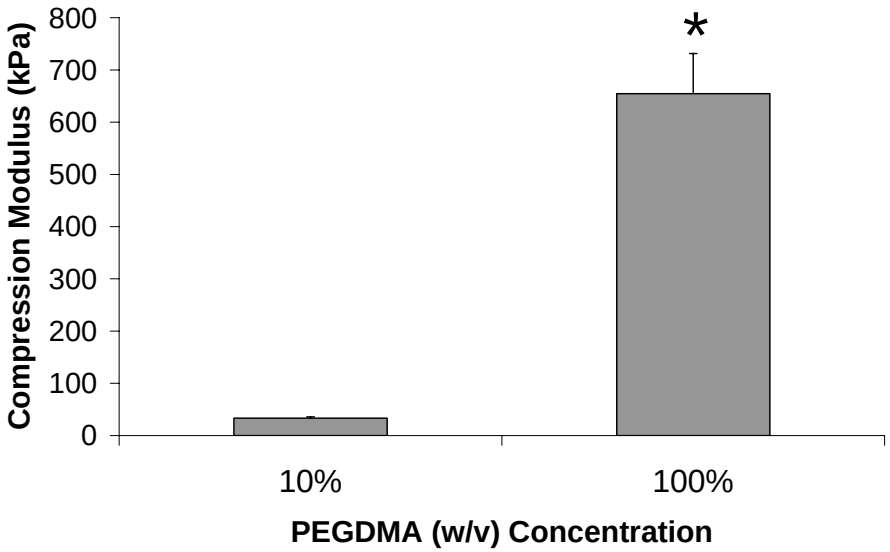

Figure 5.8 **Fluorescence micrograph of D1 seeded cells onto fibronectin-modified scaffolds. Phase contrast (A) and fluorescence microscopic (B) digital images captured after 24 hour D1 cell seeding onto fibronectin-modified PEGDA scaffolds (taken with a 10X objective). Calcein AM stained viable cells green as seen in (B). Scaffolds were fabricated using 1:10 molar ratio of PEGDA:MAA using DMD μSL. EDC/sulfo-NHS chemistry was used to activate the carboxyl group of MAA, and thus fibronectin was successfully conjugated to the amine reactive functional group; D1 cells efficiently attached to DMD-fabricated scaffolds. White bar is equal to 200 μm.**

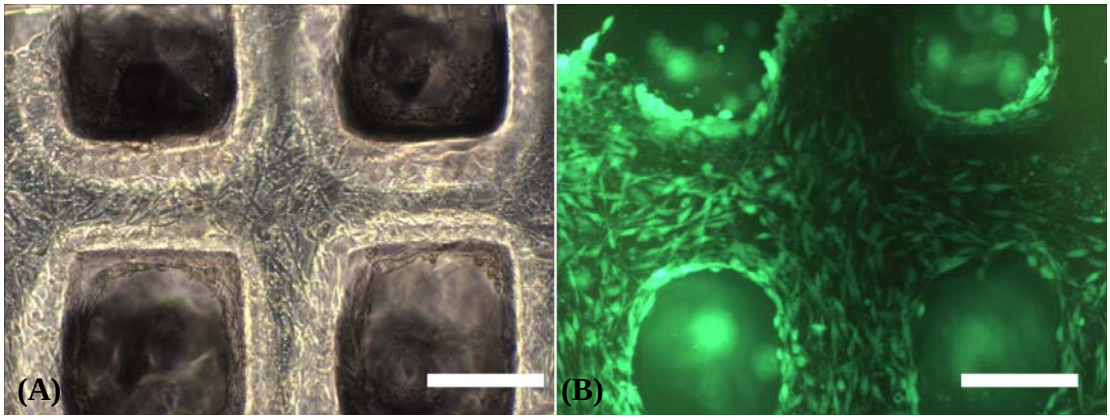

Figure 5.9 Gene expression analysis: D1 versus primary MSCs. D1 and primary MSCs were seeded onto separate fibronectin-modified DMD μSL fabricated scaffolds. After 2 weeks in osteogenic culture, total RNA was removed, and gene analysis was investigated through real time RT-PCR and gel electrophoresis. Comparing the ΔC_T gene values of each cell type showed that the immortalized D1 cell line expressed higher levels of each gene during PCR than the primary bone-marrow derived cells. Figure (A) illustrates an end-point agarose gel for both cell types, indicating that all osteogenic genes studied were expressed. Figure (B) depicts a quantitative measure of the gene expression fold change for D1 cells when compared to primary bone marrow-derived cells. Bars represent standard error of n=4 samples (*: $P < 0.02$).

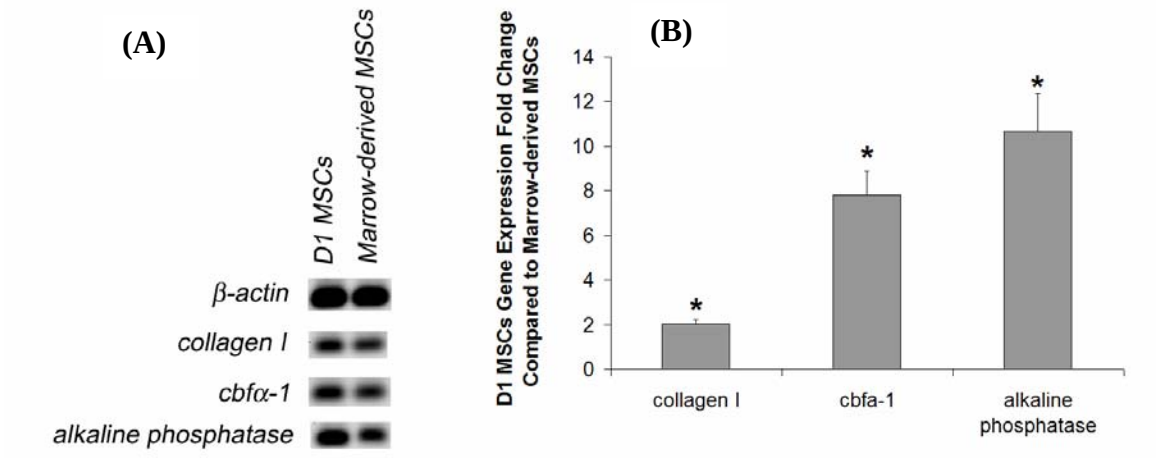

Figure 5.10 Effects of channel size and geometry on the osteogenesis of D1 Cells seeded onto DMD μSL fabricated scaffolds. Scaffold channel size and geometry were varied, and D1 cells were seeded onto DMD μSL fabricated scaffolds. After 2 weeks in culture, end-point and real time RT-PCR were performed to determine gene presence and gene expression fold changes compared to undifferentiated D1 cells. Based on real time PCR results (A-C), 0.4 mm by 0.4 mm channel size and square channel geometry had the highest gene expression fold change for all the bone-specific genes analyzed. All four genes were present for all channel parameters studied (D). Bars represent standard error of n=4 samples. Collagen I and cbfα-1 expressions were significantly highest for 0.4 mm by 0.4 mm within the varying channel dimension group (* : $P < 0.03$). Cbfα-1 expression was significantly highest the for square channel geometry within the varying channel shape group (* : $P < 0.03$). Collagen I and cbfα-1 expressions for 0.2 mm by 0.2 mm channel dimension was significantly lower than 0.4 mm by 0.4 mm (#: $P < 0.03$). Collagen I and cbfα-1 expressions for the circle channel geometry was significantly lower than the square channel geometry (% : $P < 0.05$). No significant difference was observed in (C).

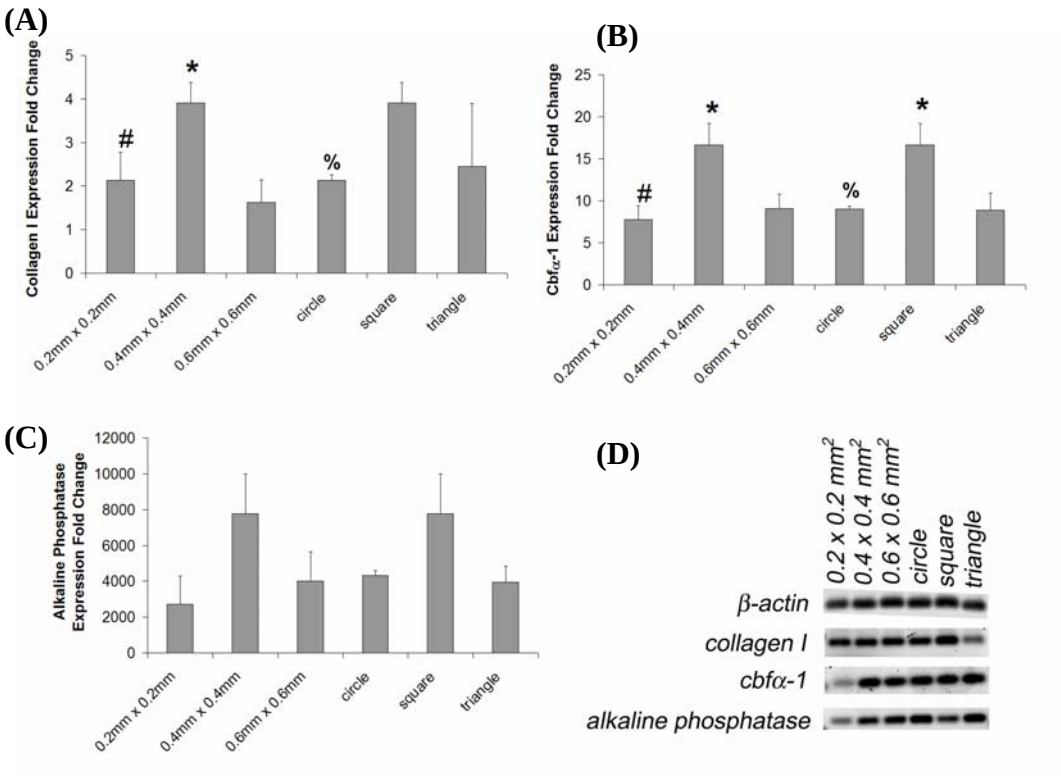

5.5 REFERENCES

1. Kawata, S., et al., *Finer features for functional microdevices.* Nature, 2001. **412**(6848): p. 697-8.
2. Khademhosseini, A., et al., *Microscale technologies for tissue engineering and biology.* Proc Natl Acad Sci U S A, 2006.
3. Zhang, H., et al., *Microrobotics and MEMS-based fabrication techniques for scaffold-based tissue engineering.* Macromol Biosci, 2005. **5**(6): p. 477-89.
4. Hollister, S.J., *Porous scaffold design for tissue engineering.* Nat Mater, 2005. **4**(7): p. 518-24.
5. Weigel, T., G. Schinkel, and A. Lendlein, *Design and preparation of polymeric scaffolds for tissue engineering.* Expert Rev Med Devices, 2006. **3**(6): p. 835-51.
6. Li, W.J., et al., *A three-dimensional nanofibrous scaffold for cartilage tissue engineering using human mesenchymal stem cells.* Biomaterials, 2005. **26**(6): p. 599-609.
7. Ren, J., et al., *Repair of mandibular defects using MSCs-seeded biodegradable polyester porous scaffolds.* J Biomater Sci Polym Ed, 2007. **18**(5): p. 505-17.
8. Mapili, G., et al., *Laser-layered microfabrication of spatially patterned functionalized tissue-engineering scaffolds.* J Biomed Mater Res B Appl Biomater, 2005. **75**(2): p. 414-24.
9. Lu, Y., et al., *A digital micro-mirror device-based system for the microfabrication of complex, spatially patterned tissue engineering scaffolds.* J Biomed Mater Res A, 2006.

10. Alhadlaq, A. and J.J. Mao, *Tissue-engineered osteochondral constructs in the shape of an articular condyle.* J Bone Joint Surg Am, 2005. **87**(5): p. 936-44.
11. Rahaman, M.N. and J.J. Mao, *Stem cell-based composite tissue constructs for regenerative medicine.* Biotechnol Bioeng, 2005. **91**(3): p. 261-84.
12. Karageorgiou, V. and D. Kaplan, *Porosity of 3D biomaterial scaffolds and osteogenesis.* Biomaterials, 2005. **26**(27): p. 5474-91.
13. Jin, Q.M., et al., *Effects of geometry of hydroxyapatite as a cell substratum in BMP-induced ectopic bone formation.* J Biomed Mater Res, 2000. **52**(4): p. 491-9.
14. Peppas, N.A., *Hydrogels*, in *Biomaterials Science*, A.S.H. Buddy D. Ratner, Frederick J. Schoen, and Jack E. Lemons, Editor. 1996, Academic Press: San Diego. p. 60-64.
15. Elisseeff, J., et al., *Advances in skeletal tissue engineering with hydrogels.* Orthod Craniofac Res, 2005. **8**(3): p. 150-61.
16. Tiller, J.C., et al., *Improving biomaterial properties of collagen films by chemical modification.* Biotechnol Bioeng, 2001. **73**(3): p. 246-52.
17. Nuttelman, C.R., M.C. Tripodi, and K.S. Anseth, *Synthetic hydrogel niches that promote hMSC viability.* Matrix Biol, 2005. **24**(3): p. 208-18.
18. Cui, Q., G.J. Wang, and G. Balian, *Pluripotential marrow cells produce adipocytes when transplanted into steroid-treated mice.* Connect Tissue Res, 2000. **41**(1): p. 45-56.
19. Dahir, G.A., et al., *Pluripotential mesenchymal cells repopulate bone marrow and retain osteogenic properties.* Clin Orthop Relat Res, 2000(379 Suppl): p. S134-45.

20. Livak, K.J. and T.D. Schmittgen, *Analysis of relative gene expression data using real time quantitative PCR and the 2^-DDCT method.* Methods, 2001. **25**: p. 402-408.

21. Liu, V.A. and S.N. Bhatia, *Three-dimensional photopatterning of hydrogels containing living cells.* Biomedical Microdevices, 2002. **4**(4): p. 257-266.

22. Bryant, S.J., et al., *Photo-patterning of porous hydrogels for tissue engineering.* Biomaterials, 2007. **28**(19): p. 2978-86.

23. Williams, C.G., et al., *In vitro chondrogenesis of bone marrow-derived mesenchymal stem cells in a photopolymerizing hydrogel.* Tissue Eng, 2003. **9**(4): p. 679-88.

24. Nuttelman, C.R., M.C. Tripodi, and K.S. Anseth, *In vitro osteogenic differentiation of human mesenchymal stem cells photoencapsulated in PEG hydrogels.* J Biomed Mater Res, 2004. **68A**(4): p. 773-82.

25. Rossert, J. and B. de Crombrugghe, *Type I Collagen: Structure, Synthesis, and Regulation*, in *Principles of Bone Biology*, J.P. Bilezikian, L.G. Raisz, and G.A. Rodan, Editors. 1996, Academic Press: San Diego. p. 127-142.

26. Ren, X.D., W.B. Kiosses, and M.A. Schwartz, *Regulation of the small GTP-binding protein Rho by cell adhesion and the cytoskeleton.* Embo J, 1999. **18**(3): p. 578-85.

27. Bidwell, J.P., et al., *Nuclear matrix proteins and osteoblast gene expression.* J Bone Miner Res, 1998. **13**(2): p. 155-67.

28. Taylor, A.F., et al., *Mechanically stimulated osteocytes regulate osteoblastic activity via gap junctions.* Am J Physiol Cell Physiol, 2007. **292**(1): p. C545-52.

29. Tsuruga, E., et al., *Pore size of porous hydroxyapatite as the cell-substratum controls BMP-induced osteogenesis.* J Biochem (Tokyo), 1997. **121**(2): p. 317-24.

CHAPTER SIX

Preliminary Studies: Simultaneous Differentiation of Mesenchymal Stem Cells within a Multi-Layered Scaffold

6.1 INTRODUCTION

The ultimate goal for creating complex, spatially-patterned scaffolds with temporal release-kinetics of biomolecules is to mimic the physiological microenvironment of differentiating stem cells. Though differentiation is complex and requires a specific cascade of intracellular signaling to occur, numerous studies in cellular biology and tissue engineering have enabled us to better understand stem cell behavior. Creating hybrid structures composed of multiple cell types has gained much interest in the past decade due to a myriad of milestones in single phenotype differentiation of stem cells [1-3]. Composite tissue engineering has successfully created hybrid tissue types by combining multiple, committed cell types within a single construct or scaffold; however, a large gap exists in understanding how stem cells in the physiological environment undergo simultaneous differentiation into various cell types.

Here we present preliminary results for the simultaneous differentiation of mesenchymal stem cells using the D1 ORL UVA immortalized cell line. D1 cells were encapsulated in photo-polymerizable poly(ethylene glycol) (PEGDA) in bulk form (i.e., irradiated with a long wave ultra-violet lamp) and differentiated into both bone- and cartilage-like cells within specific regions of a single scaffold. We discuss the biochemical factors used within each region to cue for either osteogenesis or chondrogenesis. Results gained from these studies can be used to create complex,

spatially patterned scaffolds using DMD μSL, as presented in *Chapter Four* and *Chapter Five*.

6.2 MATERIALS AND METHODS

6.2.1 RGD and Heparin Conjugation to PEG

YRGDS (tyrosine-arginine-glycine-aspartic acid-serine, Bachem Biosciences Inc., Torrance, CA) was reacted in equimolar amounts with acryloyl-PEG-*N*-hydroxysuccinimide (acryl-PEG-NHS, Mw 3400 Nektar Therapeutics Inc.) using 50 mM sodium bicarbonate buffer (pH 8.2). Briefly, acryl-PEG-NHS in 200μL of sodium bicarbonate buffer was added in drop-wise fashion to the YRGDS in sodium bicarbonate buffer (1mg/mL). The reaction was completed in a dark environment for 3 hours at room temperature. Unreacted YRGDS was removed with a Microsep™ Centrifugal Device (1K membrane, Pall Corporation, East Hills, NY), lyophilized, and stored at -20°C until further use.

To create a heparin moiety onto PEG-acrylates, ethylenediamine (EDA) was first reacted in excess with acryl-PEG-NHS at a 5:1 molar ratio to yield acryl-PEG-NH_2, similar to the method for RGD conjugation. The reaction was completed for 3 hours at room temperature in a dark environment followed by extensive dialysis (Tube-o-dialyzer, MWCO 1000, Geno Technologies, St. Louis, MO) of unreacted EDA. Samples were frozen and lyophilized for 24 hours. Periodated heparin (Mw 10,000 Celsus Laboratories Inc., USA) was reacted in equimolar amounts for 3 hours in a dark environment with acryl-PEG-NH_2 to yield acryl-PEG-heparin in the presence of 50 mM $NaBH_3CN$ as the reducing agent. Heparin, containing aldehyde moieties, undergoes Schiff-base reactions

with organic amines, and if treated with $NaBH_3CN$, the Schiff-base intermediate is reduced to its corresponding amine, forming an irreversible bond. Centrifugation (Pall Macrosep®, MWCO 10,000) was performed to eliminate the reducing agent and unreacted components. The product was lyophilized and stored in a dessicator at -20°C until further use.

6.2.2 D1 Cell Culture

D1 ORL UVA (ATCC, Manassas, VA) bone marrow progenitor cell line was used to study the tissue engineering properties of the multi-layered scaffolds photo-polymerized by a long wave ultra-violet (UV) lamp (Blak Ray®, Ted Pella Inc., Redding, CA). Primary medium was composed of 10% (w/v) fetal bovine serum (ATCC) and 1% (w/v) penicillin streptomyocin (Gibco) in Dulbecco's Modified Eagle's Medium (ATCC). D1 cells were passaged no more than 10 times during the course of the differentiation studies.

6.2.3 Fabrication of Multi-layered Scaffolds

Formulations of the macromer solutions were varied for the osteogenic and chondrogenic layers, as this contributes to the hybrid differentiation of D1 within a single scaffold. All chemicals and reagents were either filter sterilized (0.2μm filter) or placed under UV light in a tissue culture hood 24 hours prior to cell encapsulation experiments.

The macromer solution use to create the osteogenic layer was composed of 10% (w/v) PEGDA (Mw 3400, Nektar Therapeutics) in PBS with 0.05 wt% Irgacure 2959 (Ciba Technologies Inc.). D1 cells were added to the macromer solution at a concentration of 20 x 10^6 cells/mL. The following were also added to the solution prior to polymerization: 2 ng/mL FGF-2, 1 mM acryl-PEG-heparin, 2 mM acryl-PEG-RGD,

and soluble 10 mM β-glycerophosphate. A total volume of 125 μL was used to create the first layer of the scaffold by placing the macromer solution in a cuvette cap as the mold. The homogenous solution was then polymerized in a sterile tissue culture hood for 5 minutes using a long wave UV lamp.

The chondrogenic layer was composed of 20% w/v PEGDA in PBS and 0.05 wt% Irgacure 2959. D1 cell density utilized was 40 x 10^6 cells/mL, which was twice the amount used for the osteogenic solution. Furthermore, 10 ng/mL of TGF-β1 and 1.0 mM acryl-PEG-heparin were also added to the chondrogenic macromer solution. A total volume of 125 μL of solution was then pipetted onto the top of the initial polymerized osteogenic layer. It was irradiated under a UV lamp for another 5 minute period. These double-layered hydrogels were each placed in a well of a 6-well plate and cultured with D1 primary medium supplemented with 10^{-8} M of dexamethasone and 5 μg/mL of ascorbic acid-2-phosphate for a period of 4 weeks (n=4). A schematic is illustrated of how each layer of the scaffold was formulated in **Figure 6.1**. Control scaffolds, cultured in primary medium only, were composed of the same cell encapsulation densities and PEGDA concentrations for each layer. β-glycerophosphate, acryl-PEG-RGD, acryl-PEG-heparin, and growth factors were not encapsulated within these layers.

6.2.4 Viability of Encapsulated D1 Cells

Multi-layered scaffolds cultured in primary medium (control scaffolds) were removed from culture and stained with 2 μM calcein AM for 30 minutes at room temperature, which stained viable cells green. A thin-slice was obtained from the middle of cell-hydrogel systems since this part of the scaffold had the least amount of nutrient/waste transport. Samples were analyzed through fluorescence microscopy, and digital images were captured.

6.2.5 Histology

At a 4 week time point, double-layered scaffolds were removed from culture and fixed in 10% formalin at 4°C for an overnight period. Fixed scaffolds were then dehydrated for paraffin embedding using 1-hr sequential steps in the following order: 80%, 95%, 95% ethanol in dH_2O, 100% ethanol, 50/50 ethanol/Citrisolv, 100% Citrisolv, 100% Citrisolv, 60°C molten paraffin, and 60°C molten paraffin for an overnight period. Paraffin-embedded scaffolds were sliced in transverse sections at 10 μm using a rotary microtome. Sections were stained for differentiation at the interface of the osteogenic and chondrogenic layers. Von Kossa was used to stain matrix mineralization black (bone formation), and safranin O was used to stain excessive proteoglycan secretion red (cartilage formation).

6.3 RESULTS

Cells encapsulated in bulk-form using a UV lamp remained viable after 2 weeks in culture as illustrated in **Figure 6.2** with calcein AM staining. The dimensions of the entire double-layered scaffold was measured to be approximately 4mm x 4mm x 3mm (*length* x *width* x *height*). Preliminary studies using safranin O and von Kossa staining of paraffin-embedded samples after 4 weeks in culture demonstrated the simultaneous differentiation of D1 progenitor cells. Sections stained with safranin O showed that cells in the cartilage layer stained redder in color than cells in the osteogenic layer, thus indicating a higher proteoglycan secretion from these cells (**Figure 6.3**). Since proteoglycans and glycosaminoglycans make up approximately 70% of the cartilage matrix, safranin O staining is a common histological method for marking cartilage

formation. Matrix calcification as determined through von Kossa staining (black color) showed that increased mineralization occurred in the bone-specific layer and not so much in the cartilage layer (**Figure 6.4**). There was some mineralization seen in the chondrogenic layer, and this was possibly due to the diffusion of β-glycerophosphate out of the osteogenic layer. These histological methods were just initial analyses for matrix secretion by the encapsulated D1 cells, and a more thorough evaluation of gene expression, such as *in situ* hybridization, could be performed to ultimately determine mRNA synthesis from differentiating cell types.

6.4 DISCUSSION

Preliminary studies with bulk-polymerized scaffolds indicate that D1 cells have the potential to simultaneously differentiate into both bone and cartilage, if given the proper conditions. The osteogenic region of the scaffold contained acryl-PEG-RGD because osteoblasts require a signaling sequence that is triggered by cell anchorage to a substrate. Cell anchorage through $\alpha_V\beta_3$ integrins activates the Rho signaling pathway for dense cytoskeleton organization, thus changing cell shape and mechanics [4]. Additionally FGF-2, also known as basic fibroblast growth factor, was encapsulated within this layer as it has been long noted in literature to be an important, early mitogen that allows marrow-derived stromal cells to undergo the osteogenic differentiation. FGF-2 is known to cause the auto-phosphorylation of tyrosine receptor kinases due to receptor clustering, thus activating the mitogen-activated protein kinase (MAPK) pathway. Transcription factor, AP-1, thus gets activated, which signals for the onset of cell proliferation . Cbfα-1 is also activated, which is another commonly studied transcription factor that marks pre-osteoblast type cells [5].

Adding heparin to the osteogenic macromer solution, in the form of acryl-PEG-heparin, also aids in sequestering FGF-2 within this particular layer and helps prevent diffusion into the chondrogenic layer and medium. Soluble β-glycerophosphate was also added to induce mineralization by increasing alkaline phosphatase activity, a highly exhibited enzymatic activity in pre-mature osteocytes. A future consideration in incorporating β-glycerophosphate within scaffolds could be to directly conjugate this inorganic molecule to PEG polymer, thereby preventing its diffusion to neighboring regions [6].

The chondrogenic layer encapsulated the growth factor, TGF-β1, known to differentiate marrow-derived progenitor cells into chondrocytes. This growth factor is also localized in this layer by binding to acryl-PEG-heparin. Additionally the amount of D1 cells encapsulated in the chondrogenic layer was increased from $20x10^6$ D1/mL to $40x10^6$ D1/mL since chondrocytes are physiologically found more condensed. Acryl-PEG-RGD was not included in the macromer solution because chondrocytes tend to adopt a more rounded shape and do not require cell anchorage. PEGDA concentration was increased from 10% to 20% w/v in order to increase crosslinking density and compressive stress, thereby mimicking physiological cartilage. These preliminary results could be used to further determine optimal conditions for the osteogenesic and chondrogenesic properties of marrow-derived progenitor cells, such as the following, but not limited to: (1) *in vitro* culture time period, (2) variations in cell density, (3) variations in PEGDA macromer concentration, (4) RGD, or heparin concentrations, and (5) differences in degradation rates of degradable polymers. Once these basal parameters have been determined through bulk-polymerized scaffolds, more complex architectures could be created through DMD μSL, as discussed in *Chapter Four* and *Chapter Five*.

Figure 6.1 Schematic of Multi-Layered Scaffold for the Simultaneous Differentiation of D1 Cells. These schematic lists the components of a multi-layered scaffold conducive of D1 hybrid differentiation into Bone- and cartilage-like cells.

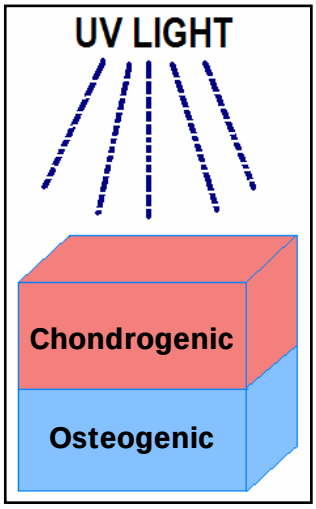

CARTILAGE LAYER:

- 125 µL of 20% w/v PEGDA
- 0.05 wt% Irgacure 2959
- 40 x 10^6 D1/mL
- 10 ng/mL TGF-β1
- 1.0 mM acryl-PEG-hepain

BONE LAYER:

- 125 µL of 10% w/v PEGDA
- 0.05 wt% Irgacure 2959
- 20 x 10^6 D1/mL
- 2 ng/mL FGF-2
- 1 mM acryl-PEG-heparin
- 2 mM acryl-PEG-RGD
- 10 mM β-glycerophosphate

Figure 6.2 **At a two-week time point, double-layered scaffolds cultured in basal medium were removed from culture and stained with 2 μM calcein AM for 30 minutes at room temperature. A thin-slice was obtained from the middle of the cell-hydrogel construct using a surgical scalpel to determine if encapsulated D1 cells remained viable after a 2 week culture period. Calcein AM stains viable cells green. Digital images were captured and fluorescence micrographs (B) revealed that encapsulated D1 cells remained viable. Image depicted in (C) is an overlay of the brightfield micrograph in (A) and fluorescence micrograph in (B).**

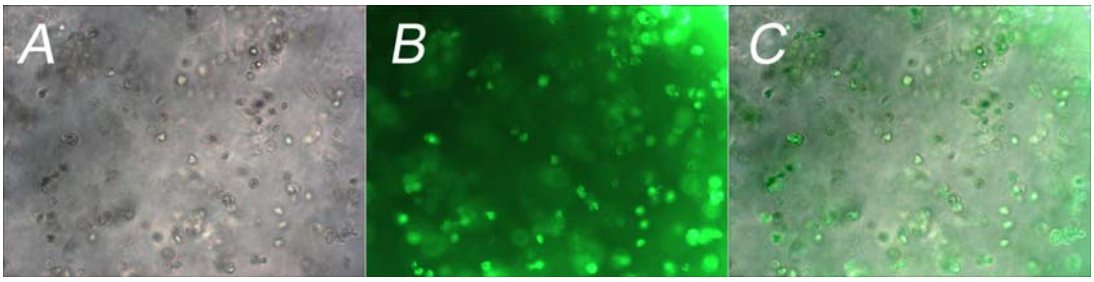

Figure 6.3 **Safranin O stains proteoglycans red, which comprises 70% of cartilage matrix. The chondrogenic layer (A) showed cells to be redder in color than cells in the osteogenic layer (B), possibly indicating that each layer was differentiating into different lineages. Presence of GAGs and proteoglycans secreted by cells were observed to be more abundant in the cartilage layer that the osteogenic layer. (Brightfield microscopy taken with a 40X objective)**

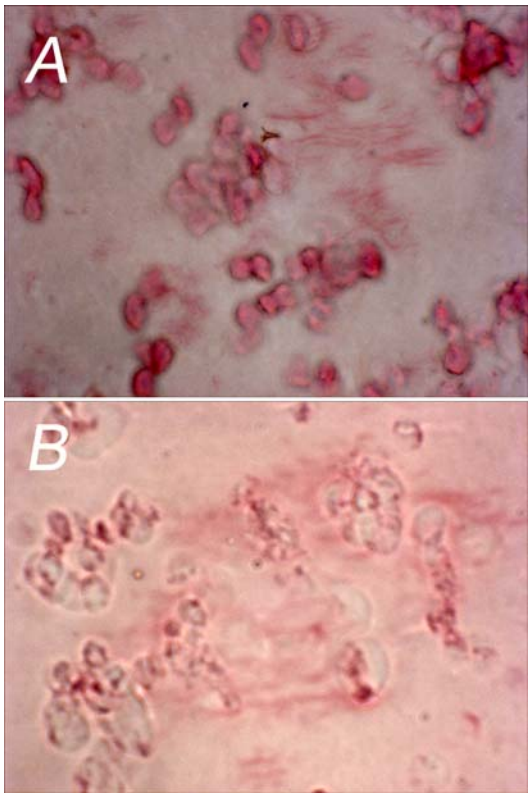

Figure 6.4 **Von Kossa stains extracellular matrix mineralization black. (A) The osteogenic layer (below the white dotted line) mineralized to a greater extent than the chondrogenic layer (above the white dotted line). Von Kossa staining was performed on paraffin-embedded samples that were in culture for 4 weeks. Increased mineralization (black color) is abundantly seen in the bone layer, with some mineralization in the chondrogenic layer. Pink color is cell nuclei staining due to nuclear fast red. (B) von Kossa staining was also performed on negative control scaffolds that were cultured in primary medium. No mineralization was observed.**

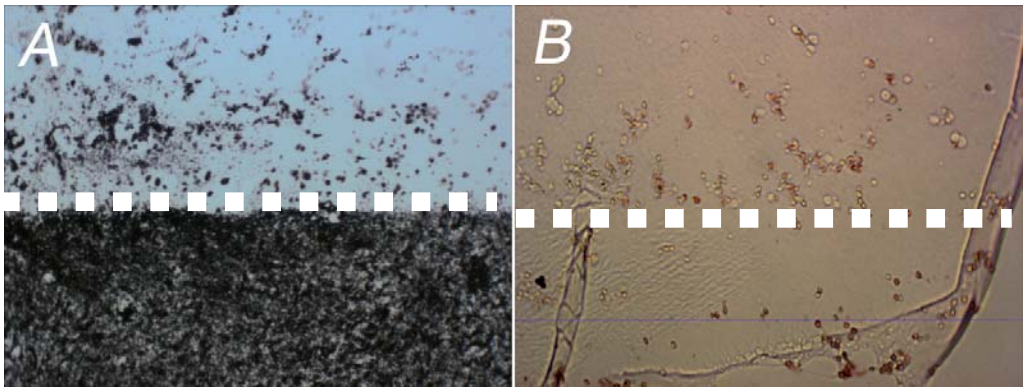

6.4 REFERENCES

1. Gao, J. and A.I. Caplan, *Mesenchymal stem cells and tissue engineering for orthopaedic surgery.* Chir Organi Mov, 2003. **88**(3): p. 305-16.

2. Rahaman, M.N. and J.J. Mao, *Stem cell-based composite tissue constructs for regenerative medicine.* Biotechnol Bioeng, 2005. **91**(3): p. 261-84.

3. Alhadlaq, A. and J.J. Mao, *Tissue-engineered osteochondral constructs in the shape of an articular condyle.* J Bone Joint Surg Am, 2005. **87**(5): p. 936-44.

4. McBeath, R., et al., *Cell shape, cytoskeletal tension, and RhoA regulate stem cell lineage commitment.* Dev Cell, 2004. **6**(4): p. 483-95.

5. Franceschi, R.T. and G. Xiao, *Regulation of the osteoblast-specific transcription factor, Runx2: responsiveness to multiple signal transduction pathways.* J Cell Biochem, 2003. **88**(3): p. 446-54.

6. Nuttelman, C.R., M.C. Tripodi, and K.S. Anseth, *Synthetic hydrogel niches that promote hMSC viability.* Matrix Biol, 2005. **24**(3): p. 208-18.

CHAPTER SEVEN

Conclusions and Future Directions

7.1 SUMMARY

We have demonstrated novel, yet feasible, approaches in microfabricating complex, spatially patterned three-dimensional (3D) scaffolds for use in tissue engineering and stem cell behavior studies. Ultra-violet (UV)-based layer-by-layer stereolithography methods were used to create intricate, polymer architectures with varying pore geometry and dimensions in the micro-scale. We show that temporally-released polymer microparticles can also be encapsulated in spatially-patterned regions of a single scaffold in a pre-designed fashion. These degradable, controlled-release microparticles could entrap biochemical cues that are specific to the differentiation of a cell lineage, thereby creating a construct that can differentiate a single stem cell population into hybrid tissue structures. Furthermore extracellular matrix components (ECM), such as small amino acid sequences, fibronectin and heparan sulfates, were covalently conjugated to the polymer to create a more biomimetic niche in which mesenchymal stem cells (MSCs) can attach, proliferate, and differentiate into multiple cell types, as illustrated in **Figure 7.1**. This figure illustrates the overall goal discussed in this dissertation and how compartmentalized stem cell differentiation could be mediated. ECM-functionalized, microfabricated scaffolds could provide the means to study progenitor cell populations under patterned, complex microenvironments and ultimately aid in creating pre-designed, hybrid tissue/organ structures.

7.2 CONCLUSIONS WITH LASER-BASED STEREOLITHOGRAPHY AND FUTURE DIRECTIONS

Chapter Three discussed a laser-based, layer-by-layer, photo-polymerization process for developing porous, polymer scaffolds in the micrometer scale. This technique allowed for precise, pre-designed, spatial distribution of single or multiple molecules within the scaffold as well as the fabrication of intricate architectures. This laser-based, stereolithographic system provided a raster-scanning style of polymerization using photo-crosslinkable poly(ethylene glycol) diacrylates (PEGDA). The patterning of complex architectures was achieved by manually moving a translational stage in the x-y direction.

We also illustrated that functionalizing PEGDA scaffolds with RGD and heparin ensures sufficient cell attachment and allows for spatial sequestration of patterned growth factors, specifically basic fibroblast growth factor (FGF-2). FGF-2 was demonstrated to be localized in certain regions of a scaffold due to the presence of heparin, which is known to bind and protect growth factors from heat degradation. Heparin also enhanced growth factor chemical signaling by clustering FGF-2 to cell tyrosine kinase receptors, thus enabling their phosphorylation. FGF-2 is a crucial signaling molecule for the osteogenic differentiation of MSCs; therefore concentrations of this protein in specific regions of a scaffold can facilitate localized bone formation. Furthermore, RGD, a small amino acid sequence derived from fibronectin, enabled protein and cellular attachment to the non-fouling PEGDA polymer.

Two future directions specific to the laser-based manufacturing of the scaffold could be taken. First, the viability rate of encapsulated cells could be increased by increasing the speed of the layer-by-layer fabrication process. Secondly, staggered layers or overhanging structures, to ensure pore interconnectivity, have yet to be achieved with

this system due to an increased laser depth of focus and monomer cross-linking in pre-existing layers. In traditional stereolithography, such overhanging structures are quite prevalent and are generally accomplished using a sacrificial filler material. Using advanced SL techniques such as this could allow for more complex structures.

Another recommendation for enhancing this system to is determine the effects of biochemical cross-contamination between the uses of various types of solutions. Although our results indicated that we can successfully pattern several components, it remained to be seen how complex the patterning can be before mixing becomes a problem. However, we believe that even simple 3D spatial patterns can provide us with unique insights on cell behavior under complex microenvironments.

7.3 CONCLUSIONS AND FUTURE DIRECTIONS WITH DIGITAL MICROMIRROR DEVICE (DMD)-BASED STEREOLITHOGRAPHY

We demonstrated in *Chapter Four* that DMD-μSL was another powerful stereolithographic technology that can create pre-designed, spatially patterned scaffolds for applications in stem cell and tissue engineering. We have developed a simple and feasible, layer-by-layer micro-stereolithography system consisting of an UV light source, a digital micro-mirror masking device, and a conventional computer projector, that allows fabrication of complex internal features along with precise spatial distribution of biological factors inside a single scaffold. These scaffolds were suitable for the encapsulation of single or multiple cell types in a spatially distributed fashion. The main advantage of using this scaffold fabrication system over the laser-based system presented in *Chapter Three* or other stereolithography methods was that the photo-polymerization of an entire single layer is achieved simultaneously, and ultimately a 3D construct was achieved by "building" subsequent layers by exchanging polymer solution in between.

Functionalizing the patterned scaffolds with fibronectin after fabrication created a microenvironment suitable for the attachment, proliferation, and differentiation of MSCs. By the addition of methacrylic acid to the PEGDA macromer solution, carboxyl activation (from methacrylic acid) could bind with free amine groups from fibronectin. Post-processing these scaffolds using standard EDC/sulfo-NHS bio-conjugation methods allowed fibronectin to be successfully conjugated to the surfaces of the scaffolds. MSCs were seeded onto the spatially patterned scaffolds and efficiently attach. Similarly to the scaffolds created with the laser-based SL system, these spatially patterned, DMD-fabricated scaffolds could ultimately consist of intricate architectures that combine both spatial and controlled-release kinetics of biochemical factors, creating a suitable environment for studying hybrid tissue formation from a single stem cell population.

In this research project, MSCs were successfully encapsulated with DMD-μSL. A promising next step would be to use multiple progenitor or committed cell types, mimicking a more complex physiological tissue/organ. The ability to do both cell encapsulation and seeding would be the most optimum for incorporating cells within the structures.

7.4 CONCLUSIONS AND FUTURE DIRECTIONS WITH THE OSTEOGENIC DIFFERENTIATION MSCS ON DMD-FABRICATED TISSUE ENGINEERING SCAFFOLDS

In *Chapter Five*, the osteogenic properties of murine MSCs are further analyzed using patterned PEGDA scaffolds fabricated by the DMD-μSL system. MSC differentiation in bulk-polymerized PEGDA scaffolds, created using a long wave UV lamp, is also investigated in this chapter. This particular study involve encapsulating MSCs in bulk-form within increasingly concentrated PEGDA solutions to determine changes in osteogenic gene expression levels when compared to undifferentiated MSCs.

Results obtained from this investigation allowed us to realize a limitation with the DMD-SL system: when MSCs were encapsulated in a scaffold with a high PEGDA concentration (100% w/v in PBS), maturation of osteoblasts was inhibited due to decreased cell nutrient and waste transport and changes in compression moduli. Currently the DMD-μSL system can encapsulate cells without losing feature resolution only when using a high macromer concentration (100% w/v PEGDA in PBS). Lower PEGDA concentrations could be used to create the scaffolds, but increased exposure time to polymerize the macromer solution could ultimately decrease cell viability.

Instead of encapsulation, MSCs were then seeded onto fibronectin-modified patterned scaffolds after fabrication, and osteogenic medium was used to culture the cell-scaffold systems. Scaffold channel size and geometry were varied, while keeping wall dimension and overall scaffold thickness constant. Additionally channel volumes of scaffolds with varying pore geometry were also kept constant. After 2 week in culture, osteoblast gene expression levels (collagen I, cbfα-1, and alkaline phosphatase) were analyzed, and the highest MSCs differentiation gene expressions were determined to be on scaffolds with a channel dimension of 0.4 mm by 0.4 mm and with a square channel geometry. It was also determined in these studies that an immortalized MSCs cell line, D1 ORL UVA, expressed higher osteoblast gene expression than primary bone-marrow derived cells when cultured in osteogenic medium for 2 weeks; therefore all osteoblast differentiation studies were used with the D1 immortalized cell line to remove cell source as a originator of variance.

Other limitations to the DMD-μSL system that could be further investigated are light scattering and increased curing depth during the photo-curing process of several layers. Challenges with light scattering affected previously fabricated layers of multi-layered scaffolds, causing macromer crosslinking to decrease feature resolution within

these existing layers. More intricate structures requiring several layers cause the bottom layers to lose interconnective porosity. However, this drawback can be resolved using a UV quencher dye that absorbs scattered light within the bottom regions of the polymer solution. Additionally a dye quencher can act to decrease the curing depth of the projected light at the focal plane, thereby providing thinner, or more resolved, layers. We conclude that complex, polymer scaffolds fabricated with UV stereolithography can mimic the niche in which MSCs can differentiate into multiple cell types. By combining knowledge gained from stem cell biology and spatio-temporally patterned scaffolds, hybrid tissue structures from a single stem cell population can ultimately be achieved. *Chapter Six* discusses preliminary studies with hybrid tissue formation by encapsulating MSCs in a multi-layered scaffold. Specific biochemical parameters were added within separate layers of a multi-layered scaffold to induce the simultaneous differentiation of bone- and cartilage-like cells. Histology on these composite scaffolds was performed after a 4 week culture period *in vitro*. Future work involves determining optimum parameters for these biochemical factors, and then utilizing these results within DMD μSL fabricated scaffolds.

Figure 7.1 Schematic of Overall Project Goal

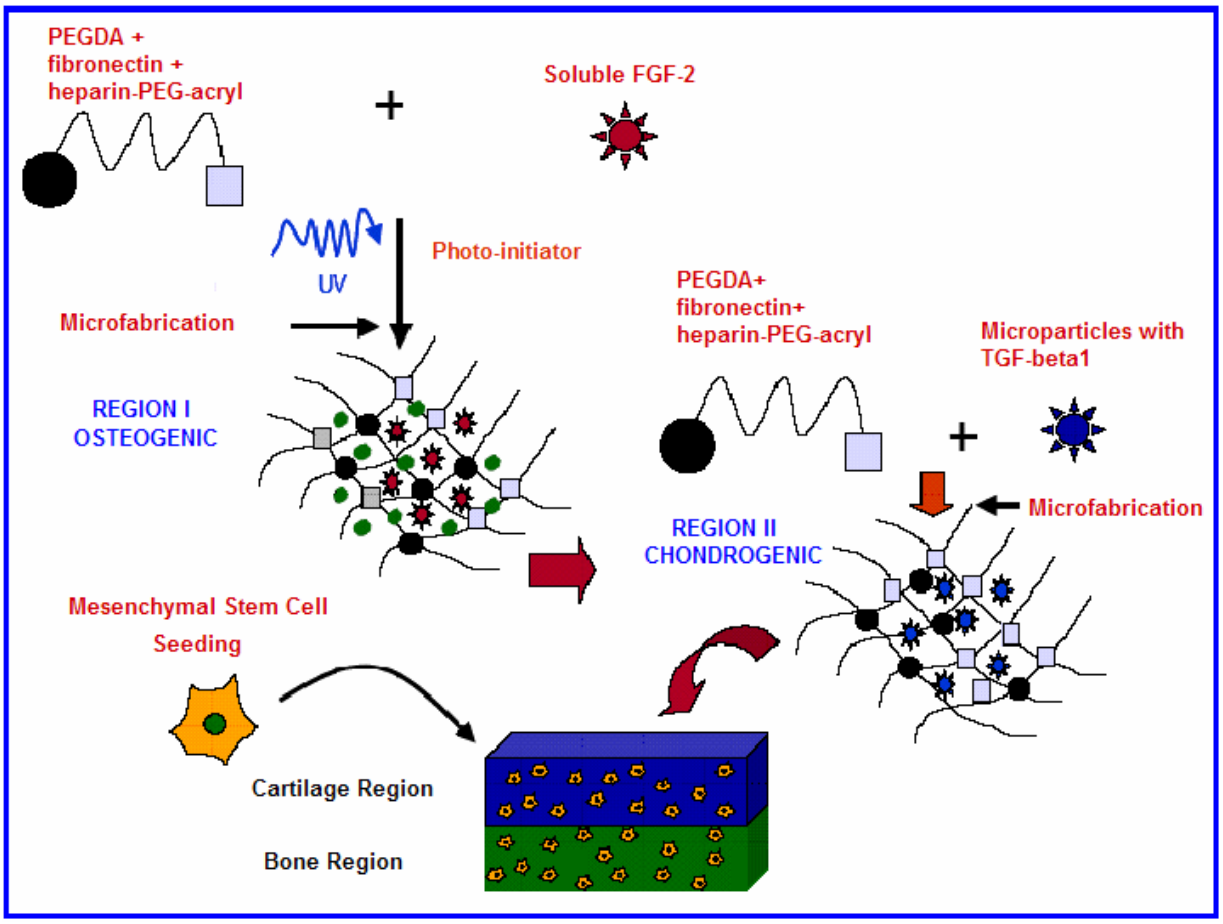

Appendix

APPENDIX A

Visible Light-based Digital Micromirror Device (DMD) Micro-Stereolithography

A.1 INTRODUCTION

Photo-polymerization is considered to be an attractive process in the biomedical sciences due to a myriad of applications [1, 2] in solidifying a liquid macromer solution to match a defect site. We have studied two forms of stereolithography processes that involve the use of photo-polymerizing acrylated monomers, as discussed in *Chapters There and Four*. During the initial stages of creating a digital micro-mirror device-based micro-stereolithography system (DMD μSL), both visible and ultra-violet (UV) light sources were considered in fabricating complex tissue engineering scaffolds. This appendix discusses polymerization and cell viability results with two types of visible photoinitiating systems studied with the encapsulation of murine OP9 stromal cells: 2,4,5,7-tetraiodo-6-hydroxy-3-fluorone (H-Nu 535) and camphorquinone (CQ). Additionally a profile of light intensity versus photomask pixel luminance used with the visible-DMD μSL was also determined. Based on this analysis, we utilized the UV-based DMD μSL system to ultimately create scaffolds for stem cell differentiation studies.

A.2 MATERIALS AND METHODS

A.2.1 Visible DMD-μSL

The visible-based stereolithography system used in this study was fabricated the same way the UV-based DMD-μSL was created in *Chapter Four*. The high intensity white light originally built into the commercial projector (PB2120, BenQ, Taiwan) was used for this system. This was the only modification to the system, as described in *Chapter Four*. The commercial projector was coupled to a digital micro-mirror device (DMD™, Texas Instruments) and the patterns of each layer were drawn in a series of Microsoft PowerPoint slides. These patterns were then executed onto the DMD chip to generate a dynamic mask.

Visible light was modulated according to the defined mask on the DMD chip and went through a reduction-projection lens assembly to form an image on the surface of the photo-crosslinkable macromer solution. The illuminated area was solidified simultaneously under one exposure, while the dark regions remained liquid. This system consisted of five major components: a DMD chip embedded within the projector as a dynamic mask, a visible light source, a projection lens assembly, a translation stage with capable of micrometer movements, and a container to hold the macromer solution.

A.2.2 H-Nu 535 Visible Photoinitiating System

Concentrations of 10% and 30% w/v poly(ethylene glycol) diacrylate (PEGDA) in PBS were utilized when evaluating a visible photoinitiator (H-Nu 535, Spectra Group Limited, Inc.) and the DMD μSL system. The visible photoinitiator comes with three components: H-Nu 535, Uvacure 1600 OPPI (a coinitiator), and a liquid amine group, which provides hydrogens for a more efficient rate of initiation. These components were not soluble in the macromer solution alone and were therefore added to *N*-vinyl pyrrolidone (*n*-PVP) at a concentration of 10% (w/v). Furthermore these components

were heated at 50°C for approximately 2 hours, as recommended by the manufacturer. Upon solubilizing, the photoinitiator was added to the PEGDA solutions, at concentrations ranging from 0.05-0.10% (w/v) in macromer solution. Minimum exposure time to pattern-polymerize PEGDA macromer solution was determined.

A.2.3 Cell Viability

Each component of the visible-based DMD μSL system was evaluated separately to determine if any of the components were toxic to cells. While creating a white photomask on MS PowerPoint (255 pixel luminance value), OP9 cells seeded in a 96-well plate (~50,000 cells/cm^2) were irradiated for 1, 2.5, 5,10, and 15 minutes (n=5). A maximum irradiation time of 15 minutes was chosen because this was the maximum time the cells would have to endure for the polymerization of a single hydrogel layer while using a low photoinitiator concentration. Methyl thiazolyl tetrazolium (MTT) assay was completed after a 24 hour incubation period to determine relative survival when compared to non-irradiated cells.

Cyto-toxicity of H-Nu 535, OPPI coinitiator, and the liquid amine group without visible light irradiation was determined individually. To evaluate for photoinitiator cell toxicity, each photoinitiating component was directly placed in a monolayer culture of OP9 cells (density of 50,000 cells/cm^2) at two different concentrations: 0.05 and 0.1% (w/v). MTT assay was performed after a 24-hour incubation period with the initiators. *n*-PVP alone was also filter sterilized and directly added to separate OP9 cell culture wells. After a 24 hour incubation time, cultures were observed through microscopy.

A.2.4 Camphorquinone Visible Photoinitiating System

Camphorquinone (CQ) was another visible photoinitiator used to study patterned-polymerization of visible DMD μSL. Cell viability using this photoinitiating system was previously studied by Bryant et. al. [3]. Macromer solutions of 30% and 100% (w/v) PEGDA with 0.05 wt% CQ system were used to encapsulate OP9 cells (density $3x10^6$ cells/mL) for approximately 7 and 18 minutes respectively, using DMD μSL. A 10 μL PEG-cell solution was placed onto a coverslip and irradiated using a high intensity solid photomask (255 pixel luminance). Cell-gel systems were washed extensively with sterile PBS and were incubated for a 24 hour period before performing MTT assay (n=3).

To determine if cells could be effectively encapsulated using visible DMD μSL, OP9 cells were added to 30% (w/v) PEGDA in PBS and 0.05 wt% CQ photoinitiator. Cell densities tested were 1×10^6 and 5×10^6 OP9 cells/mL of macromer solution. Scaffolds were observed using phase contrast microscopy, and digital images were captured.

A.3 RESULTS AND DISCUSSION

Microsoft PowerPoint was used to create slides containing different pixel luminance (ranging from 0 to 255) as a solid photomask. Using a power meter, the intensity was calculated by dividing the measured power by the area of irradiation. The area of irradiation from the visible DMD μSL was measured to be 3 mm x 4 mm (or 0.12 cm^2). **Figure A.1** illustrates intensity versus pixel luminance graph. Increasing pixel luminance from 0 to 255 resulted in increased intensity. The minimum amount of time required to polymerize either 10% or 30% (w/w) of PEGDA in PBS using H-Nu 535

photointiator without losing feature resolution was determined, and these results are summarized in **Table A.1**.

Visible light from the DMD μSL system did not exclusively effect cell viability as determined through MTT and depicted in **Figure A.2** (n=2). Relative cell survival was above 80% for all exposure times studied without the use of photoinitiating systems. Because it was determined that visible light was not toxic to cells, components of the H-Nu 535 photoinitiating system was studied. H-Nu 535, OPPI coinitiator, and liquid amine group were individually added to OP9 cells and resulted in 41% cell viability or higher, as illustrated in **Figure A.3**. It was found that these components had varying levels of toxicity on an individual basis. OPPI had the greatest affect on cell apoptosis with a 41% mean relative survival rate for both concentrations studied. The amine liquid group varied for the 0.05 and 0.10%, with a mean relative survival rate of 87% and 41%, respectively. H-Nu 535 had a mean survival rate of at least 66%. Because these chemicals are not soluble in aqueous solutions, it was necessary to add them into *n*-PVP before solubilizing in macromer solutions. Cell cultures treated with the photoinitiator in *n*-PVP detached from the plate, showing that this specific photoinitiating system is cyto-toxic. Furthermore, it was also determined that direct addition of sterile *n*-PVP to OP9 cells resulted in complete cell death after a 24 hour incubation time. All cells were observed floating in the medium when compared to the control group.

Using CQ photoinitiating system to encapsulate D1 cells with visible DMD μSL resulted in the relative mean survival rates for 30% and 100% to be less than 65% and 56%, respectively, when compared to OP9 cells cultured in monolayer. Literature discusses that CQ photoinitiator is not cyto-toxic at levels below 0.01 wt%; however the PEGDA concentrations used in this study did not polymerize at such a low photoinitiator concentration, and 0.05 wt% was the lowest concentration necessary to obtain PEGDA

crosslinking using DMD μSL. Furthermore when cells were encapsulated using patterned photomasks, feature resolution was lost during photo-polymerization (**Figure A.5**). Increased concentrations of cells within the macromer solution (from 1 x 10^6 to 5 x 10^6 OP9 cells/mL) caused increased light diffraction, thus polymerizing other areas of the scaffolds. **Figure A.5B** shows that an entire layer was polymerized when using a cell density of 5 x 10^6 OP9 cells/mL, and no scaffold porosity could be observed.

Based on these photo-polymerization studies, it was determined that the H-Nu 535 photoinitiating system was not cyto-compatible due to the necessity of *n*-PVP solution. However, *n*-PVP itself was also found to be detrimental to cells. Furthermore, CQ photoinitiator polymerizes PEGDA solution with OP9 cells using DMD μSL and is a more common compound used in dental applications. Although CQ proves to be a promising chemical compound to initiate chain polymerization, feature resolution of scaffolds was still not attainable when encapsulating cells. These studies confirmed that ultra-violet based DMD μSL (as discussed in *Chapter Four*) was a better method of fabricating pre-designed, spatially patterned scaffolds, since shorter wavelengths are higher in energy.

Table A.1 Minimum Polymerization Time Using Visible Photoinitiator

Solution	Minimum Time for Polymerization (minutes)
10% (w/w) PEG in PBS; 0.05 wt% H-Nu 535	14
10% (w/w) PEG in PBS; 0.07 wt% H-Nu 535	10
10% (w/w) PEG in PBS; 0.10 wt% H-Nu 535	8-10
30% (w/w) PEG in PBS; 0.05 wt% H-Nu 535	6
30% (w/w) PEG in PBS; 0.07 wt% H-Nu 535	6-8
30% (w/w) PEG in PBS; 0.10 wt% H-Nu 535	6

Figure A.1 Visible DMD-μSL Intensity versus Luminance

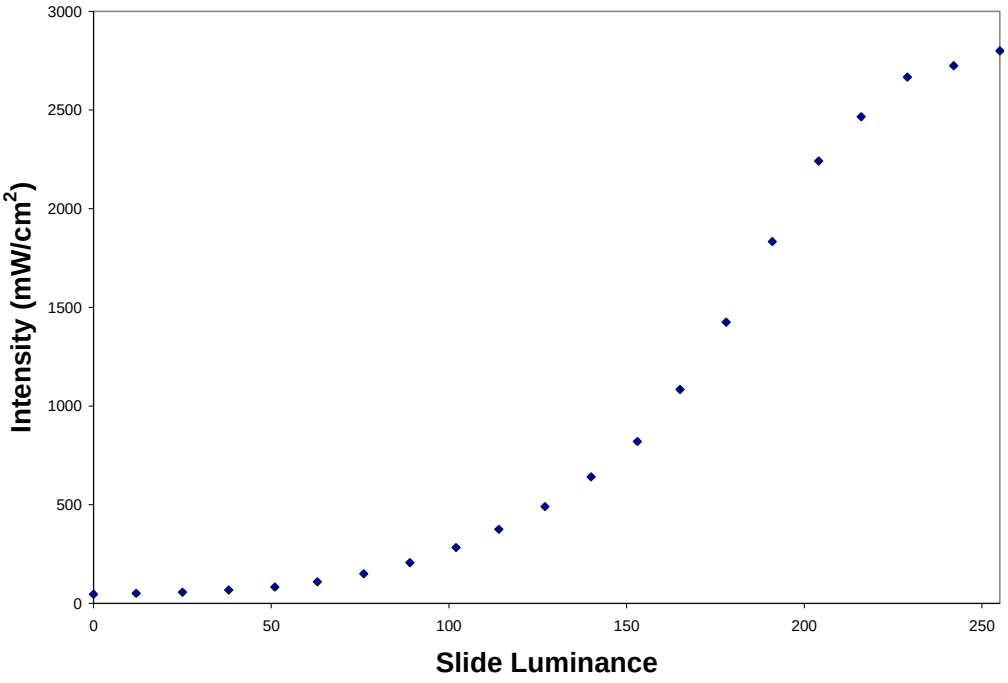

Figure A.2 Cell Viability of Irradiated Cells using Visible DMD μSL. MTT assay shows that visible light irradiation using DMD μSL does not effect OP9 cell viability after 24 hours in culture. Exposure times varied from 0 to 15 minutes, and relative survival did not go below 80% when compared to OP9 cells that were not exposed to DMD μSL visible light (n=5).

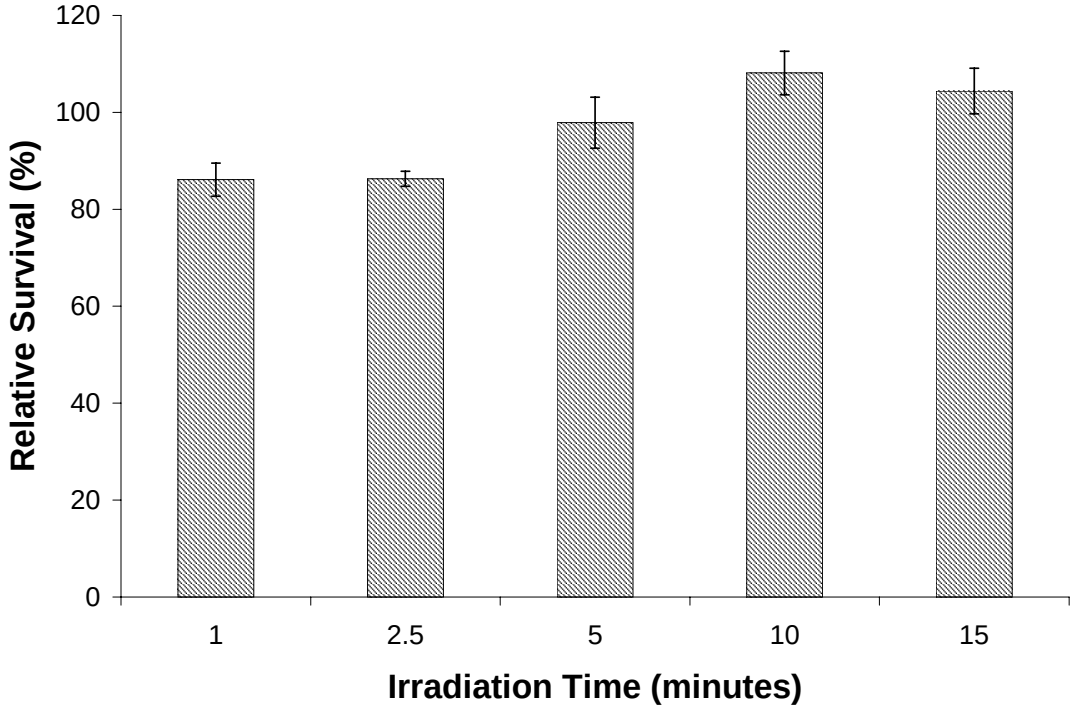

Figure A.3 Cell Viability of H-Nu 535 Photoinitiating System. MTT assay shows that individual components of the H-Nu 535 photoinitiating system were toxic to OP9 cells, even without visible light exposure. OPPI component seemed to be the most toxic with approximately 41% relative survival mean for both concentrations evaluated. H-Nu 535 had over 65% relative survival mean for both concentrations. The amine component greatly reduced cell viability at a higher concentration. Relative survival was determined by comparing to scaffolds that did not contain photoinitiator. Bars represent standard error n = 3 samples.

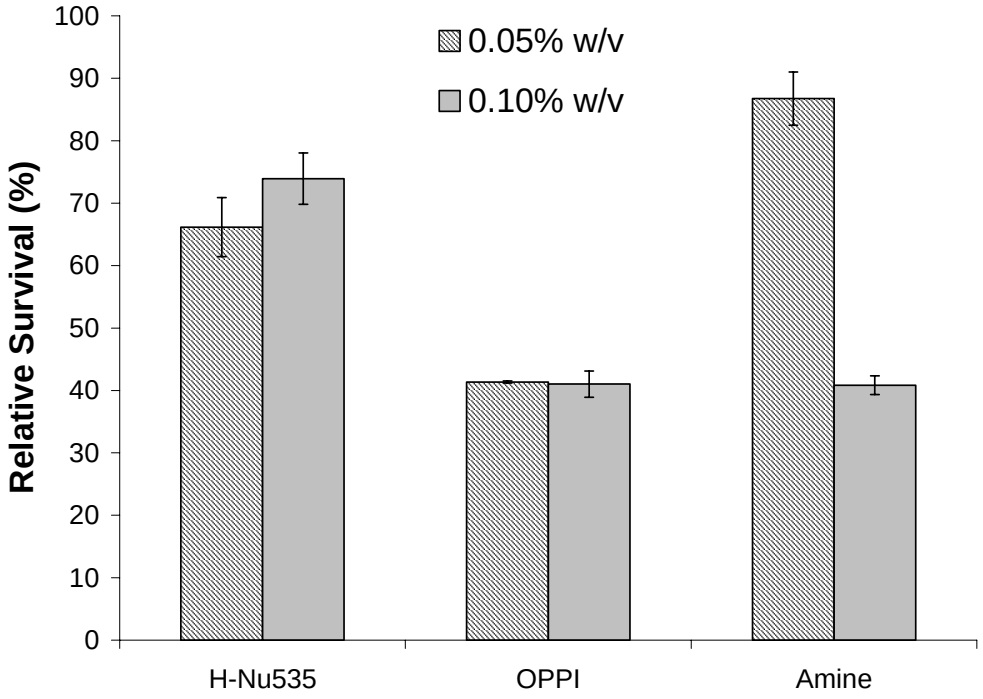

Figure A.4 Cell viability of encapsulated OP9 cells using visible DMD μSL and camphorquinone photoinitiating system at a concentration of 0.05% (w/v) was evaluated using MTT assay. After a 24 hour incubation period, relative mean survival rates of encapsulated D1 cells were determined to be less that 65% for the 30% (w/v) PEGDA solution and 56% for the 100% (w/v) PEGDA solution. Bars represent standard error with n=3 samples.

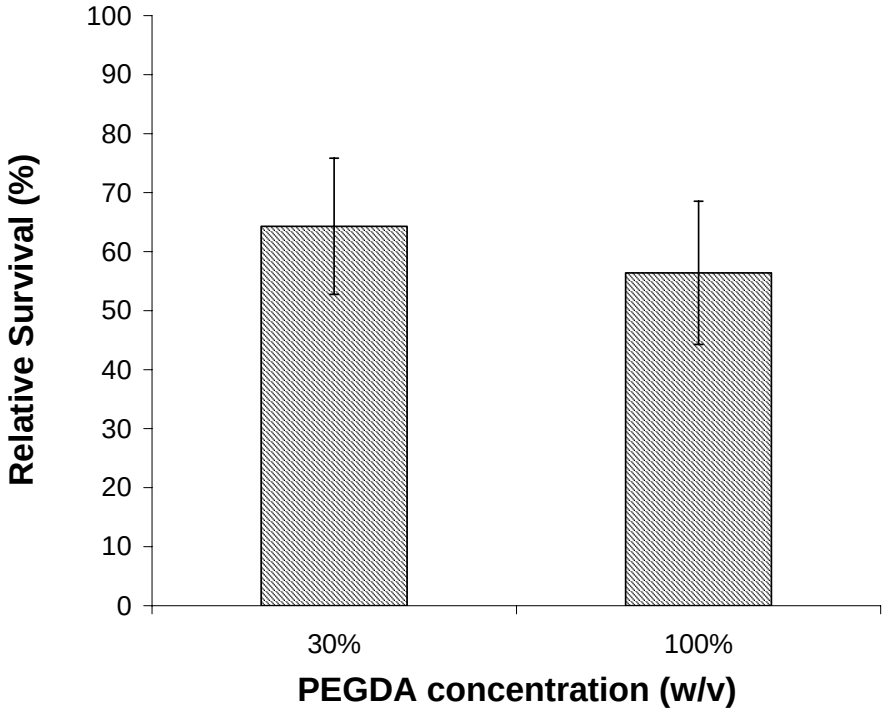

Figure A.5 **Scaffolds Encapsulating Cells using Visible DMD μSL. Patterned scaffolds were formulated with 30% PEGDA and polymerized for 10 minutes using visible DMD μSL. (A) OP9 cells were encapsulated in scaffolds at a density of $1x10^6$ OP9/mL with a wall thickness dimension of 200μm. Cells were encapsulated but feature resolution was sacrificed. (B) This scaffold encapsulated a higher OP9 density ($5x10^6$ OP9/mL) and the entire scaffold layer was polymerized while using a patterned photomask. Scaffold wall dimension was kept constant. These results indicate that visible DMD-mSL does not encapsulate OP9 within spatially-patterned scaffolds. Diffraction due to the presence of cells causes polymerization all throughout the layer, even with a patterned photomask. Feature resolution is lost when cells are added into the macromer solution; therefore UV DMD μSL was ultimately chosen to create these patterned scaffolds. Black scale bar is equal to 500 μm.**

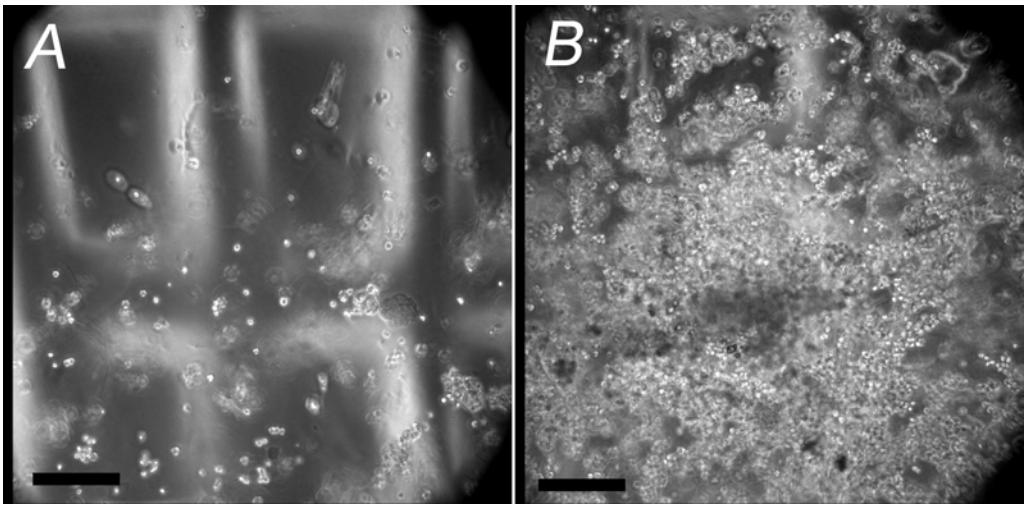

A.4 REFERENCES

1. Maffezzoli, A., et al., *Photopolymerization of dental composite matrices.* Biomaterials, 1994. **15**(15): p. 1221-8.
2. Burkoth, A.K. and K.S. Anseth, *A review of photocrosslinked polyanhydrides: in situ forming degradable networks.* Biomaterials, 2000. **21**(23): p. 2395-404.
3. Bryant, S.J., C.R. Nuttelman, and K.S. Anseth, *Cytocompatibility of UV and visible light photoinitiating systems on cultured NIH/3T3 fibroblasts in vitro.* J Biomater Sci Polym Ed, 2000. **11**(5): p. 439-57.

APPENDIX B

Basic Fibroblast Growth Factor (FGF-2) Release from Heparin-modified Poly(ethylene glycol) Hydrogels

B.1 INTRODUCTION

FGF-2 is a well-characterized protein that binds to heparan sulfates glycosaminoglycans (GAGs) while promoting cell proliferation and playing a critical role in osteoblast formation from mesenchymal progenitor cells. Because proteins and other growth factors are unstable under physiological conditions due to heat and pH changes, heparin acts to stabilize FGF-2 both *in vivo* and *in vitro*. In our studies, heparin is used to not only protect the signaling provided by FGF-2, but to localize this particular growth factor within a specific region of a patterned scaffold. As initially stated in specific aim 2, sequestration studies of basic fibroblast growth factor (FGF-2) to heparin modified scaffolds were to be studied. This section summarizes experimental attempts in quantifying FGF-2 release studies from heparin-modified scaffolds and future recommendations to further analyze conflicting results obtained from this study.

B.2 MATERIALS AND METHODS

B.2.1 Heparin Conjugation to PEG Monomer

As previously reported, heparin was conjugated to acryl-PEG by first reacting ethylenediamine (EDA) in excess with acryloyl-PEG-*N*-hydroxysuccinimide (acryl-PEG-NHS, Nektar Therapeutics) at a 5:1 molar ratio to yield acryl-PEG-NH_2. The reaction

was completed for 3 hours at room temperature in a dark environment followed by dialysis (Tube-o-dialyzer, MWCO 1000, Geno Technologies, St. Louis, MO) to remove unreacted EDA. Samples were frozen and lyophilized for 24 hours.

Periodated heparin (Mw 10,000 Celsus Laboratories Inc., USA) was then reacted in equimolar amounts for 3 hours in a dark environment with acryl-PEG-NH_2 to yield acryl-PEG-heparin in the presence of 50 mM $NaBH_3CN$ as the reducing agent. Filtration through centrifugation (Pall Macrosep®, MWCO 10,000) was performed to eliminate the reducing agent and unreacted components. The product was lyophilized and stored in a dessicator at -20°C until further use.

B.2.2 Native PAGE

To ensure FGF-2 binds to synthesized acryl-PEG-heparin, native polyacrylamide gel electrophoresis (PAGE) was performed on FGF-2 and acryl-PEG-heparin samples. A total amount of 200 ng FGF-2 (Cell Sciences) was added to 4 mg acryl-PEG-heparin (1:20,000 molar ratio FGF-2:acryl-PEG-hep) using 100μL of PBS as the buffer solution. The samples were placed on a rotator at 37°C for a 2 hour binding period. A pre-cast polyacrylamide gel (4-20% Ready Gel, Tris-HCL, Bio-Rad) was used to load acryl-PEG-heparin with and without FGF-2. Silver staining method was used to stain for bound FGF-2.

B.2.3 Cumulative Release of FGF-2 from Heparin-modified PEGDA Hydrogels

FGF-2 (4 ng) was encapsulated in a 200μL solution of 20% w/v poly(ethylene glycol) diacrylate (PEGDA) in PBS and 0.1 wt% Irgacure 2959 using a long wave ultra-violet (UV) lamp and an irradiation time of 10 minutes (n=3). A 1.0 mM concentration

of acryl-PEG-heparin was then added to another 200µl 20% PEGDA, as well as 4 ng of FGF-2 (n=3); these hydrogels were also created by polymerizing with a UV lamp for 10 minutes (n=3). Each hydrogel was placed in 4 mL of PBS and rotated at 37°C. 150µL was extracted from each sample at (1, 6hr, 12hr, 24hr, 48hr, 7d, 14d, and 21d time points) and replaced with fresh 150µL PBS each time. Sandwich ELISA (R&D Systems) was performed on these extracted solutions to determine the cumulative release of FGF-2 from the heparin-modified and unmodified PEGDA hydrogels.

B.3 RESULTS AND DISCUSSION

FGF-2 binding affinity to acryl-PEG-heparin was not affected after periodated-heparin conjugation to acryl-PEG-NH_2, as illustrated with native PAGE in **Figure B.1**. Silver staining marks nanogram amounts of protein dark brown/black, and lane 2 in this figure shows that FGF-2 is present and bound to heparin-modified PEG. The negative control, acryl-PEG-heparin without any FGF-2, does not stain brown/black, thus indicating that the presence of a band is exclusively due to FGF-2. Heparin is a type of GAGs composed of repeating disaccharide units made up of alternating uronic acid and glucosamine residues. GAGs usually have extended conformations that occupy a huge volume relative to their mass and are highly negatively charged. Heparin plays an important role chemical signaling between cells by binding to certain molecules, such as FGF-2, and causing their aggregation. This clustering causes FGF-2 to crosslink, thus activating their transmembrane tyrosine kinase receptors. FGF-2 affinity to heparin is mainly due to ionic interactions with some hydrogen bonding, van der Waals, and hydrophobic interactions.

It was initially speculated that encapsulated FGF-2 would be sequestered more in PEGDA scaffolds containing heparin; however FGF-2 release studies from heparin-

modified and unmodified bulk-polymerized gels do not confirm this hypothesis. The first study was performed over a 48 hour period, as illustrated in **Figure B.2(A)**, and scaffolds with 1.0 mM acryl-PEG-heparin actually released 3% more FGF-2 than scaffolds without. This study was then repeated for a longer incubation time period of 21 days total since the initial study was only completed for a 48 hour period. Results from this study confirmed the same release data from the initial studies: increased FGF-2 release was observed from heparin-modified scaffolds, as depicted in **Figure B.2B**.

Future studies recommended to further analyze these conflicting results involve studying the mesh sizes between the modified and unmodified scaffolds. There could also be the possibility of unpolymerized acryl-PEG-heparin that has not diffused out of the polymerized hydrogels. The supernatant solution should also be analyzed of unconjugated acryl-PEG-heparin, thus also increasing the amount of FGF-2 in the solution. Instead of encapsulating FGF-2, the protein could also be added to the supernatant solution of the hydrogels after washing the scaffold extensively to remove unreacted acryl-PEG-heparin. Since heparin has a high density of negative charges, cations (such as Na^+) are attracted, causing hydrogels to be more osmotically active with large volumes of water diffusing into the polymer mesh. The mesh sizes of both polymer meshes should also be evaluated to compare FGF-2 diffusion throughout the scaffold.

Figure B.1 Native PAGE and silver staining indicate that FGF-2 still binds to heparin even after conjugation to acryl-PEG-NH_2. Lane 1 shows acryl-PEG-heparin without FGF-2 (as the negative control) and lane 2 shows acryl-PEG-heparin with FGF-2. Silver staining stains proteins a dark brown color, and this staining is only observed in lane 2 due to the presence of FGF-2. The negative control (lane 1) does not stain for protein, indicating that acryl-PEG-heparin exclusively does not stain during the addition of silver staining components.

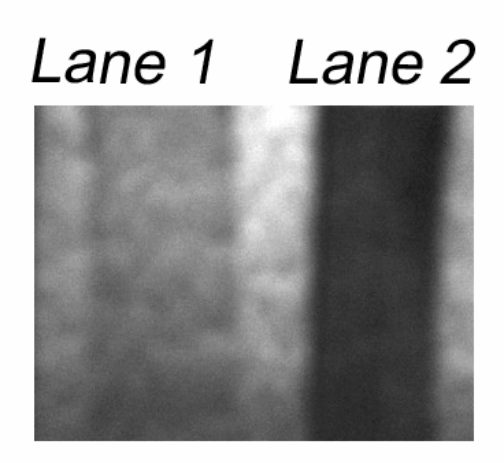

Figure B.2 **FGF-2 release from unmodified PEGDA and PEGDA with 1.0 mM acryl-PEG-heparin was determined through sandwich ELISA. Graph (A) depicts a time period of 48 hr and graph (B) depicts a time period of 21 days. Results were contrary to what was hypothesized: hydrogels modified with heparin released more FGF-2 than hydrogels that did not contain any heparin, even for a 3 week incubation period. Bars indicate standard error between experimental repeats.**

(A)

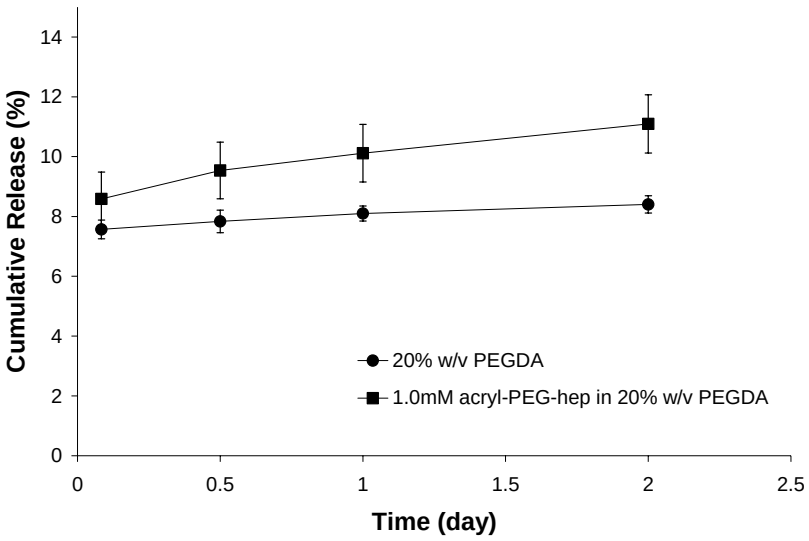

(B)

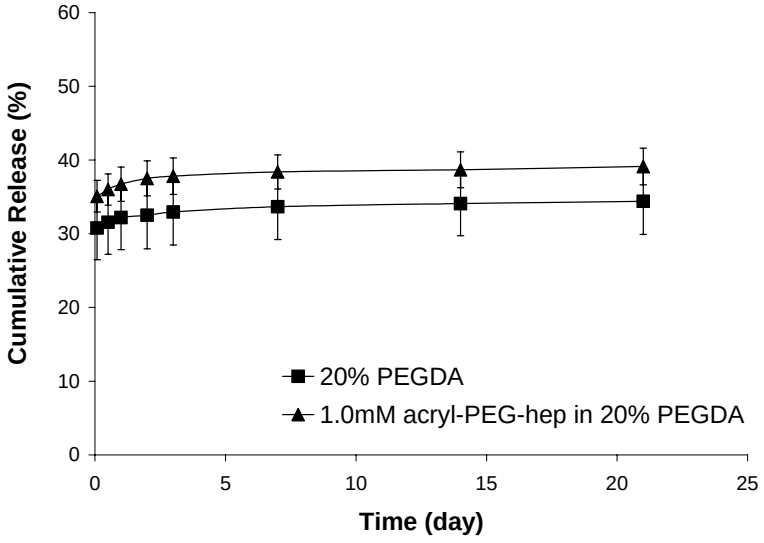

Bibliography

Ahsan, T. and R.M. Nerem, Bioengineered tissues: the science, the technology, and the industry. Orthod Craniofac Res, 2005. **8**(3): p. 134-40.

Alhadlaq, A. and J.J. Mao, Tissue-engineered osteochondral constructs in the shape of an articular condyle. J Bone Joint Surg Am, 2005. **87**(5): p. 936-44.

Allen, B.L., M.S. Filla, and A.C. Rapraeger, Role of heparan sulfate as a tissue-specific regulator of FGF-4 and FGF receptor recognition. J Cell Biol, 2001. **155**(5): p. 845-58.

Altman, G.H., et al., Cell differentiation by mechanical stress. Faseb J, 2002. **16**(2): p. 270-2.

Anderson, D.G., et al., Biomaterial microarrays: rapid, microscale screening of polymer-cell interaction. Biomaterials, 2005. **26**(23): p. 4892-7.

Anseth, K.S., V.R. Shastri, and R. Langer, Photopolymerizable degradable polyanhydrides with osteocompatibility. Nat Biotechnol, 1999. **17**(2): p. 156-9.

Banfi, A., et al., Replicative aging and gene expression in long-term cultures of human bone marrow stromal cells. Tissue Eng, 2002. **8**(6): p. 901-10.

Barry, F., et al., The SH-3 and SH-4 antibodies recognize distinct epitopes on CD73 from human mesenchymal stem cells. Biochem Biophys Res Commun, 2001. **289**(2): p. 519-24.

Barry, F.P., et al., The monoclonal antibody SH-2, raised against human mesenchymal stem cells, recognizes an epitope on endoglin (CD105). Biochem Biophys Res Commun, 1999. **265**(1): p. 134-9.

Bertsch, A., Lorenz, H., Renaud, P., 3D microfabrication by combining microstereolithography and thick resist UV lithography. Sensors and Actuators A, 1999. **73**: p. 14-23.

Bertsch, A., Bernhard, P., Vogt, C., and Renaud, P., Rapid Prototyping of Small Size Objects. Rapid Prototyping Journal, 2000. **6**(4): p. 259-266.

Bianchi, G., et al., Ex vivo enrichment of mesenchymal cell progenitors by fibroblast growth factor 2. Exp Cell Res, 2003. **287**(1): p. 98-105.

Bidwell, J.P., et al., Nuclear matrix proteins and osteoblast gene expression. J Bone Miner Res, 1998. **13**(2): p. 155-67.

Boland, T., et al., Cell and organ printing 2: fusion of cell aggregates in three-dimensional gels. Anat Rec A Discov Mol Cell Evol Biol, 2003. **272**(2): p. 497-502.

Bolland, B.J., et al., Adult mesenchymal stem cells and impaction grafting: a new clinical paradigm shift. Expert Rev Med Devices, 2007. **4**(3): p. 393-404.

Borden, M., M. Attawia, and C.T. Laurencin, The sintered microsphere matrix for bone tissue engineering: in vitro osteoconductivity studies. J Biomed Mater Res, 2002. **61**(3): p. 421-9.

Borden, M., et al., Structural and human cellular assessment of a novel microsphere-based tissue engineered scaffold for bone repair. Biomaterials, 2003. **24**(4): p. 597-609.

Brandley, B.K. and R.L. Schnaar, Covalent attachment of an Arg-Gly-Asp sequence peptide to derivatizable polyacrylamide surfaces: support of fibroblast adhesion and long-term growth. Anal Biochem, 1988. **172**(1): p. 270-8.

Bruder, S.P., et al., Monoclonal antibodies reactive with human osteogenic cell surface antigens. Bone, 1997. **21**(3): p. 225-35.

Bruder, S.P., et al., Mesenchymal stem cell surface antigen SB-10 corresponds to activated leukocyte cell adhesion molecule and is involved in osteogenic differentiation. J Bone Miner Res, 1998. **13**(4): p. 655-63.

Brun, P., et al., Chondrocyte aggregation and reorganization into three-dimensional scaffolds. J Biomed Mater Res, 1999. **46**(3): p. 337-46.

Bryant, S.J. and K.S. Anseth, Hydrogel properties influence ECM production by chondrocytes photoencapsulated in poly(ethylene glycol) hydrogels. J Biomed Mater Res, 2002. **59**(1): p. 63-72.

Bryant, S.J., et al., Encapsulating chondrocytes in degrading PEG hydrogels with high modulus: engineering gel structural changes to facilitate cartilaginous tissue production. Biotechnol Bioeng, 2004. **86**(7): p. 747-55.

Bryant, S.J., et al., Photo-patterning of porous hydrogels for tissue engineering. Biomaterials, 2007. **28**(19): p. 2978-86.

Bryant, S.J., C.R. Nuttelman, and K.S. Anseth, Cytocompatibility of UV and visible light photoinitiating systems on cultured NIH/3T3 fibroblasts in vitro. J Biomater Sci Polym Ed, 2000. **11**(5): p. 439-57.

Burdick, J.A. and K.S. Anseth, Photoencapsulation of osteoblasts in injectable RGD-modified PEG hydrogels for bone tissue engineering. Biomaterials, 2002. **23**(22): p. 4315-23.

Burkoth, A.K. and K.S. Anseth, A review of photocrosslinked polyanhydrides: in situ forming degradable networks. Biomaterials, 2000. **21**(23): p. 2395-404.

Caplan, A.I., Embryonic development and the principles of tissue engineering. Novartis Found Symp, 2003. **249**: p. 17-25; discussion 25-33, 170-4, 239-41.

Caplan, A.I., Review: mesenchymal stem cells: cell-based reconstructive therapy in orthopedics. Tissue Eng, 2005. **11**(7-8): p. 1198-211.

Caplan, A.I. and S.P. Bruder, Mesenchymal stem cells: building blocks for molecular medicine in the 21st century. Trends Mol Med, 2001. **7**(6): p. 259-64.

Carstens, M.H., M. Chin, and X.J. Li, In situ osteogenesis: regeneration of 10-cm mandibular defect in porcine model using recombinant human bone morphogenetic protein-2 (rhBMP-2) and Helistat absorbable collagen sponge. J Craniofac Surg, 2005. **16**(6): p. 1033-42.

Chang, Y.L., C.M. Stanford, and J.C. Keller, Calcium and phosphate supplementation promotes bone cell mineralization: implications for hydroxyapatite (HA)-enhanced bone formation. J Biomed Mater Res, 2000. **52**(2): p. 270-8.

Chen, C.S., et al., Cell shape provides global control of focal adhesion assembly. Biochem Biophys Res Commun, 2003. **307**(2): p. 355-61.

Chen, C.S., et al., Micropatterned surfaces for control of cell shape, position, and function. Biotechnol Prog, 1998. **14**(3): p. 356-63.

Cho, J.H., et al., Chondrogenic differentiation of human mesenchymal stem cells using a thermosensitive poly(N-isopropylacrylamide) and water-soluble chitosan copolymer. Biomaterials, 2004. **25**(26): p. 5743-51.

Chou, L., B. Marek, and W.R. Wagner, Effects of hydroxylapatite coating crystallinity on biosolubility, cell attachment efficiency and proliferation in vitro. Biomaterials, 1999. **20**(10): p. 977-85.

Cui, Q., G.J. Wang, and G. Balian, Pluripotential marrow cells produce adipocytes when transplanted into steroid-treated mice. Connect Tissue Res, 2000. **41**(1): p. 45-56.

Dahir, G.A., et al., Pluripotential mesenchymal cells repopulate bone marrow and retain osteogenic properties. Clin Orthop Relat Res, 2000(379 Suppl): p. S134-45.

Dang, J.M., et al., Temperature-responsive hydroxybutyl chitosan for the culture of mesenchymal stem cells and intervertebral disk cells. Biomaterials, 2006. **27**(3): p. 406-18.

Datta, N., et al., In vitro generated extracellular matrix and fluid shear stress synergistically enhance 3D osteoblastic differentiation. Proc Natl Acad Sci U S A, 2006.

Davis, K.A. and K.S. Anseth, Controlled release from crosslinked degradable networks. Crit Rev Ther Drug Carrier Syst, 2002. **19**(4-5): p. 385-423.

Deligianni, D.D., et al., Effect of surface roughness of hydroxyapatite on human bone marrow cell adhesion, proliferation, differentiation and detachment strength. Biomaterials, 2001. **22**(1): p. 87-96.

Deng, W., et al., In vitro differentiation of human marrow stromal cells into early progenitors of neural cells by conditions that increase intracellular cyclic AMP. Biochem Biophys Res Commun, 2001. **282**(1): p. 148-52.

Dennis, J.E. and A.I. Caplan, Bone Marrow Mesenchymal Stem Cells, in Stem Cells Handbook, S. Sell, Editor. 2004, Humana Press: Totowa. p. 107-18.

Ehara, A., et al., Effects of alpha-TCP and TetCP on MC3T3-E1 proliferation, differentiation and mineralization. Biomaterials, 2003. **24**(5): p. 831-6.

El-Ghannam, A., Bone reconstruction: from bioceramics to tissue engineering. Expert Rev Med Devices, 2005. **2**(1): p. 87-101.

Elisseeff, J., et al., Photoencapsulation of chondrocytes in poly(ethylene oxide)-based semi-interpenetrating networks. J Biomed Mater Res, 2000. **51**(2): p. 164-71.

Elisseeff, J., et al., Controlled-release of IGF-I and TGF-beta1 in a photopolymerizing hydrogel for cartilage tissue engineering. J Orthop Res, 2001. **19**(6): p. 1098-104.

Elisseeff, J., et al., Advances in skeletal tissue engineering with hydrogels. Orthod Craniofac Res, 2005. **8**(3): p. 150-61.

Feinberg, S.E., et al., Image-based biomimetic approach to reconstruction of the temporomandibular joint. Cells Tissues Organs, 2001. **169**(3): p. 309-21.

Filla, M.S., P. Dam, and A.C. Rapraeger, The cell surface proteoglycan syndecan-1 mediates fibroblast growth factor-2 binding and activity. J Cell Physiol, 1998. **174**(3): p. 310-21.

Flaim, C.J., S. Chien, and S.N. Bhatia, An extracellular matrix microarray for probing cellular differentiation. Nat Methods, 2005. **2**(2): p. 119-25.

Franceschi, R.T. and G. Xiao, Regulation of the osteoblast-specific transcription factor, Runx2: responsiveness to multiple signal transduction pathways. J Cell Biochem, 2003. **88**(3): p. 446-54.

Fujimura, K., et al., The effect of fibroblast growth factor-2 on the osteoinductive activity of recombinant human bone morphogenetic protein-2 in rat muscle. Arch Oral Biol, 2002. **47**(8): p. 577-84.

Gao, J. and A.I. Caplan, Mesenchymal stem cells and tissue engineering for orthopaedic surgery. Chir Organi Mov, 2003. **88**(3): p. 305-16.

Gleizes, P.E., et al., Basic fibroblast growth factor (FGF-2) internalization through the heparan sulfate proteoglycans-mediated pathway: an ultrastructural approach. Eur J Cell Biol, 1995. **66**(1): p. 47-59.

Goessler, U.R., et al., In-vitro analysis of the expression of TGFbeta -superfamily-members during chondrogenic differentiation of mesenchymal stem cells and chondrocytes during dedifferentiation in cell culture. Cell Mol Biol Lett, 2005. **10**(2): p. 345-62.

Gojo, S., et al., In vivo cardiovasculogenesis by direct injection of isolated adult mesenchymal stem cells. Exp Cell Res, 2003. **288**(1): p. 51-9.

Gomes, M.E., et al., In Vitro Localization of Bone Growth Factors in Constructs of Biodegradable Scaffolds Seeded with Marrow Stromal Cells and Cultured in a Flow Perfusion Bioreactor. Tissue Eng, 2006. **12**(1): p. 177-188.

Gravel, M., et al., Responses of mesenchymal stem cell to chitosan-coralline composites microstructured using coralline as gas forming agent. Biomaterials, 2006. **27**(9): p. 1899-906.

Grayson, W.L., T. Ma, and B. Bunnell, Human mesenchymal stem cells tissue development in 3D PET matrices. Biotechnol Prog, 2004. **20**(3): p. 905-12.

Griffith, L.G., Emerging design principles in biomaterials and scaffolds for tissue engineering. Ann N Y Acad Sci, 2002. **961**: p. 83-95.

Halstenberg, S., et al., Biologically engineered protein-graft-poly(ethylene glycol) hydrogels: a cell adhesive and plasmin-degradable biosynthetic material for tissue repair. Biomacromolecules, 2002. **3**(4): p. 710-23.

Hanada, K., J.E. Dennis, and A.I. Caplan, Stimulatory effects of basic fibroblast growth factor and bone morphogenetic protein-2 on osteogenic differentiation of rat bone marrow-derived mesenchymal stem cells. J Bone Miner Res, 1997. **12**(10): p. 1606-14.

Hedberg, E.L., et al., Controlled release of an osteogenic peptide from injectable biodegradable polymeric composites. J Control Release, 2002. **84**(3): p. 137-50.

Hern, D.L. and J.A. Hubbell, Incorporation of adhesion peptides into nonadhesive hydrogels useful for tissue resurfacing. J Biomed Mater Res, 1998. **39**(2): p. 266-76.

Hersel, U., C. Dahmen, and H. Kessler, RGD modified polymers: biomaterials for stimulated cell adhesion and beyond. Biomaterials, 2003. **24**(24): p. 4385-415.

Holland, T.A., Y. Tabata, and A.G. Mikos, Dual growth factor delivery from degradable oligo(poly(ethylene glycol) fumarate) hydrogel scaffolds for cartilage tissue engineering. J Control Release, 2005. **101**(1-3): p. 111-25.

Hollister, S.J., Porous scaffold design for tissue engineering. Nat Mater, 2005. **4**(7): p. 518-24.

Hollister, S.J., et al., An image-based approach for designing and manufacturing craniofacial scaffolds. Int J Oral Maxillofac Surg, 2000. **29**(1): p. 67-71.

Hollister, S.J., R.D. Maddox, and J.M. Taboas, Optimal design and fabrication of scaffolds to mimic tissue properties and satisfy biological constraints. Biomaterials, 2002. **23**(20): p. 4095-103.

Holtorf, H.L., et al., Scaffold mesh size affects the osteoblastic differentiation of seeded marrow stromal cells cultured in a flow perfusion bioreactor. J Biomed Mater Res A, 2005. **74**(2): p. 171-80.

Holtorf, H.L., J.A. Jansen, and A.G. Mikos, Ectopic bone formation in rat marrow stromal cell/titanium fiber mesh scaffold constructs: effect of initial cell phenotype. Biomaterials, 2005. **26**(31): p. 6208-16.

Holtorf, H.L., J.A. Jansen, and A.G. Mikos, Flow perfusion culture induces the osteoblastic differentiation of marrow stroma cell-scaffold constructs in the absence of dexamethasone. J Biomed Mater Res A, 2005. **72**(3): p. 326-34.

Hubbell, J.L.W.a.J.A., Polymeric biomaterials with degradation sites for proteases involved in cell migration. Macromolecules, 1999. **32**: p. 241-244.

Hutmacher, D.W., Scaffolds in tissue engineering bone and cartilage. Biomaterials, 2000. **21**(24): p. 2529-43.

Hutmacher, D.W., M. Sittinger, and M.V. Risbud, Scaffold-based tissue engineering: rationale for computer-aided design and solid free-form fabrication systems. Trends Biotechnol, 2004. **22**(7): p. 354-62.

Itoga, K., et al., Cell micropatterning using photopolymerization with a liquid crystal device commercial projector. Biomaterials, 2004. **25**(11): p. 2047-53.

Itoga, K., et al., Micropatterned surfaces prepared using a liquid crystal projector-modified photopolymerization device and microfluidics. J Biomed Mater Res A, 2004. **69**(3): p. 391-7.

Jaiswal, R.K., et al., Adult human mesenchymal stem cell differentiation to the osteogenic or adipogenic lineage is regulated by mitogen-activated protein kinase. J Biol Chem, 2000. **275**(13): p. 9645-52.

Jaiswal, R.K., et al., Adult human mesenchymal stem cell differentiation to the osteogenic or adipogenic lineage is regulated by mitogen-activated protein kinase. J Biol Chem, 2000. **275**(13): p. 9645-52.

Jansen, J.A., et al., Growth factor-loaded scaffolds for bone engineering. J Control Release, 2005. **101**(1-3): p. 127-36.

Jeong, B., et al., Biodegradable block copolymers as injectable drug-delivery systems. Nature, 1997. **388**(6645): p. 860-2.

Jin, Q.M., et al., Effects of geometry of hydroxyapatite as a cell substratum in BMP-induced ectopic bone formation. J Biomed Mater Res, 2000. **52**(4): p. 491-9.

Johnstone, B., et al., In vitro chondrogenesis of bone marrow-derived mesenchymal progenitor cells. Exp Cell Res, 1998. **238**(1): p. 265-72.

Karageorgiou, V. and D. Kaplan, Porosity of 3D biomaterial scaffolds and osteogenesis. Biomaterials, 2005. **26**(27): p. 5474-91.

Kasturi, S.P., K. Sachaphibulkij, and K. Roy, Covalent conjugation of polyethyleneimine on biodegradable microparticles for delivery of plasmid DNA vaccines. Biomaterials, 2005. **26**(32): p. 6375-85.

Kawaguchi, H., et al., Stimulation of fracture repair by recombinant human basic fibroblast growth factor in normal and streptozotocin-diabetic rats. Endocrinology, 1994. **135**(2): p. 774-81.

Kawata, S., et al., Finer features for functional microdevices. Nature, 2001. **412**(6848): p. 697-8.

Khademhosseini, A., et al., Microscale technologies for tissue engineering and biology. Proc Natl Acad Sci U S A, 2006.

Kim, T.K., et al., Experimental model for cartilage tissue engineering to regenerate the zonal organization of articular cartilage. Osteoarthritis Cartilage, 2003. **11**(9): p. 653-64.

Kimoto, T., et al., Continuous administration of basic fibroblast growth factor (FGF-2) accelerates bone induction on rat calvaria--an application of a new drug delivery system. J Dent Res, 1998. **77**(12): p. 1965-9.

Klompmaker, J., et al., Porous polymer implant for repair of meniscal lesions: a preliminary study in dogs. Biomaterials, 1991. **12**(9): p. 810-6.

Klompmaker, J., et al., Porous polymer implants for repair of full-thickness defects of articular cartilage: an experimental study in rabbit and dog. Biomaterials, 1992. **13**(9): p. 625-34.

Koh, W.G., A. Revzin, and M.V. Pishko, Poly(ethylene glycol) hydrogel microstructures encapsulating living cells. Langmuir, 2002. **18**(7): p. 2459-62.

Kokubo, T., Bioactive glass ceramics: properties and applications. Biomaterials, 1991. **12**(2): p. 155-63.

Kuznetsov, S.A., et al., Circulating skeletal stem cells. J Cell Biol, 2001. **153**(5): p. 1133-40.

Lalani, Z., et al., Spatial and temporal localization of transforming growth factor-beta1, bone morphogenetic protein-2, and platelet-derived growth factor-A in healing tooth extraction sockets in a rabbit model. J Oral Maxillofac Surg, 2003. **61**(9): p. 1061-72.

Li, Q., et al., Biodegradable and photocrosslinkable polyphosphoester hydrogel. Biomaterials, 2006. **27**(7): p. 1027-34.

Li, W.J., et al., Multilineage differentiation of human mesenchymal stem cells in a three-dimensional nanofibrous scaffold. Biomaterials, 2005. **26**(25): p. 5158-66.

Li, W.J., et al., A three-dimensional nanofibrous scaffold for cartilage tissue engineering using human mesenchymal stem cells. Biomaterials, 2005. **26**(6): p. 599-609.

Li, X., et al., Chemical characteristics and cytocompatibility of collagen-based scaffold reinforced by chitin fibers for bone tissue engineering. J Biomed Mater Res B Appl Biomater, 2005.

Li, Z., et al., Controlled gene delivery system based on thermosensitive biodegradable hydrogel. Pharm Res, 2003. **20**(6): p. 884-8.

Lieb, E., et al., Poly(D,L-lactic acid)-poly(ethylene glycol)-monomethyl ether diblock copolymers control adhesion and osteoblastic differentiation of marrow stromal cells. Tissue Eng, 2003. **9**(1): p. 71-84.

Lim, J.Y. and H.J. Donahue, Biomaterial characteristics important to skeletal tissue engineering. J Musculoskelet Neuronal Interact, 2004. **4**(4): p. 396-8.

Lin, A.S., et al., Microarchitectural and mechanical characterization of oriented porous polymer scaffolds. Biomaterials, 2003. **24**(3): p. 481-9.

Lin, C.Y., N. Kikuchi, and S.J. Hollister, A novel method for biomaterial scaffold internal architecture design to match bone elastic properties with desired porosity. J Biomech, 2004. **37**(5): p. 623-36.

Lin, X., et al., Heparan sulfate proteoglycans are essential for FGF receptor signaling during Drosophila embryonic development. Development, 1999. **126**(17): p. 3715-23.

Liu, L., et al., Preparation and characterization of collagen-hydroxyapatite composite used for bone tissue engineering scaffold. Artif Cells Blood Substit Immobil Biotechnol, 2003. **31**(4): p. 435-48.

Liu, V.A. and S.N. Bhatia, Three-dimensional photopatterning of hydrogels containing living cells. Biomedical Microdevices, 2002. **4**(4): p. 257-266.

Livak, K.J. and T.D. Schmittgen, Analysis of relative gene expression data using real time quantitative PCR and the 2^-DDCT method. Methods, 2001. **25**: p. 402-408.

Lo, H., M.S. Ponticiello, and K.W. Leong, Fabrication of controlled release biodegradable foams by phase separation. Tissue Engineering, 1995. **1**(1): p. 15-28.

Lu, Y., et al., A digital micro-mirror device-based system for the microfabrication of complex, spatially patterned tissue engineering scaffolds. J Biomed Mater Res A, 2006.

Ma, H.L., et al., Neocartilage from human mesenchymal stem cells in alginate: implied timing of transplantation. J Biomed Mater Res A, 2005. **74**(3): p. 439-46.

Mackay, A.M., et al., Chondrogenic differentiation of cultured human mesenchymal stem cells from marrow. Tissue Eng, 1998. **4**(4): p. 415-28.

Maffezzoli, A., et al., Photopolymerization of dental composite matrices. Biomaterials, 1994. **15**(15): p. 1221-8.

Mann, B.K., et al., Smooth muscle cell growth in photopolymerized hydrogels with cell adhesive and proteolytically degradable domains: synthetic ECM analogs for tissue engineering. Biomaterials, 2001. **22**(22): p. 3045-51.

Mapili, G., et al., Laser-layered microfabrication of spatially patterned functionalized tissue-engineering scaffolds. J Biomed Mater Res B Appl Biomater, 2005. **75**(2): p. 414-24.

Martin, I., et al., Fibroblast growth factor-2 supports ex vivo expansion and maintenance of osteogenic precursors from human bone marrow. Endocrinology, 1997. **138**(10): p. 4456-62.

Maruo, S. and K. Ikuta, New microstereolithography (Super-IH process) to create 3D freely movable micromechanism without sacrificial layer technique, in MHS'98: Proceedings of the 1998 International Symposium on Micromechatronics and Human Science. 1998. p. 115.

McBeath, R., et al., Cell shape, cytoskeletal tension, and RhoA regulate stem cell lineage commitment. Dev Cell, 2004. **6**(4): p. 483-95.

Meinel, L., et al., Silk implants for the healing of critical size bone defects. Bone, 2005. **37**(5): p. 688-98.

Meinel, L., et al., Engineering cartilage-like tissue using human mesenchymal stem cells and silk protein scaffolds. Biotechnol Bioeng, 2004. **88**(3): p. 379-91.

Meinel, L., et al., Engineering bone-like tissue in vitro using human bone marrow stem cells and silk scaffolds. J Biomed Mater Res A, 2004. **71**(1): p. 25-34.

Meirelles Lda, S. and N.B. Nardi, Murine marrow-derived mesenchymal stem cell: isolation, in vitro expansion, and characterization. Br J Haematol, 2003. **123**(4): p. 702-11.

Metters, A.T., K.S. Anseth, and C.N. Bowman, Fundamental studies of biodegradable hydrogels as cartilage replacement materials. Biomed Sci Instrum, 1999. **35**: p. 33-8.

Mondrinos, M.J., et al., Engineering Three-Dimensional Pulmonary Tissue Constructs. Tissue Eng, 2005.

Muggli, D.S., A.K. Burkoth, and K.S. Anseth, Crosslinked polyanhydrides for use in orthopedic applications: degradation behavior and mechanics. J Biomed Mater Res, 1999. **46**(2): p. 271-8.

Muggli, D.S., A.K. Burkoth, and K.S. Anseth, Crosslinked polyanhydrides for use in orthopedic applications: degradation behavior and mechanics. J Biomed Mater Res, 1999. **46**(2): p. 271-8.

Murphy, W.L., et al., Effects of a bone-like mineral film on phenotype of adult human mesenchymal stem cells in vitro. Biomaterials, 2005. **26**(3): p. 303-10.

Musina, R.A., E.S. Bekchanova, and G.T. Sukhikh, Comparison of mesenchymal stem cells obtained from different human tissues. Bull Exp Biol Med, 2005. **139**(4): p. 504-9.

Nagaya, N., et al., Transplantation of mesenchymal stem cells improves cardiac function in a rat model of dilated cardiomyopathy. Circulation, 2005. **112**(8): p. 1128-35.

Nakagawa, T. and T. Tagawa, Ultrastructural study of direct bone formation induced by BMPs-collagen complex implanted into an ectopic site. Oral Dis, 2000. **6**(3): p. 172-9.

Nazarov, R., H.J. Jin, and D.L. Kaplan, Porous 3-D scaffolds from regenerated silk fibroin. Biomacromolecules, 2004. **5**(3): p. 718-26.

Nishimura, N., et al., A new bioactive bone cement: its histological and mechanical characterization. J Appl Biomater, 1991. **2**(4): p. 219-29.

Noth, U., et al., Anterior cruciate ligament constructs fabricated from human mesenchymal stem cells in a collagen type I hydrogel. Cytotherapy, 2005. **7**(5): p. 447-55.

Nuttelman, C.R., M.C. Tripodi, and K.S. Anseth, In vitro osteogenic differentiation of human mesenchymal stem cells photoencapsulated in PEG hydrogels. J Biomed Mater Res, 2004. **68A**(4): p. 773-82.

Nuttelman, C.R., M.C. Tripodi, and K.S. Anseth, Synthetic hydrogel niches that promote hMSC viability. Matrix Biol, 2005. **24**(3): p. 208-18.

Nuttelman, C.R., M.C. Tripodi, and K.S. Anseth, Dexamethasone-functionalized gels induce osteogenic differentiation of encapsulated hMSCs. J Biomed Mater Res A, 2006. **76**(1): p. 183-95.

Ong, J.L., et al., Osteoblast precursor cell activity on HA surfaces of different treatments. J Biomed Mater Res, 1998. **39**(2): p. 176-83.

Orban, J.M., K.G. Marra, and J.O. Hollinger, Composition options for tissue-engineered bone. Tissue Eng, 2002. **8**(4): p. 529-39.

Orlic, D., et al., Bone marrow cells regenerate infarcted myocardium. Nature, 2001. **410**(6829): p. 701-5.

Otto, W.R. and J. Rao, Tomorrow's skeleton staff: mesenchymal stem cells and the repair of bone and cartilage. Cell Prolif, 2004. **37**(1): p. 97-110.

Park, A., B. Wu, and L.G. Griffith, Integration of surface modification and 3D fabrication techniques to prepare patterned poly(L-lactide) substrates allowing regionally selective cell adhesion. J Biomater Sci Polym Ed, 1998. **9**(2): p. 89-110.

Park, H., et al., Delivery of TGF-beta1 and chondrocytes via injectable, biodegradable hydrogels for cartilage tissue engineering applications. Biomaterials, 2005. **26**(34): p. 7095-103.

Peppas, N.A., Hydrogels, in Biomaterials Science, A.S.H. Buddy D. Ratner, Frederick J. Schoen, and Jack E. Lemons, Editor. 1996, Academic Press: San Diego. p. 60-64.

Perry, T.E., et al., Thoracic Surgery Directors Association Award. Bone marrow as a cell source for tissue engineering heart valves. Ann Thorac Surg, 2003. **75**(3): p. 761-7; discussion 767.

Peter, S.J., et al., Effects of transforming growth factor beta1 released from biodegradable polymer microparticles on marrow stromal osteoblasts cultured on poly(propylene fumarate) substrates. J Biomed Mater Res, 2000. **50**(3): p. 452-62.

Petka, W.A., et al., Reversible hydrogels from self-assembling artificial proteins. Science, 1998. **281**(5375): p. 389-92.

Pittenger, M.F., et al., Multilineage potential of adult human mesenchymal stem cells. Science, 1999. **284**(5411): p. 143-7.

Pittenger, M.F., J.D. Mosca, and K.R. McIntosh, Human mesenchymal stem cells: progenitor cells for cartilage, bone, fat and stroma. Curr Top Microbiol Immunol, 2000. **251**: p. 3-11.

Pye, D.A., et al., Regulation of FGF-1 mitogenic activity by heparan sulfate oligosaccharides is dependent on specific structural features: differential requirements for the modulation of FGF-1 and FGF-2. Glycobiology, 2000. **10**(11): p. 1183-92.

Quarto, N. and F. Amalric, Heparan sulfate proteoglycans as transducers of FGF-2 signalling. J Cell Sci, 1994. **107 (Pt 11)**: p. 3201-12.

Raghunath, J., et al., Advancing cartilage tissue engineering: the application of stem cell technology. Curr Opin Biotechnol, 2005. **16**(5): p. 503-9.

Rahaman, M.N. and J.J. Mao, Stem cell-based composite tissue constructs for regenerative medicine. Biotechnol Bioeng, 2005. **91**(3): p. 261-84.

Rahmoune, H., et al., Interaction of heparan sulfate from mammary cells with acidic fibroblast growth factor (FGF) and basic FGF. Regulation of the activity of basic FGF by high and low affinity binding sites in heparan sulfate. J Biol Chem, 1998. **273**(13): p. 7303-10.

Reddi, A.H. and N.S. Cunningham, Initiation and promotion of bone differentiation by bone morphogenetic proteins. J Bone Miner Res, 1993. **8 Suppl 2**: p. S499-502.

Ren, J., et al., Repair of mandibular defects using MSCs-seeded biodegradable polyester porous scaffolds. J Biomater Sci Polym Ed, 2007. **18**(5): p. 505-17.

Ren, X.D., W.B. Kiosses, and M.A. Schwartz, Regulation of the small GTP-binding protein Rho by cell adhesion and the cytoskeleton. Embo J, 1999. **18**(3): p. 578-85.

Rezania, A. and K.E. Healy, The effect of peptide surface density on mineralization of a matrix deposited by osteogenic cells. J Biomed Mater Res, 2000. **52**(4): p. 595-600.

Richard, C., M. Roghani, and D. Moscatelli, Fibroblast growth factor (FGF)-2 mediates cell attachment through interactions with two FGF receptor-1 isoforms and extracellular matrix or cell-associated heparan sulfate proteoglycans. Biochem Biophys Res Commun, 2000. **276**(2): p. 399-405.

Richardson, T.P., et al., Polymeric system for dual growth factor delivery. Nat Biotechnol, 2001. **19**(11): p. 1029-34.

Rickard, D.J., et al., Isolation and characterization of osteoblast precursor cells from human bone marrow. J Bone Miner Res, 1996. **11**(3): p. 312-24.

Ringeisen, B.R., et al., Jet-based methods to print living cells. Biotechnol J, 2006. **1**(9): p. 930-48.

Robey, P.G., Bone Matrix Proteoglycans and Glycoproteins, in Principles of Bone Biology, J.P. Bilezikian, L.G. Raisz, and G.A. Rodan, Editors. 1996, Academic Press: San Diego. p. 155-65.

Romanov, Y.A., et al., Mesenchymal stem cells from human bone marrow and adipose tissue: isolation, characterization, and differentiation potentialities. Bull Exp Biol Med, 2005. **140**(1): p. 138-43.

Rossert, J. and B. de Crombrugghe, Type I Collagen: Structure, Synthesis, and Regulation, in Principles of Bone Biology, J.P. Bilezikian, L.G. Raisz, and G.A. Rodan, Editors. 1996, Academic Press: San Diego. p. 127-142.

Ruel-Gariepy, E., et al., A thermosensitive chitosan-based hydrogel for the local delivery of paclitaxel. Eur J Pharm Biopharm, 2004. **57**(1): p. 53-63.

Sachlos, E. and J.T. Czernuszka, Making tissue engineering scaffolds work. Review: the application of solid freeform fabrication technology to the production of tissue engineering scaffolds. Eur Cell Mater, 2003. **5**: p. 29-39; discussion 39-40.

Sanchez-Ramos, J., et al., Adult bone marrow stromal cells differentiate into neural cells in vitro. Exp Neurol, 2000. **164**(2): p. 247-56.

Schmitt, J.M., et al., Bone morphogenetic proteins: an update on basic biology and clinical relevance. J Orthop Res, 1999. **17**(2): p. 269-78.

Schnaar, R.L., B.G. Langer, and B.K. Brandley, Reversible covalent immobilization of ligands and proteins on polyacrylamide gels. Anal Biochem, 1985. **151**(2): p. 268-81.

Schonherr, E. and H.J. Hausser, Extracellular matrix and cytokines: a functional unit. Dev Immunol, 2000. **7**(2-4): p. 89-101.

Sharma, B. and J.H. Elisseeff, Engineering structurally organized cartilage and bone tissues. Ann Biomed Eng, 2004. **32**(1): p. 148-59.

Shea, C.M., et al., BMP treatment of C3H10T1/2 mesenchymal stem cells induces both chondrogenesis and osteogenesis. J Cell Biochem, 2003. **90**(6): p. 1112-27.

Shin, H., S. Jo, and A.G. Mikos, Modulation of marrow stromal osteoblast adhesion on biomimetic oligo[poly(ethylene glycol) fumarate] hydrogels modified with Arg-Gly-Asp peptides and a poly(ethyleneglycol) spacer. J Biomed Mater Res, 2002. **61**(2): p. 169-79.

Shin, H., et al., Osteogenic differentiation of rat bone marrow stromal cells cultured on Arg-Gly-Asp modified hydrogels without dexamethasone and beta-glycerol phosphate. Biomaterials, 2005. **26**(17): p. 3645-54.

Shin, H., et al., Attachment, proliferation, and migration of marrow stromal osteoblasts cultured on biomimetic hydrogels modified with an osteopontin-derived peptide. Biomaterials, 2004. **25**(5): p. 895-906.

Shin, M., H. Yoshimoto, and J.P. Vacanti, In vivo bone tissue engineering using mesenchymal stem cells on a novel electrospun nanofibrous scaffold. Tissue Eng, 2004. **10**(1-2): p. 33-41.

Simmons, C.A., et al., Cyclic strain enhances matrix mineralization by adult human mesenchymal stem cells via the extracellular signal-regulated kinase (ERK1/2) signaling pathway. J Biomech, 2003. **36**(8): p. 1087-96.

Simmons, P.J., et al., Isolation, characterization and functional activity of human marrow stromal progenitors in hemopoiesis. Prog Clin Biol Res, 1994. **389**: p. 271-80.

Simmons, P.J. and B. Torok-Storb, Identification of stromal cell precursors in human bone marrow by a novel monoclonal antibody, STRO-1. Blood, 1991. **78**(1): p. 55-62.

Solchaga, L.A., et al., FGF-2 enhances the mitotic and chondrogenic potentials of human adult bone marrow-derived mesenchymal stem cells. J Cell Physiol, 2005. **203**(2): p. 398-409.

Subramanian, A. and H.Y. Lin, Crosslinked chitosan: its physical properties and the effects of matrix stiffness on chondrocyte cell morphology and proliferation. J Biomed Mater Res A, 2005. **75**(3): p. 742-53.

Sun, C., Fang, N., Wu, D.M., and Zhang, X., Projection micro-stereolithography using digital micro-mirror dynamic mask. Sensors and Acutuators A-Physical, 2005. **121**(1): p. 113-120.

Sun, J.S., et al., The effects of calcium phosphate particles on the growth of osteoblasts. Journal of Biomedical Materials Research, 1997. **37**(3): p. 324-34.

Taboas, J.M., et al., Indirect solid free form fabrication of local and global porous, biomimetic and composite 3D polymer-ceramic scaffolds. Biomaterials, 2003. **24**(1): p. 181-94.

Taipale, J. and J. Keski-Oja, Growth factors in the extracellular matrix. Faseb J, 1997. **11**(1): p. 51-9.

Takahashi, Y. and Y. Tabata, Homogeneous seeding of mesenchymal stem cells into nonwoven fabric for tissue engineering. Tissue Eng, 2003. **9**(5): p. 931-8.

Takahashi, Y., M. Yamamoto, and Y. Tabata, Enhanced osteoinduction by controlled release of bone morphogenetic protein-2 from biodegradable sponge composed of gelatin and beta-tricalcium phosphate. Biomaterials, 2005. **26**(23): p. 4856-65.

Tan, J.L., et al., Simple approach to micropattern cells on common culture substrates by tuning substrate wettability. Tissue Eng, 2004. **10**(5-6): p. 865-72.

Temenoff, J.S., et al., Thermally cross-linked oligo(poly(ethylene glycol) fumarate) hydrogels support osteogenic differentiation of encapsulated marrow stromal cells in vitro. Biomacromolecules, 2004. **5**(1): p. 5-10.

Tiller, J.C., et al., Improving biomaterial properties of collagen films by chemical modification. Biotechnol Bioeng, 2001. **73**(3): p. 246-52.

Tsang, V.L. and S.N. Bhatia, Three-dimensional tissue fabrication. Adv Drug Deliv Rev, 2004. **56**(11): p. 1635-47.

Tsuruga, E., et al., Pore size of porous hydroxyapatite as the cell-substratum controls BMP-induced osteogenesis. J Biochem (Tokyo), 1997. 121(2): p. 317-24.

Tsutsumi, S., et al., Retention of multilineage differentiation potential of mesenchymal cells during proliferation in response to FGF. Biochem Biophys Res Commun, 2001. **288**(2): p. 413-9.

Vacanti, J.P. and R. Langer, Tissue engineering: the design and fabrication of living replacement devices for surgical reconstruction and transplantation. Lancet, 1999. **354 Suppl 1**: p. SI32-4.

Vacanti, J.P., et al., Selective cell transplantation using bioabsorbable artificial polymers as matrices. J Pediatr Surg, 1988. **23**(1 Pt 2): p. 3-9.

Vozzi, G., et al., Fabrication of PLGA scaffolds using soft lithography and microsyringe deposition. Biomaterials, 2003. **24**(14): p. 2533-40.

Wake, M.C., et al., Effects of biodegradable polymer particles on rat marrow-derived stromal osteoblasts in vitro. Biomaterials, 1998. **19**(14): p. 1255-68.

Wake, M.C., et al., Effects of biodegradable polymer particles on rat marrow-derived stromal osteoblasts in vitro. Biomaterials, 1998. **19**(14): p. 1255-68.

Wakitani, S., T. Saito, and A.I. Caplan, Myogenic cells derived from rat bone marrow mesenchymal stem cells exposed to 5-azacytidine. Muscle Nerve, 1995. **18**(12): p. 1417-26.

Walsh, S., et al., Expression of the developmental markers STRO-1 and alkaline phosphatase in cultures of human marrow stromal cells: regulation by fibroblast growth factor (FGF)-2 and relationship to the expression of FGF receptors 1-4. Bone, 2000. **27**(2): p. 185-95.

Wang, D.A., et al., Bioresponsive phosphoester hydrogels for bone tissue engineering. Tissue Eng, 2005. **11**(1-2): p. 201-13.

Wang, F.S., et al., Superoxide mediates shock wave induction of ERK-dependent osteogenic transcription factor (CBFA1) and mesenchymal cell differentiation toward osteoprogenitors. J Biol Chem, 2002. **277**(13): p. 10931-7.

Wang, J., H.Q. Mao, and K.W. Leong, A novel biodegradable gene carrier based on polyphosphoester. J Am Chem Soc, 2001. **123**(38): p. 9480-1.

Wang, Y., et al., In vitro cartilage tissue engineering with 3D porous aqueous-derived silk scaffolds and mesenchymal stem cells. Biomaterials, 2005. **26**(34): p. 7082-94.

Weigel, T., G. Schinkel, and A. Lendlein, Design and preparation of polymeric scaffolds for tissue engineering. Expert Rev Med Devices, 2006. **3**(6): p. 835-51.

Williams, C.G., et al., In vitro chondrogenesis of bone marrow-derived mesenchymal stem cells in a photopolymerizing hydrogel. Tissue Eng, 2003. **9**(4): p. 679-88.

Williams, J.T., et al., Cells isolated from adult human skeletal muscle capable of differentiating into multiple mesodermal phenotypes. Am Surg, 1999. **65**(1): p. 22-6.

Woodbury, D., et al., Adult rat and human bone marrow stromal cells differentiate into neurons. J Neurosci Res, 2000. **61**(4): p. 364-70.

Worster, A.A., et al., Chondrocytic differentiation of mesenchymal stem cells sequentially exposed to transforming growth factor-beta1 in monolayer and insulin-like growth factor-I in a three-dimensional matrix. J Orthop Res, 2001. **19**(4): p. 738-49.

Wozney, J.M., The bone morphogenetic protein family and osteogenesis. Molecular Reproduction and Development, 1992. **32**(1): p. 160-7.

Yang, X.B., et al., Human osteoprogenitor growth and differentiation on synthetic biodegradable structures after surface modification. Bone, 2001. **29**(6): p. 523-31.

Yarlagadda, P.K., M. Chandrasekharan, and J.Y. Shyan, Recent advances and current developments in tissue scaffolding. Biomed Mater Eng, 2005. **15**(3): p. 159-77.

Yoshikawa, H. and A. Myoui, Bone tissue engineering with porous hydroxyapatite ceramics. J Artif Organs, 2005. **8**(3): p. 131-6.

Young, C.S., et al., Tissue-engineered hybrid tooth and bone. Tissue Eng, 2005. **11**(9-10): p. 1599-610.

Zaleskas, J.M., et al., Contractile forces generated by articular chondrocytes in collagen-glycosaminoglycan matrices. Biomaterials, 2004. **25**(7-8): p. 1299-308.

Zegzula, H.D., et al., Bone formation with use of rhBMP-2 (recombinant human bone morphogenetic protein-2). J Bone Joint Surg Am, 1997. **79**(12): p. 1778-90.

Zein, I., et al., Fused deposition modeling of novel scaffold architectures for tissue engineering applications. Biomaterials, 2002. **23**(4): p. 1169-85.

Zhang, G., et al., A PEGylated Fibrin Patch for Mesenchymal Stem Cell Delivery. Tissue Eng, 2006. **12**(1-2): p. 9-19.

Zhang, H., et al., Microrobotics and MEMS-based fabrication techniques for scaffold-based tissue engineering. Macromol Biosci, 2005. **5**(6): p. 477-89.

Zhang, X., X.N. Jiang, and C. Sun, Micro-stereolithography of polymeric and ceramic microstructures. Sensors and Actuators A, 1999. **77**: p. 149-156.

Zhao, F., et al., Effects of hydroxyapatite in 3-D chitosan-gelatin polymer network on human mesenchymal stem cell construct development. Biomaterials, 2006. **27**(9): p. 1859-67.

Vita

Mary Gazell Mapili Call was born in Manila, Philippines on May 14, 1980, daughter of Reynaldo B. and Maria B. Mapili. After graduating from Little Rock Central High School in Little Rock, Arkansas, in 1998, she pursued her undergraduate studies at the University of Arkansas in Fayetteville. During the summer semester of 2000 and spring semester of 2001, Gazell worked at the Dow Chemical Company as a cooperative engineering student. In May 2002, she received her Bachelor of Science degree in Chemical Engineering at the University of Arkansas in Fayetteville.

With a strong interest in the biomedical sciences, Gazell began her Ph.D. studies in August 2002 at the University of Texas in Austin at the Department of Biomedical Engineering. She received her Master of Science degree in May 2006 and continued her efforts in studying stem cell behavior within complex, polymer environments. Gazell presented her work at several, leading biomedical conferences and published two first author papers in peer reviewed journals. In April 2006, Gazell was the recipient of the international "Ph.D. Student Award for Outstanding Research" given by the Society for Biomaterials in Pittsburgh, Pennsylvania. Gazell is married to Seth Call and currently resides in Austin, Texas with her husband.

Permanent address: 10814 Sans Souci Place, Austin, Texas 78759

This dissertation was typed by Mary Gazell Mapili Call.